Fall 2010

Classification of EMG signals to control a prosthetic hand using time-frequesncy representations and Support Vector Machines

Juan Manuel Fontana

CLASSIFICATION OF EMG SIGNALS TO CONTROL A PROSTHETIC HAND USING TIME-FREQUENCY REPRESENTATIONS AND SUPPORT VECTOR MACHINES

by

Juan Manuel Fontana, B.S.

A Dissertation Presented in Partial Fulfillment
of the Requirements for the Degree
Doctor of Philosophy

COLLEGE OF ENGINEERING AND SCIENCE
LOUISIANA TECH UNIVERSITY

November 2010

LOUISIANA TECH UNIVERSITY

THE GRADUATE SCHOOL

09/21/2010

Date

We hereby recommend that the dissertation prepared under our supervision by Juan Manuel Fontana

entitled

CLASSIFICATION OF EMG SIGNALS TO CONTROL A PROSTHETIC HAND USING TIME-FREQUENCY REPRESENTATIONS AND SUPPORT VECTOR MACHINES

be accepted in partial fulfillment of the requirements for the Degree of Doctor of Philosophy in Biomedical Engineering

Supervisor of Dissertation Research

Head of Department

Department

Recommendation concurred in:

Advisory Committee

Approved:

Director of Graduate Studies

Approved:

Dean of the Graduate School

Dean of the College

GS Form 13a
(6/07)

ABSTRACT

Myoelectric signals (MES) are viable control signals for externally-powered prosthetic devices. They may improve both the functionality and the cosmetic appearance of these devices. Conventional controllers, based on the signal's amplitude features in the control strategy, lack a large number of controllable states because signals from independent muscles are required for each degree of freedom (DoF) of the device. Myoelectric pattern recognition systems can overcome this problem by discriminating different residual muscle movements instead of contraction levels of individual muscles. However, the lack of long-term robustness in these systems and the design of counter-intuitive control/command interfaces have resulted in low clinical acceptance levels. As a result, the development of robust, easy to use myoelectric pattern recognition-based control systems is the main challenge in the field of prosthetic control.

This dissertation addresses the need to improve the controller's robustness by designing a pattern recognition-based control system that classifies the user's intention to actuate the prosthesis. This system is part of a cost-effective prosthetic hand prototype developed to achieve an acceptable level of functional dexterity using a simple to use interface. A Support Vector Machine (SVM) classifier implemented as a directed acyclic graph (DAG) was created. It used wavelet features from multiple surface EMG channels strategically placed over five forearm muscles. The classifiers were evaluated across seven subjects. They were able to discriminate five wrist motions with an accuracy of

91.5%. Variations of electrode locations were artificially introduced at each recording session as part of the procedure, to obtain data that accounted for the changes in the user's muscle patterns over time. The generalization ability of the SVM was able to capture most of the variability in the data and to maintain an average classification accuracy of 90%.

Two principal component analysis (PCA) frameworks were also evaluated to study the relationship between EMG recording sites and the need for feature space reduction. The dimension of the new feature set was reduced with the goal of improving the classification accuracy and reducing the computation time. The analysis indicated that the projection of the wavelet features into a reduced feature space did not significantly improve the accuracy and the computation time. However, decreasing the number of wavelet decomposition levels did lower the computational load without compromising the average signal classification accuracy.

Based on the results of this work, a myoelectric pattern recognition-based control system that uses an SVM classifier applied to time-frequency features may be used to discriminate muscle contraction patterns for prosthetic applications.

APPROVAL FOR SCHOLARLY DISSEMINATION

The author grants to the Prescott Memorial Library of Louisiana Tech University the right to reproduce, by appropriate methods, upon request, any or all portions of this Dissertation. It is understood that "proper request" consists of the agreement, on the part of the requesting party, that said reproduction is for his personal use and that subsequent reproduction will not occur without written approval of the author of this Dissertation. Further, any portions of the Dissertation used in books, papers, and other works must be appropriately referenced to this Dissertation.

Finally, the author of this Dissertation reserves the right to publish freely, in the literature, at any time, any or all portions of this Dissertation.

Author _____

Date 10/20/2010

GS Form 14
(5/03)

TABLE OF CONTENTS

LIST OF TABLES

TABLE OF FIGURES

ACKNOWLEDGMENTS

I would like to take this opportunity to express gratitude to the people that played an important role in my four years as graduate student. First of all, I would like to give special thanks to my partner of life, my adorable wife Natalia, for her unconditional love and understanding and for making me laugh every time I was frustrated. I would never have achieved this goal without you by my side.

To my loving family in Argentina: for being so close to me despite of the many miles and for moulding me into the person I am today. To my mother and first Math teacher Mabel: for motivating me with her strength, fortitude and constant prayers. To my father Juan: for encouraging me to progress through each stage of my life. To my sisters, Marive and Luciana, and their families: for showing me that goals become easier to reach with effort and commitment. To my Nono Herminio: for being such a wonderful role model. To my wife's family: for their support and affection.

To all my friends who helped me in one way or another along this journey. To my best friend and lab partner Cristian: for sharing this walk along the project and for inspiring me with his hard work and passion for making a difference in the lives of those in need. To Dr. Pedro Derosa and Dr. Daniela Mainardi: for their sincere and generous friendship and for their disinterested help throughout this stage of my life. To Ivan Diaz, Carlos Montes and Juan M. Lopez: for backing me up during all these years not only with their talks, advice and words of encouragement but also with countless barbecue nights.

To all my friends in Argentina: for being always there for me when they would rather be anywhere else.

To my advisor Dr. Alan W.L. Chiu: for his mentorship throughout these years at Louisiana Tech University and for his constant guidance in the beginning of my researcher career. To all the committee members Dr. Steven Jones, Dr. Stan Cronk, Dr. Eric Guilbeau and Dr. Weizhong Dai for their time and valuable comments and contributions to the final version of this manuscript. Finally, I want to thank the College of Engineering and Science at Louisiana Tech University for the financial support.

CHAPTER 1

INTRODUCTION

1.1. Problem Statement

In the United States, 1.7 million people live with limb loss, and it is projected that this number will double by the year 2050 [1]. Dysvascular amputations constitute the leading cause of limb loss followed by trauma-related amputations [2]. However, the majority of upper limb amputations are related to injuries and only 3% are related to vascular diseases [1, 3]. Limb replacement is a complex process influenced by many factors. Lower limb amputations are 20 times more frequent than the upper limb amputations. However, the damage produced by upper limb loss is more detrimental [4] because the dexterity of the hand plays a major role in carrying out the different activities of daily living. The replacement of an upper extremity impacts the amputees' life socially, psychologically and economically. The social impact arises from the altered cosmetic appearance and the reduced limb functionality. The psychological impact arises directly from the absence of the limb. Part of the economic impact, for most people, is the cost of replacing the absent extremity. Consequently, a properly designed upper limb prosthetic device should address all three of these issues that emerge from the amputation.

The prosthesis has to be comfortable, functional, and aesthetically pleasing to be acceptable. Existing prostheses are mostly focused on one of these attributes so they do

not present an appropriate balance among them and this may be the reason of the high rejection rate [5]. Upper limb amputees have two different options for prosthetics: a) *passive prostheses* that do not actively grasp but have excellent cosmetic appearance; and b) *active prostheses* (also called functional prosthetics), which allow the user to hold and manipulate objects but with lower attractive appearance. Passive prostheses lack functionality but they can look incredibly natural. They present only few user concerns, mostly related to glove problems and strap irritation [6]. On the other hand, functional prostheses can help people perform different activities of daily living but the comfort and the cost are limiting factors. Body-powered (cable controlled) and externally-powered (electrically powered) are the two main types of functional upper limb prostheses.

Currently, the use of *myoelectric signals* (MES) in the control strategy of active prostheses [7-9] offers a viable alternative for body-powered control by providing more functionality and better cosmetic appearance [10, 11], as signals recorded during voluntary muscle contractions are translated into different prosthetic actions. Conventional use of signal amplitude as the feature for control lacks a large number of controllable states because independent muscles are required for each degree of freedom (DoF). Myoelectric pattern recognition systems can overcome this problem if the set of features describing a specific muscle activation pattern is repeatable at particular electrode locations [12]. Multiple prosthetic actions can be created by discriminating different muscle states instead of individual muscle contraction amplitudes. Many pattern recognition [13-16] and feature extraction algorithms [17-20] have been proposed for prosthetic applications. Although patterns were successfully classified on both able subjects and amputees, these methods lack the long-term robustness and intuitive

command interfaces of historical body-powered prostheses. The long term robustness is associated to the ability of the control system to adjust to changes in the user's myoelectric patterns over time. The intuitiveness in the control is related to the cognitive burden of the user, who has to be able to actuate the prosthetic's functions in the most natural way. Therefore, the development of a robust, easy to use myoelectric pattern recognition-based control system that accurately discriminates several voluntary muscles contractions is a major need in the field of prosthetic control.

1.2. Prosthetic Hand Project Overview

The need of a new generation of upper limb prosthetics motivated the development of a cost effective prosthetic hand with a user friendly control interface. Advanced signal processing tools and an automatic control algorithm have been incorporated into the myoelectric hand to allow replacement of expensive, specialized actuators and sensors with less expensive components and to reduce the cognitive burden associated with the actuation of the device. Figure 1 illustrates the scheme of the proposed prosthesis. High-level control is used to interpret the user's intention to actuate the hand prototype, which was specially designed and fabricated for this project. Low-level control then automatically performs the grasping task. Low level feedback gives both grasping force and joint position information to the control, whereas a vibrotactile feedback system (high level feedback) gives an indirect sense of touch to the user.

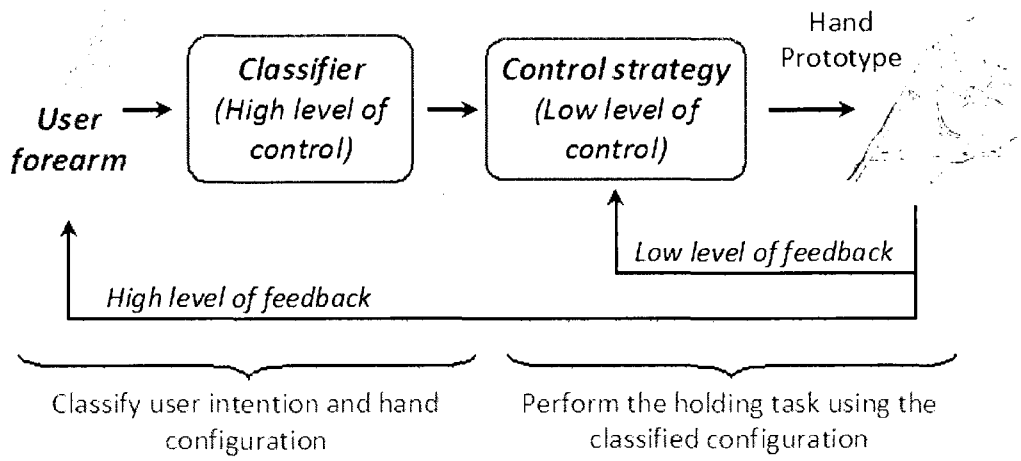

Figure 1. General scheme of the proposed device. The intention of the user is translated into actions of the hand. The control algorithm will automatically modulate the grasping force. This dissertation focuses only on the classification of the user intention.

MES recorded from the body surface of the forearm are classified into different patterns that represent the user's intention to actuate the prosthetic hand to different configurations. Once the action is selected, the control strategy is activated to automatically modulate the grasping force. The prosthetic hand is continuously monitored by the low level control to prevent slippage of the object. The combination of a signal classifier with an automatic grasping scheme leads to a robust system that is more natural and easier to control. The user simply has to select the grasping configuration and the control system will modulate the holding task automatically. Minimal further monitoring of the prosthesis is needed during the grasping task, which considerably decreases the psychological effort of the user.

This dissertation focuses on the high level control, which involves the development of a myoelectric pattern recognition-based control system. The methods used to classify the different motion patterns are extensively explained in this manuscript. The validation of the proposed control system is achieved through the evaluation of the

accuracy in the classification of four different wrist movements, which were selected as the motions that could activate four different functions of the prosthetic hand.

1.3. Goals

The main goal of this work is to develop a robust myoelectric pattern recognition-based control system for upper limb prosthetics that involves a minimum user effort. When a prosthetic device is controlled by electromyographic signals generated by the muscles of the residual limb, three main aspects have to be taken into account to get a successful control [21]:

- The different movements produced must be accurately classified.
- User control must be intuitive and must require low psychological effort.
- The system response time should not introduce perceivable delay.

A pattern recognition scheme will help to achieve an easy to use interface since the user has to perform a simple muscle contraction to actuate the device. The implementation Support Vector Machines (SVM) as the signal classifier will help to achieve high accuracy in the classification because of its high generalization property. The SVM model is a linear function that can be calculated with low computational load.

The specific aims of this project include:

- Implement and evaluate SVM signal classification technique for the discrimination of five different muscle contraction classes.
- Minimize the effect caused by variations in the electrode location to reduce the user effort to setup the device.
- Implement and evaluate the myoelectric pattern recognition system for a real-time control of a prosthetic hand.

1.4. Myoelectric Control System Overview

The myoelectric pattern recognition-based control system presented in this work classifies several users' muscle contractions to actuate a prosthetic hand. Figure 2 illustrates the four main blocks of the control system. Surface myolectric signals are recorded and conditioned for feature extraction. A classifier takes the reduced set of features and determines the appropriate function of the prosthesis.

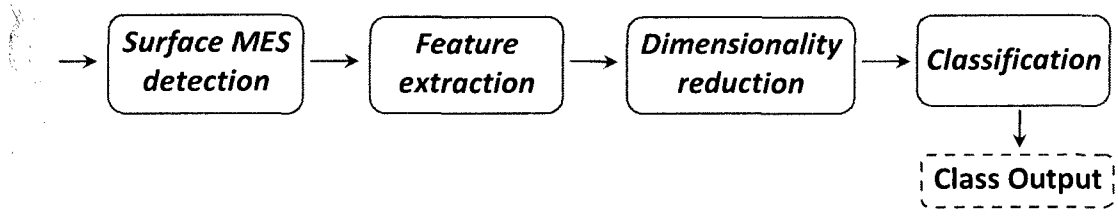

Figure 2. Block diagram of the myoelectric pattern recognition-based control system proposed.

In the following paragraphs a brief explanation of the contents covered on each block is introduced. The dimensionality reduction block is presented after the classification stage because it was implemented as a potential method to improve the performance of the whole pattern recognition system.

MES detection

As the prosthetic hand under development was designed to be a non-invasive device, MES were recorded from the surface of the skin. Five forearm muscles were selected, whose activation is directly associated with four different wrist movements: abduction, adduction, extension and flexion. Seven bipolar channels were distributed along the selected muscles, and the reference electrode was placed on the wrist. The recorded signal was filtered to eliminate both low frequency motion artifacts and power

line noise. The amplitude of the filtered signal was normalized into 256-points non-overlapped windows.

Feature Extraction

To extract the information contained in the cleaned MES, the Discrete Wavelet Transform (DWT) was applied to each 256-point moving time window segment of muscle contraction. This time-frequency representation of the signal overcomes both time and frequency features because the mother wavelets functions resemble the motor unit actions potentials that represent the gross EMG signal. The DWT mapped the windowed signal into a set of wavelets coefficients, whose number depended on the level of depth decomposed. To reduce the amount of information obtained, the wavelet coefficients' energy was averaged at each frequency resolution level. The reduced features of each channel were combined into a single feature vector to give a D-dimensional wavelet feature vector (D = No. of decomposition levels $\times$ No. of channels).

Classification

The four specific wrist movements performed by the user were decoded into four different actions of the prosthetic hand. A rest muscle state was translated as no action for the device. Therefore, the classifier was responsible for the correct classification of five different motion classes. It incorporated the information received from the feature vector into a mathematical description of the decision boundary that separated the classes. SVM, implemented as a directed acyclic graph (DAG), was used as the classification algorithm because it can generalize and classify both linear and nonlinear data. Multiple binary SVM classifiers were trained to discriminate the classes using the Gaussian Radial Basis Function (GRBF) kernel. The selection of the best model parameters, as well as

classification accuracy achieved after training one classifier per subject was examined. The classifier also incorporated minor variations in electrode locations so potential trial-to-trial changes produced by either a misalignment of the socket or long-term use can be accommodated. It was hypothesized that the SVM algorithm will be able to compensate for these variations. To test this hypothesis a training strategy was proposed. Signals from different recording sessions simulated the electrode placement variations. The improvement in the SVM classification accuracy was evaluated as data from the different sessions were added to the training set. The performance of the classifier was also evaluated by calculating the sensitivity and specificity.

Dimensionality Reduction

A feature projection framework based on Principal Component Analysis (PCA) was implemented with the aim to expedite the processing time and improve the classification accuracy of the myoelectric control system. It was hypothesized that the implementation of a PCA feature projection framework will gather the relevant discriminatory information from the original features set, producing an improvement in the classification accuracy of the signal classifier. In addition, a reduction in the dimensionality of the new feature set will expedite the processing time in the decision stage. Two PCA frameworks were tested for dimensionality reduction. The effect of reducing the feature dimension was analyzed in classification accuracy and processing time. The analysis was also extended to determine the effect of these feature projection frameworks on the performance of the classifier as more data were incorporated in the training process to account for the variations of electrode placement.

CHAPTER 2

BACKGROUND AND LITERATURE REVIEW

Electromyography (EMG) is a well known technique that records the electrical activity produced by the skeletal muscles. By means of appropriate detection methods, the signals generated can be used to determine when a muscle is contracted or if an intention of a movement exists. This important tool allows the control of assistive devices by means of voluntary contractions produced by the subject. This type of control is referred to as *myoelectric control*. It can enable people with disabilities such as amputation, cerebral palsy, and spinal cord injury to communicate with the external environment and to perform tasks that would otherwise be impossible. In the case of prosthetic devices, signals from the muscles on the residual extremity can be used to activate different functions of the artificial limb.

This chapter reviews the basic principles of myoelectric signal generation and the past and present techniques that use these signals in the control strategy of upper limb prostheses. The chapter begins with the origin of electromyographic signals and the two main detection methods. Several applications that use analysis and interpretation of EMG are mentioned. Conventional and pattern recognition-based myoelectric control techniques are presented later in this chapter. The latter technique is explained in more detail since it was implemented in this work.

2.1. Nature of Myoelectric Signals

Electromyographic (EMG) signals represent the electrical activity generated when skeletal muscles are contracted after an action potential stimulated the muscle fibers. Myelinated large nerve fibers originated from α-motor neurons located in the anterior horn of the spinal cord innervate the skeletal muscle fibers. The terminal branches of a single motor neuron excite multiple muscle fibers forming a *motor unit* (MU) (Figure 3). The number of muscle fibers innervated by one nerve fiber range from 10 in the extraocular muscles to over 500 in large limb muscles [22]. The motor unit is the smallest part of a muscle that the central nervous system can control individually. A normal muscle is formed by a random distribution of the muscle fibers of a motor unit that are intermingled with muscle fibers belonging to 20-50 different motor units [23].

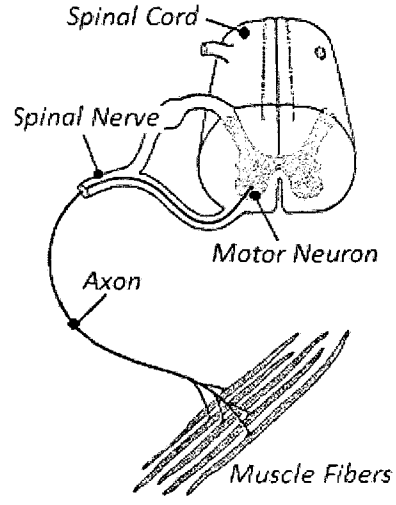

Figure 3. Nerve fiber originated in the spinal cord innervates several muscle fibers forming a motor unit (MU).

A single motor neuron controls the muscle fiber through special synaptic junctions called *motor end plates* (Figure 4.a). The action potential (AP) transmitted from

the brain down to the neuromuscular junction initiates a sequence of electrochemical events at the pre-synaptic nerve terminal. An excitatory transmitter Acetylcholine (Ach) is released into the synaptic cleft producing an increment in the electrical potential inside the muscle fiber in the positive direction by opening the Ach-gated ion channels located in the fiber membrane and allowing the flow of great amount of ions to the interior of the cell. This local potential is referred to as the *end plate potential* (Figure 4.b). A depolarization in the post-synaptic membrane above a threshold level initiates an action potential in the adjacent membrane and spreads along the muscle fiber in opposite directions towards the two ends.

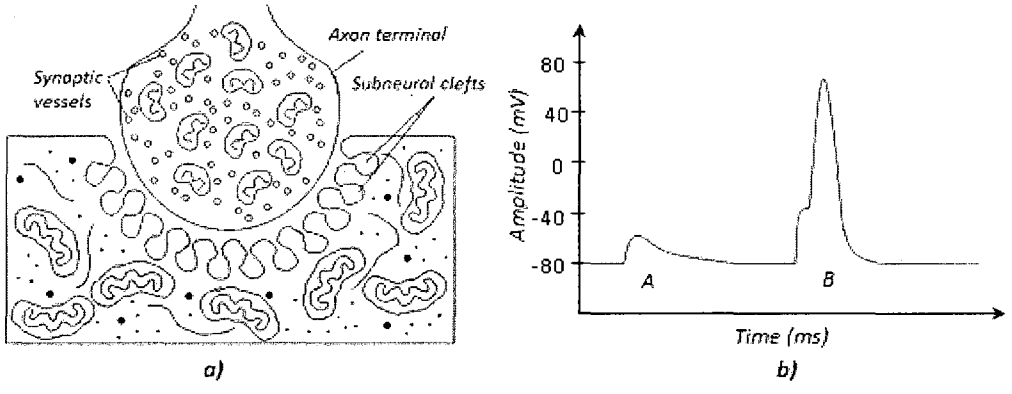

Figure 4. a) Contact point between the axon terminal and the muscle fiber membrane. b) End plate potentials: A is too weak to elicit an action potential whereas B is a normal end plate that elicits an AP.

When a motor unit is recruited, action potentials are generated on each muscle fiber innervated by the motor neuron causing a brief contraction or twitch of the muscle (delayed few milliseconds from the AP origin). The spatial-temporal superposition of the contributions of the individual fiber results in an electrical signal called *motor unit action potential* (MUAP) (Figure 5). A needle electrode placed in the contracting muscle can record this local voltage. The shape and the amplitude of the observed MUAP depend on

the geometric orientation of the active muscle fibers with respect to the recording sites as well as on the muscle tissue and on the properties of the MU. The filtering properties of the electrodes also affect the phase and the duration of the MUAP recorded [23]. In normal muscles, the typical amplitude may vary from 20 to 2000 μV [25]. The duration of the MUAP in skeletal muscles is inversely related to the conduction velocity of the muscle fiber, varying from 1 ms to 5 ms, about five times as long as in large myelinated nerves [24].

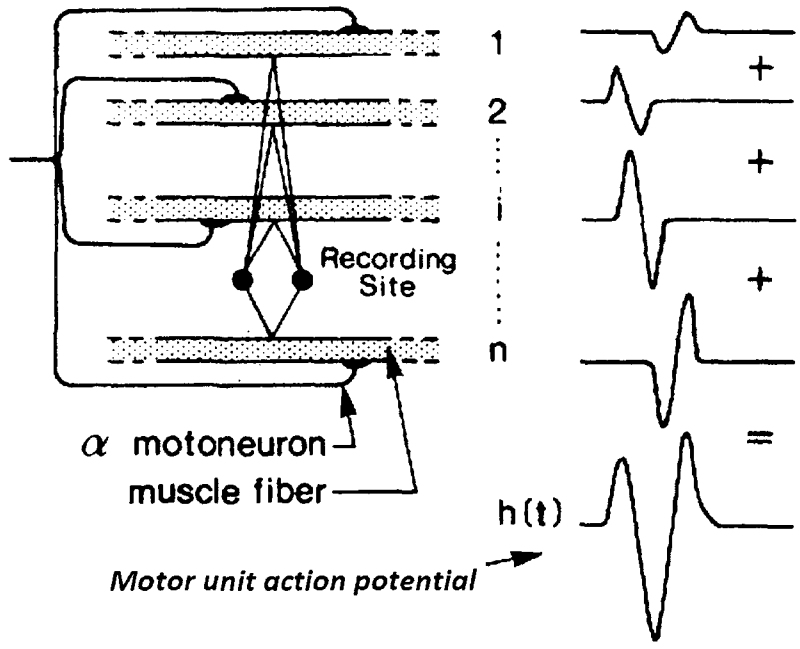

Figure 5. The motor unit action potential (MUAP) is the result of a spatial-temporal superposition of the action potentials from each muscle fiber [23].

To maintain the muscle contraction, a sequence of MUAP must be generated yielding to a train of impulses called *motor unit action potential train* (MUAPT). The time interval between the adjacent discharges is called interpulse interval (IPI) whereas the reciprocal of the average IPI is referred to as the average firing rate of the MU. The

myoelectric signal (MES) generated at the recoding sites is the summation of the contributions of the MUAPTs (Figure 6). The irregular discharges of the motor units and the different shapes of the MUAPs lead to a myoelectric signal that can be represented by a band-limited stochastic process with Gaussian amplitude distribution whose frequency spectrum ranges from DC to 500 Hz [26]. In summary, a myoelectric signal is a function of physiological and anatomical factors as well as of the filtering characteristics of the environment and the recording device.

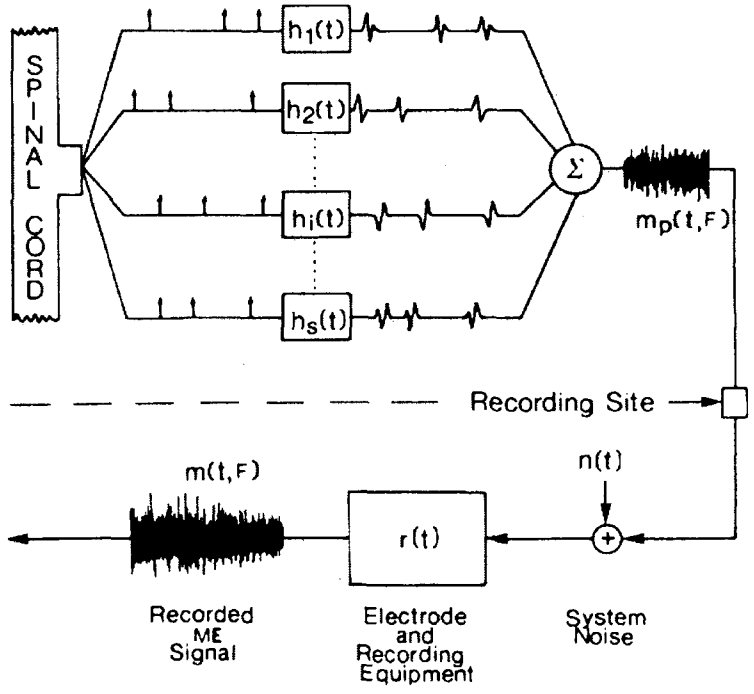

Figure 6. The myoelectric signal is the summation of the contribution of the individual motor unit action potential trains. It characteristics depends on anatomical factors and the properties of the recording equipment [23]

2.2. Detection Techniques for Myoelectric Signals

The electric potential field generated by a muscle contraction can be recorded from either *intramuscular* or *surface* electrodes. The signals from these two types of

recordings differ strongly because of the amount of biological tissue separating the active fibers and the recording sites, called *volume conductor*. In the intramuscular recordings, *needle electrodes* are inserted directly into the muscle, so the effect of volume conductor is minimal. The signal is detected close to the source and consists of the activity of a few muscle fibers belonging to 10 to 15 motor units. On the other hand, the distance between the *surface electrodes* and the sources of the signal is relevant, which produces a significant spatial lowpass filtering effect on the EMG signal. The surface electromyographic (sEMG) signal contains electric potentials from several tens of MUs, yielding global information about muscle function. The detection volume of the surface electrodes is much larger than that on the intramuscular electrodes. The sEMGs are also subject to *crosstalk,* where the signal contains information from muscles that are not relevant for the study but that are close to the recording muscle. This phenomenon is one of the most important sources of error in interpreting surface myoelectric signals [27].

Intramuscular recordings have been used to study the physiology of single motor units because they are highly selective to individual action potentials [28]. Studies have attempted to decompose the intramuscular EMG (iEMG) signals into its constituent MUAPs to understand the control strategies of muscle contractions by the neuromuscular system [29-31] (Figure 7). As an example, firing patterns have been analyzed to identify the activity of specific MUs for different force levels and contraction types [32-34]. In addition, the recruitment behavior of the human motor units was studied by decomposing the iEMG signals detected from individual muscles [35-37].

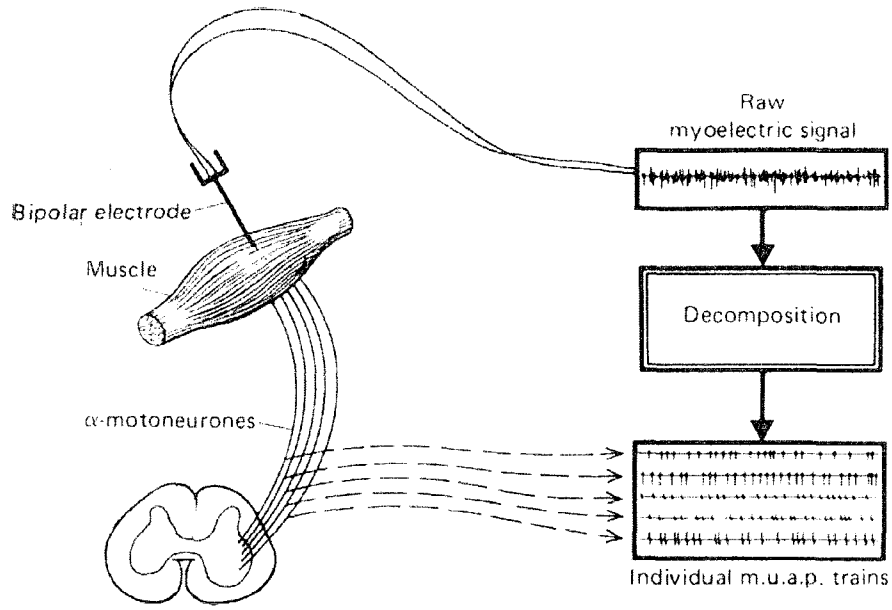

Figure 7. Decomposition of the myoelectric signals into its constituent MUAP [38].

Clinical applications of intramuscular EMG have been limited by decomposition algorithm, which require excessive processing time to generate useful information. Another factor is the necessity high-quality signals for a reliable decomposition, which can only be achieved by a meticulous placement of the needle electrodes. Present applications in the clinical environment are related to diseases affecting either the neuromuscular junction or α-motor neuron. They do not require the full decomposition of the iEMG but it uses either the shape of some motor unit action potentials or the interference signal (superposition of many motor unit responses) for the diagnosis of the pathology [39, 40]. In the field of assistive technology, current technological advances on implantable sensors have led to studies that focuses on the implementation of intramuscular EMG as a potential alternative for the control of prosthetic devices [41].

On the other hand, *surface recordings* present the advantage of being non invasive because the signal is picked up over the skin surface overlaying the examined

muscles. They have been also used for signal decomposition even though the process is considerably more complex than when using needle electrodes [42]. The main reason is the effect of the volume conductor, which strongly affects the shapes and durations of the MUAPs increasing the probability of superposition and making more difficult their correct interpretation [43]. However, advanced signal processing algorithms [42, 44, 45] and novel surface recording techniques [46, 47] have allowed decomposition of surface electrode recordings that are reliable for investigating physiological muscle properties. For example, conduction velocity of the action potentials has been estimated by detecting the motor unit activity during muscle contractions [48, 49]. In addition, the firing patterns of the MU trains and their behavior were analyzed by several investigators [50-52].

Surface EMG find important application in neurology, sports, rehabilitation medicine and in the control of assistive devices where needle electrodes are not acceptable. The study of patterns of muscle activations generated by the central nervous system can help to the analysis and diagnosis of neurological disorders. Fluctuations in the sEMG signal during normal and pathological fatigue can be tracked reflecting several aspects of the metabolic state of the muscle and the variations in the motor command during exercise [53-55]. The analysis of the function and coordination of muscles in different movements and postures as well as in skilled actions and during training is often done by means of myoelectric signals. Isometric and non-isometric contractions are studied in time and frequency domain for determining the timing of muscle activation. The linear envelope (rectification and low-pass filtering of the EMG) as well as additional smoothing techniques are used to describe the human walking and running and to estimate the muscle forces [56-59]. In rehabilitation engineering, different parameters

of the EMG signal, such as the peak amplitude or the onset and end of EMG activity are analyzed to evaluate low back pain, neck pain, pelvic floor pathologies, and motor control of the trunk muscles [60, 61].

Prosthetic devices can be controlled with sEMG signals recorded from specific muscles in residual limbs. Signal processing techniques extract relevant information from the recorded signal and map it into different actions of the prosthetic device (Figure 8). Myoelectrically controlled prostheses have several advantages over prostheses that do not use these signals; no harnesses are required to command the device, minimal muscle activity is needed to provide reliable signals, and a non-invasive technique is used for recording [9, 62, 63]. An expanded literature review on the two main types of myoelectric control of prosthetic devices is presented in the next section.

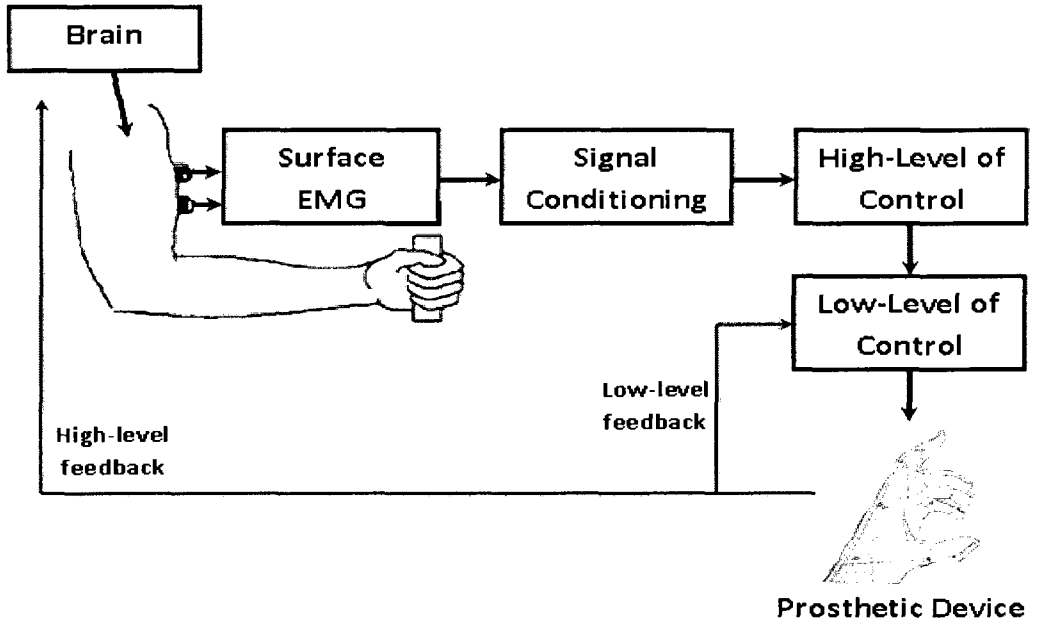

Figure 8. Block diagram showing a general scheme of a myoelectric control system.

2.3. Conventional Myoelectric Control of Prosthetic Devices

The surface myoelectric signal is widely used as an input for the actuation of upper limb prosthetic devices. Individuals with amputations or congenital deficient limbs can still voluntarily control the contraction of the remaining muscles. Appropriately located electrodes detect this activity and by means of signal processing algorithms different functions of the prosthesis can be selected. Since the 1960s, researchers had been addressing alternatives for commanding the prosthesis by discriminating several muscle states. Two major groups can be identified depending on the type of myoelectric control implemented: a) conventional control and b) pattern recognition based control. In both cases, the objective was to allow the users to actuate the device at a subconscious level, so they can focus on things other than the contraction of specific muscles [64].

Conventional myoelectric control systems extract the information of the muscle activity either from the signal's amplitude or from its rate of change. These features are used to initiate a set of commands that can be used to instruct the prosthetic device for a specific degree of freedom (DoF) in movement. Most of the commercially available myoelectric prostheses use the amplitude of the signal from an active control muscle of the user's remaining limb.

Early myoelectric systems decoded the amplitude of the signals from two independent muscles for controlling the open and close functions of the prosthesis [65, 66]. Flexor and extensor muscle activities were commonly used as the on-off switch for the *two-state actuation* of the device. These systems have a good performance, are easy to materialize and do not require excessive user effort to control. Those may have been the reasons for being the first control schemes commercially implemented in prosthetic

devices [9]. The MES detected is full-wave rectified and then smoothed or averaged using a low-pass filter. This provides a signal amplitude level that gives an indication of the variance of the raw signal, which is then used as the control input. If the amplitude level corresponding to the contraction of the control muscle rises above certain threshold (S1 and S2 in Figure 9), the associated function is activated. The disadvantage of the two-state method is that two independent muscle sites are needed to control one degree of freedom making the system impractical when more than two functions must be controlled (i.e. above elbow amputees needs to actuate three DoF: elbow, wrist, hand).

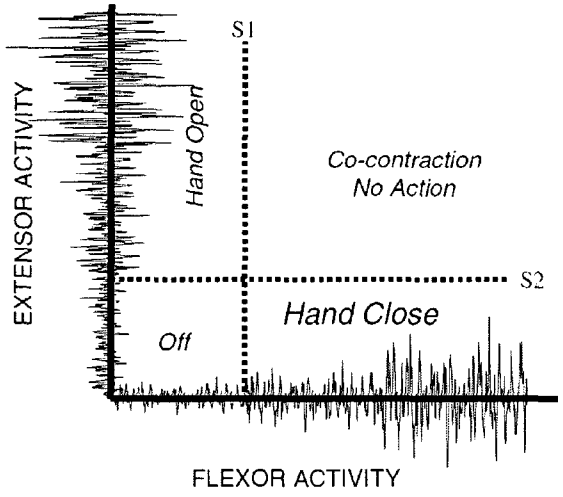

Figure 9. Basic principle of the two-state myoelectric control system using two different control muscles [9]

Three-state myoelectric control systems were developed for overcoming this limitation and were clinically tested on below-elbow and forequarter amputees [67, 68]. Each control muscle can control two functions (one DoF) of a terminal device (i.e. hand, wrist) by modulating the amplitude of the signal and comparing its value with two different threshold levels (Figure 10). When the mean absolute value (MAV) of the MES is below threshold level S1 the corresponding function is in off state; when MAV falls

between S1 and S2 one function is activated (i.e. hand open, right wrist rotation, elbow extension); finally, when the MAV of the signal is above S2 the opposite function is selected (i.e. hand close, left wrist rotation, elbow flexion). To operate the device successfully, the user needs to be trained, which implies an additional cognitive effort since the control strategy was not physiologically designed [9].

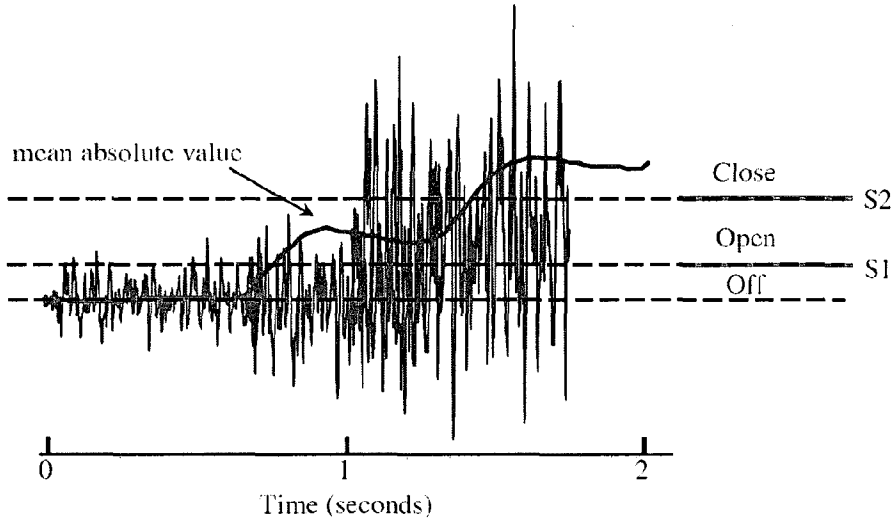

Figure 10. Three-state myoelectric control system using a single control muscle [9].

Following the same principle, myoelectric control systems attempting to select *more than three states* from one control muscle were investigated but with no promising results. The operator error and the necessity of feedback on the level of force executed made this type of control unreliable [69, 70].

A *proportional myoelectric control* of devices has been addressed as an additional approach. The velocity at which the terminal device is actuated is proportional to the amplitude of the contraction of the control muscle. The advantage of proportional control over the on-off state control is that it allows a more natural response of the device with

less psychological effort for the user. Some companies have implemented this control technique in prosthetic devices. The Boston Elbow (Liberating Technologies, Inc. [71]) was created to compensate for the absence of an arm and uses residual muscles in the stump to control the extension and flexion of the elbow joint. The speed of the movement is controlled by the intensity of the contractions performed by the remaining muscles. The Utah Arm (Motion Control, Inc. [72]), originally developed in 1981 for above elbow amputees, also uses proportional control to command elbow, wrist and hand at different velocities [73]. These three degrees of freedom cannot be controlled simultaneously, so a switch mechanism using quick co-contraction of the control muscle was implemented to select the active terminal. However, the introduction of two microcontrollers in the latest version, the Utah Arm 3, allows the user to control both the elbow and the hand at the same time but not the wrist rotation. A newer device that implemented proportional control but that was not commercially developed was the Southampton hand [74]. It was designed based on the hierarchical form employed by the central nervous system to control the hand. This task was broken up into three levels where the person simply desires to move the object (first level) and the system automatically coordinates the actions (second and third levels) to reach the objective without significant psychological effort. The first level is the myoelectric control, in which a pair of electrodes was connected to the flexor and extensor muscles of the forearm to record a bipolar EMG signal. The degree of opening of the hand was proportional to the level of contraction on one direction (extension) whereas the amount of grip force exerted by the hand was proportional to the level of contraction on the other way (flexion) (Figure 11).

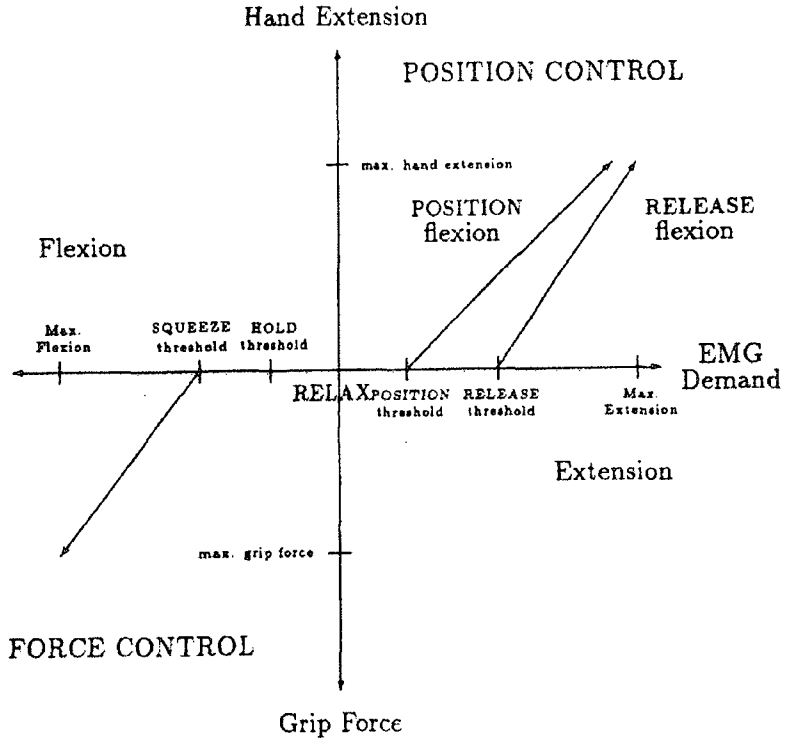

Figure 11. Proportional myoelectric control implemented in the Southampton Hand. Hand extension and grip force are controlled by extensor and flexor muscles, respectively [74].

The conventional control approaches described in this section have two common drawbacks. First, only two functions can be controlled using the same control muscle, and in the case of multifunction control (>2), the signal sources must be independent. This constitutes a limitation for high-level amputees because they require more functionality in the device but they probably don't have enough number of control sites available. Second, the psychological effort associated with the multifunction control forces the training of the users. This may become very complex because they must learn to contract several independent muscles in a coordinated way [8].

Current technological advances in computing devices and instrumentation as well as the development of complex signal processing techniques have opened the door to the

design of new strategies for multifunction myoelectric control. The discrimination among muscle states has emerged as the most reliable technique for controlling more than one degree of freedom of the prosthetic device. This technique is referred to as *pattern recognition based myoelectric control.* The next section presents a review of this technique as well as of the different methods explored by researchers to achieve a high accuracy in the selection of the prosthetic functions.

2.4. Pattern Recognition-Based Myoelectric Control

Pattern recognition-based myoelectric control systems attempt to discriminate different classes of movements by using time of frequency related signatures observed on the MES. Each class is directly related with a DoF in movement, so the user can voluntarily select and modulate the functions of the prosthetic device. These systems are based on the assumption that the set of features describing the MES of specific muscle activation's pattern is repeatable under particular electrode location [12]. The pattern recognition process encompasses a series of steps before the final control outcome can be achieved. They are represented by each one of the blocks illustrated in Figure 12.

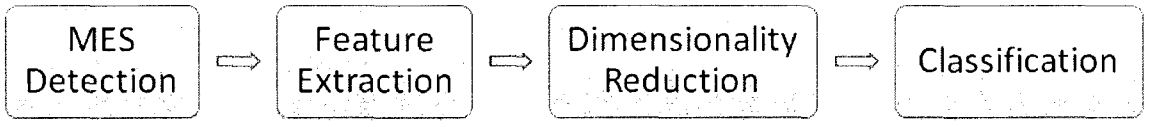

Figure 12. Block diagram of the pattern recognition process applied to the control of a prosthetic device. The surface EMG signal is detected and then conditioned for the extraction of the most relevant information. A classifier takes the reduced set of features and determines the appropriate action of the prosthesis.

Surface electrodes are strategically placed over the skin in order to record as much information as possible about the muscle activity. The measured signal is

transformed to extract important features contained in it. This feature extraction stage is one of the most critical in myoelectric control design because the overall performance of the system depends on it [8]. In some cases, the amount of information must be reduced because a large number of features may lead to a sub-optimal performance in the classification stage. The classifier takes the reduced set of features and creates a model that is able recognize the patterns present on the signal with a certain level of accuracy. These patterns are associated with different prosthetic commands, so the control system takes the output of the classifier and execute the appropriate action.

Most of the earlier myoelectric pattern recognition systems designed for multifunction myoelectric prosthesis used information from a single recording site. One of the opening systems was developed in 1975 by Graupe et al. [75]. They examined the EMG signal using autoregressive moving-average (ARMA) models and found the four-order ARMA to be the best approach. Even though the myoelectric signals are non-stationary in nature, they showed that the variation of the ARMA parameters with time was adequately small to allow an accurate discrimination of four upper-limb functions 95% of the time. Later on, they performed online tests of a slightly modified scheme on one above elbow amputee. Five classes of motion, elbow flexion, elbow extension, wrist pronation, wrist supination, and hold, were discriminated with 85% of accuracy [76]. These results were obtained after 12 hours of user training, and performance was significantly decreased with time because the signals generated by the user became modified with time.

An important contribution was made by Hudgins et al. in 1993 [77]. He found deterministic patterns in the onset of several sudden muscle contractions by representing

the EMG signal with four time-domain parameters. He implemented a control strategy that used a Multilayer Perceptron (MLP) Artificial Neural Network (ANN) classifier to discriminate among four classes of limb motion (Figure 13). This new control strategy eliminated the need for extensive user training. An average classification accuracy of 85% was obtained over normally limbed and limb-deficient subjects. A second channel was added in a subsequent study to increase the classifier performance up to 90% accurate [78]. This new multifunction controller was embedded into a hybrid control system for commanding the multiple-axis Southampton-Remedi hand [79]. The users were able select up to four different functions of the prosthesis achieving secure manipulation of objects of various sizes and compliances.

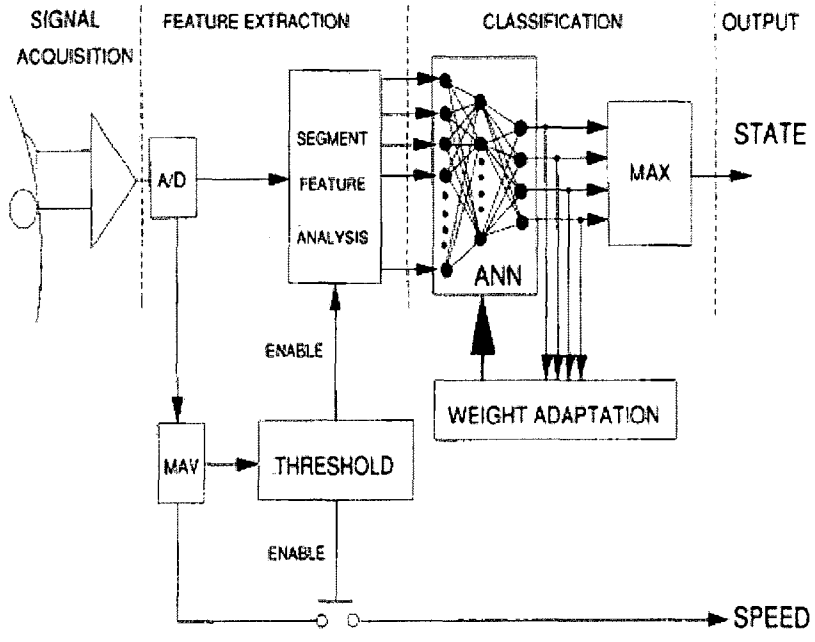

Figure 13. Pattern recognition based control system implemented by Hudgings et al. Transient MES was processed to select the output state (function). A proportional control was also added to control de speed of the function [77].

The introduction of multiple recording channels promised an improvement in the performance of the classifier for discriminating more than three functions. Two channels were used for Al-Assaf et al. to classify four elbow and wrist movements with less that 6% of classification error [80]. Doerschuk et al. recorded signals from four channels and classified four functions with more than 95% accuracy using nearest neighbor classifier trained with four ARMA coefficients per channel [81]. Englehart et al. used the same number of channels and extracted frequency domain features to classify six functions with a maximum accuracy of 98% [82]. Other research groups have implemented four or more recording channels into a multifunction pattern recognition system averaging less that 15% classification error [83-88]. One of the most significant works was developed at the Northwestern University and the Rehabilitation Institute of Chicago by Kuiken et al. They developed a system with 12 bipolar electrodes placed over chest muscles, which were reinnervated by residual arm nerves in a surgical procedure called targeted muscle reinnervation (TMR) (Figure 14). Four time domain features were used to train an ANN classifier that discriminated among 11 motion classes with an average accuracy of 88% (SD, 7%) [89].

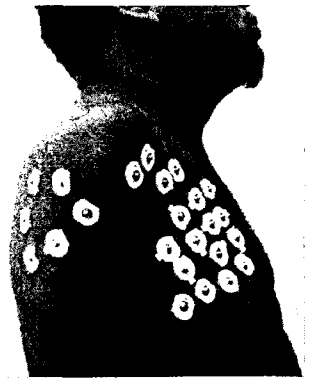

Figure 14. Placement of 12 bipolar electrodes for TMR subjects [89, 90].

Three important aspects determine the performance of the myoelectric control system of a prosthetic device: *the accuracy of movement selection, the intuitiveness of actuating control, and the response time of the system* [21]. Accurate discrimination of the movements produced by the user leads to a more precise control of the prosthesis by the user. Furthermore, more than one function of the device could be controlled using an integrated system.

During the past decades, researchers have addressed different directions in order to achieve effective pattern recognition algorithms that can be translated into real-world prosthetic applications. In the subsequent subsections, the block diagram presented in Figure 12 is used as a reference to present the most common methods followed and the most important conclusion obtained from them.

2.4.1. MES Detection

The main objective of the detection stage is the collection of unique information about different muscle contractions. The number of channels and the locations of the recording sites must be optimized to successfully discriminate among muscle states.

Myoelectric signals from several locations of the body surface can be used to activate upper limb prosthesis. The most appropriate location depends on the amputation level and on the type of application (i.e. arm or hand). Signals from biceps and triceps brachii are typically selected for describing arm movements of above elbow and elbow disarticulation amputees [79, 86, 91, 92], whereas the remaining muscles in the forearm are mainly used as recording sites in below elbow amputees [10, 21, 93-95].

Although the system performed well with one [77, 96-98] and two [78, 99-101] myoelectric channels, additional recording channels (>2) improved the classification

accuracy [82]. The muscle activity recorded from additional channels adds information about the contractions of spatially separated muscle groups. However, the incorporation of more than seven channels in the socket of a real prosthesis can be difficult [102].

2.4.2. Feature Extraction

Whereas each one of the four blocks presented in Figure 12 can be considered as a research gap that could be addressed, the feature extraction block becomes the most important because valuable information present in the raw myoelectric signal must be separated and decoded for successful discrimination of the muscle states by the classifier [8].

A considerable amount of research has been done in this area leading to a wide variety of features for representing the MES for multifunction myoelectric control. They can be grouped in three main categories: *time* domain, *frequency* domain and *time-frequency* (also called time-scale) domain.

Time domain features (TD) are frequently used for myoelectric classification because they are computationally simple [11]. They do not require a previous signal transformation in most cases, and the EMG is considered a zero-mean stochastic signal [63]. Researchers have used combinations of various features to represent the myoelectric activity, including mean absolute value, mean absolute value slope, signal variance, number of zero crossings, waveform length, number of slope sign changes, Willison amplitude, Cepstrum coefficients and AR model coefficients [77, 89, 90, 103-105]. These types of features are significantly affected by disturbances in the MES, such as those introduced by shifts in electrode locations and variations in muscle contraction efforts. The classification accuracy is considerably reduced by these physical and physiological

effects, making time-domain features unstable for their implementation in a pattern recognition system for long term use [20].

Frequency domain features present information about the signal spectrum and are influenced by two factors: the firing rate of the motor units and the morphology of the action potential travelling along the muscle fibers [106]. The power spectral density (PSD) based on the Fourier transform is commonly used to perform a spectral analysis of the myoelectric signal. The mean and median frequency of the PSD can be estimated using either the classic periodogram [107] or parametric methods such as autoregressive (AR) models [108]. Few studies have investigated the use of frequency domain features in pattern recognition schemes [109-111] because the non-stationary nature of the myoelectric signal [23] is not captured by the Fourier transform.

Time-frequency representations (TFR) are special tools used to analyze non-stationary process that capture the time and frequency information present in the observed signal. In real-time signal classification applications, linear TFRs (i.e. the short-time Fourier transform (STFT), the discrete wavelet transform (DWT) and the wavelet packet transform (WPT)) are preferable to quadratic TFRs (continuous wavelet transform (CWT)) because of their computation efficiency [11]. The linear TFRs differ mainly in the partitioning of the time-frequency plane [112] (Figure 15).

The *STFT* [113] maps the myoelectric signal into a two dimensional function of time and frequency depending on an analysis window. The size of this window determines the time frequency resolution; a short window leads to a high time resolution but poor frequency resolution whereas a long window gives low resolution in time but high in frequency. The STFT has a fixed tiling of the time-frequency space, consisting in

an identical aspect ratio for each cells, which on the size of the analysis window (Figure 15a). The *DWT* overcomes the resolution limitations of STFT by using basis functions that have time widths adapted to each frequency band [114]. This adaptation generates a variable time-frequency aspect ratio for the cells yielding a good frequency resolution at low frequencies and a good time resolution at high frequencies (Figure 15b). This tiling of the time-frequency space is appropriate for most physical signals [115]. The *WPT* is a generalization of the wavelet transform and it provides an adaptive tailing of the time-frequency space (Figure 15c). The best tailing is selected among different alternatives using an entropy cost function that minimizes the reconstruction error [116]. Computing the WPT is significantly more expensive than computing the DWT [11].

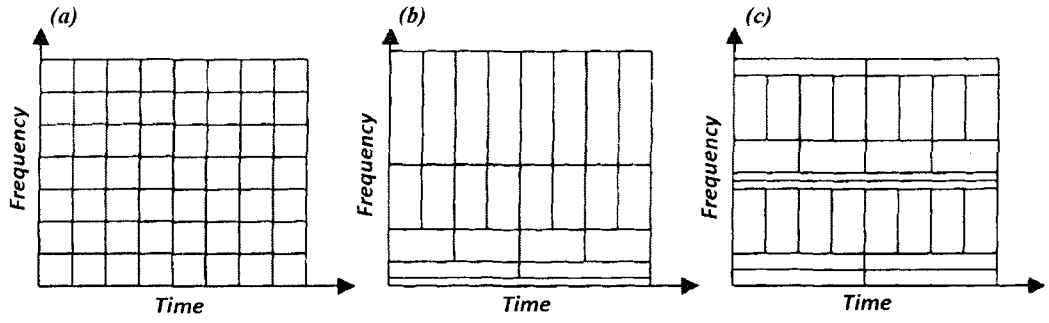

Figure 15. Time-frequency domain partitioning: (a) STFT, (b) WT and (c) WPT [115].

These three TFRs have been implemented as the method to extract relevant EMG signal information for myoelectric pattern recognition based control (STFT [117], DWT [82, 118-120] and WPT [18, 121-123]). Englehart et al. showed that for transient myoelectric signal (observed during the onset of muscle contractions [77]), the features extracted by both DWT and WPT improve the classification performance obtained using STFT features [115]. In the same work, the authors obtained better signal classification

with TFRs than with time domain features, and the wavelet packet transform presented the best overall performance. Similar results were observed by the same research group when analyzing steady-state MES [124].

2.4.3. Dimensionality Reduction

The dimensionality reduction of the feature vector was another important research direction in the myoelectric control. Depending on the technique used to extract the information from the recorded signal, the dimension of the input vector will vary. As the number of dimension increases, machine learning algorithms need more input data to generalize sufficiently well; this requirement is called the *course of dimensionality* [125]. For that reason, the main goal of this process is to obtain a reduced representation of the original feature vector by retaining information that is useful for class discrimination and discarding that which is worthless [126]. When wavelet transform is used to select the time-frequency features [127], the input vector dimension obtained will generally be larger. This dimension will need to be reduced for any practical real-time application. Depending on the objective function used, two strategies can be used to reduce dimensionality: a) *feature selection,* which finds a subset of the original feature set; and b) *feature projection,* which finds the best combination of the original features to create a new feature set [11].

Feature selection [128, 129] is a recurrent process in which the feature subset generated is evaluated and compared with previous subsets according to a certain evaluation criteria. The best subset is chosen each time until a stopping criteria is satisfied. An algorithm combining two different feature selection approaches has been proposed for reducing the dimension of the myoelectric feature vector [130]. Seven limb

motions were correctly classified 93% of the time by introducing the mutual information (MI) approach into the particle swarm optimization (PSO) algorithm.

Among different methods for feature projection, PCA [131] performs a linear projection of the original variables into a new coordinate system that captures the largest amount of variation in data. This *unsupervised* technique has been proposed for reducing the number of frequency [132] and time-frequency [133] myoelectric features presented to the classifier of a pattern recognition system. Linear discriminant analysis (LDA) was another method proposed to linearly project the features for maximizing class separability of the projected features [17]. In some cases, nonlinear projection of the original features [134] may be more appropriate for representing variables. Self-organizing feature maps (SOFM) [135] and kernel PCA (KPCA) [136] can reduce the dimensionality, but their implementation in real-time applications is restricted by the associated computational load. A linear-nonlinear feature projection algorithm composed of PCA and a SOFM had been proposed [137]. The combination PCA-SOFM process was able to achieve 97% accuracy for the classification of nine hand movements. In general, the PCA algorithm is found to be superior dimension reduction technique when it is applied to TFR input feature vectors [115, 123].

2.4.4. Classification

In a pattern-recognition-based multifunction myoelectric control, the prosthesis is actuated by means of the classification of the information received from the reduced feature vector into different classes. Each class determines a particular action of the device, which is then executed by the control system. The classification of data is a two-step process that involves the learning step and the signal classification step [138]. In the

first step, an algorithm is used to build a classifier by learning a decision function (or rules) from a training set that can be used to predict the associated class label of a given data point. In the second state a validation set is used to evaluate the model in terms of classification accuracy (percent of data that was correctly classified). If the results are considered acceptable the classifier is used to classify new data, whose class labels are unknown.

The types of classifiers used for myoelectric control can be divided into two main groups: statistical classifiers (i.e. LDA, Naive Bayes) and machine learning classifiers (i.e. ANN, Fuzzy Logic, K-nearest neighbor (kNN)). The first group was predominantly used in myoelectric control systems before the second group begins to appear. LDA classifiers are usually chosen for myoelectric signal classification because they are well understood and easily implemented. Englehart et al. combined LDA with time domain [21] and time-frequency [82] features to classify several limb motions resulting in less than 10% error rate in both cases. The low computational complexity of statistical classifiers in this category makes them suitable for real-time applications. This simplicity is the primary motivation for their continued use [13, 14, 139, 140]. A mixture of Gaussian models (GMM) [141] as well as hidden Markov models (HMM) [142] have been also proposed to decode limb motions for multifunction myoelectric control. Both methods yielded robust classifiers that could discriminate six limb movements with high classification accuracy (>90%).

A wide variety of the second group of classifiers, also called neural classifiers, has been employed. MLP neural network was presented as the signal classifier in numerous works. Their main advantage is the ability to model (learn) linear and nonlinear

relationships directly from the data and to adapt to real-time implementations [7]. One of the pioneers of the development of real-time multifunction myoelectric control, Englehart et al., implemented a MLP neural network to classify four different limb motions with an average accuracy of around 90% [77]. In their way to develop a new generation of prosthetic arm/hand, a group of researchers from John Hopkins University employed feed-forward MLP to decode movements of the hand [16]. Flexion and extension movements of each finger performed by both transradial amputees and normal-limbed subjects were classified with more than 90% accuracy. Other works utilized ANN of classifiers to identify limb movements produced by the subjects [80, 143-145]. Fuzzy networks are another type of learning classifiers that researchers have used. A fuzzy approach was introduced to classify single-site EMG signals [146]. Its performance was comparable to feed-forward artificial neural network (FFNN), but the fuzzy approach is superior in achieving higher recognition rate, less sensitivity to overtraining and higher reliability.

An ongoing method for classification is SVM [147]. SVM are based on statistical learning theory and can be thought of as a method for constructing a special kind of rule, called a linear classifier, which has the property of high level of classification on unseen data (high generalization) [148]. The use of this type of classifiers in pattern recognition-based control has recently spread. One of the first works that introduced SVM in a myoelectric pattern recognition system was published in 2007 [19]. A recognition rate of 93% was obtained by combining SVM with a generalized discriminant analysis (GDA) algorithm to create a cascaded kernel learning machine classifier for gaining high generalization ability. In another work, a linear SVM was trained to classify time-domain

features from eight classes with 92-98% accuracy [149]. Oskoei et al. proposed a real-time myoelectric control framework using SMV [150]. Its performance was superior to LDA and MLP classifiers in terms of classification accuracy (95% average for classifying 5 limb motions), robustness and computational load.

This good generalization property of SVM is extremely important for the real-time implementation of a multifunction myoelectric control because the classifier has to be able to accommodate to the changes in the user's myoelectric patterns over time [90]. These alterations may be caused by variations of electrode conductivity, spatial displacement of the electrodes from their original location or electrophysiological changes caused by muscle fatigue. SVM meets the real-time constrains, which is an important feature in prosthetic control systems.

CHAPTER 3

MYOELECTRIC SIGNAL DETECTION

The myoelectric pattern recognition-based control system starts with the recording of electromyographic (EMG) signals from a set of muscles specifically chosen. As the proposed control system is applied to actuate a prosthetic hand, it was decided to investigate five different forearm muscles as the potential sources of control. The activation of these muscles is directly associated with four different wrist movements: abduction, adduction, extension and flexion. The resting state was also considered and it is coded as the neutral state of the prosthesis (no action). Seven bipolar channels were placed over the skin's surface and distributed along the selected muscles. Their main purpose was to detect the activity of the underlying muscles when each one of the wrist motions was executed. Before proceeding to the feature extraction stage, the recorded signal must be conditioned so that the muscle contraction pattern can be correctly interpreted.

This chapter explains the recording and conditioning of the EMG signals obtained from seven able-body subjects to create the project database. The first section gives the rationale of the muscle and motion selection. A typical recording session is presented in the second section. In the last three sections of the chapter, the filtering, segmentation and normalization strategies are presented, respectively.

3.1. Movement and Muscle Selection

A pattern recognition scheme designed for multifunction myoelectric control can be implemented for discriminating any set of motions. As a proof of concept, a five-class discrimination problem involving prosthetic hand control was investigated, as below-elbow amputees represent a large proportion of prosthetic users. Four types of wrist motions were selected (Figure 16):

- *Abduction:* the thumb side of the hand is moved toward the lateral aspect (radial side) of the forearm. This movement is also called *radial deviation* of the wrist.
- *Adduction:* the little finger side of the hand is moved toward the medial aspect (ulnar side) of the forearm. This movement is also called *ulnar deviation* of the wrist.
- *Extension*: the back of the hand is moved toward the posterior aspect of the forearm.
- *Flexion*: the palm of the hand is moved to the anterior aspect of the forearm.

These constituted four different myoelectric classes that need to be discriminated by the classification algorithm for selecting a particular action of the prosthetic device. The forearm in a relaxed position was introduced as the fifth class (*Rest*) and was interpreted by the control system as the inactive class.

Figure 16. Four specific wrist motions that represent four of the classes to be discriminated: Abduction, Adduction, Extension and Flexion respectively

Activities corresponding to isometric contractions of five forearm muscles (Figure 17) were analyzed to identify different patterns in the EMG signal that can discriminate among muscle states. The five muscles were selected because they directly contribute to each of the wrist movements studied (Table 1).

Table 1. Muscles selected to record EMG signals

Muscle	**Function**
Anconeus	Assists triceps in extending forearm at elbow; stabilizes elbow joint; abducts ulna during pronation.
Extensor Carpi Ulnaris	Extends and adduct hand at wrist joint.
Extensor Digitorum	Extends hand at wrist joint; extend medial four digits at metacarpophalangeal joints.
Flexor Carpi Radialis	Flexes and abducts hand at wrist joint.
Flexor Carpi Ulnaris	Flexes and abducts hand at wrist joint.

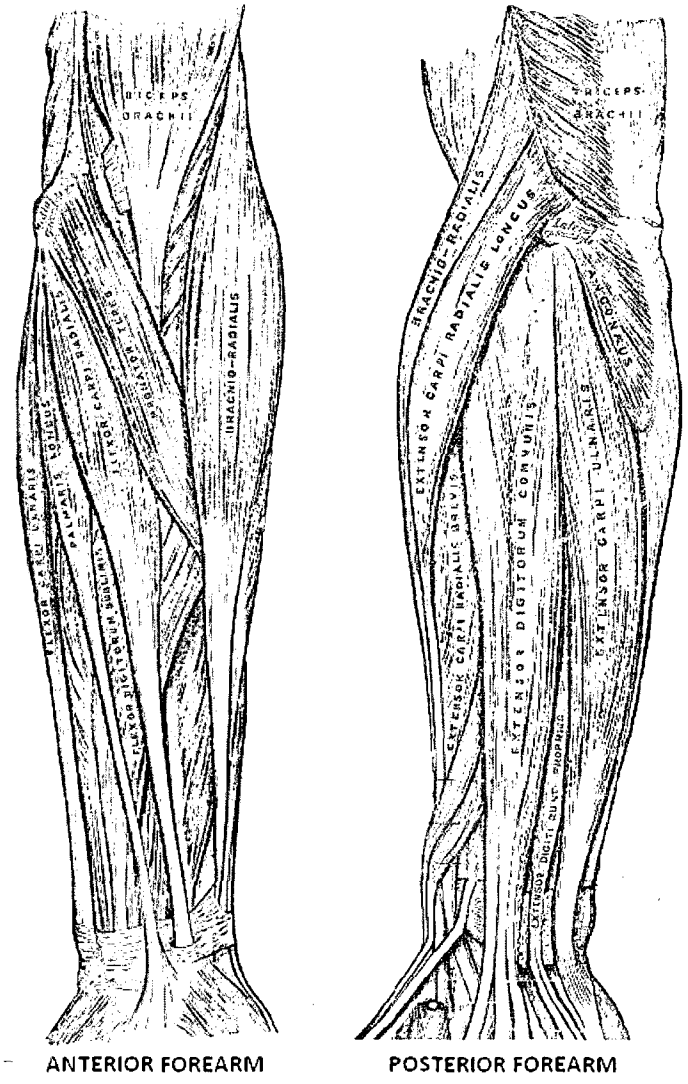

Figure 17. Location of the forearm muscles selected to record the EMG signals

3.2. Recording Sessions

In order to test the feasibility of the pattern recognition scheme proposed in this work, myoelectric signals from seven normally-limbed subjects (four males, three females, age range: 19-28 years) were collected. The data were obtained over six different recording sessions. The number of subjects was determined in order to demonstrate the performance of the system with statistically significant results. The BioRadio 150 wireless data acquisition system (CleveMed, Inc) was used to detect

muscle activity by means of seven bipolar channels distributed along the five forearm muscles introduced above. One pair of Ag/AgCl electrodes (Vermed, Inc) were placed on the Extensor Digitorum, Anconeus, and Flexor Carpi Radialis muscles (Figure 18). Two pairs of electrodes were placed on the Extensor Carpi Ulnaris and the Flexor Carpi Radialis muscles. The reference electrode was placed on the wrist (Appendix A presents a detailed explanation of the protocol).

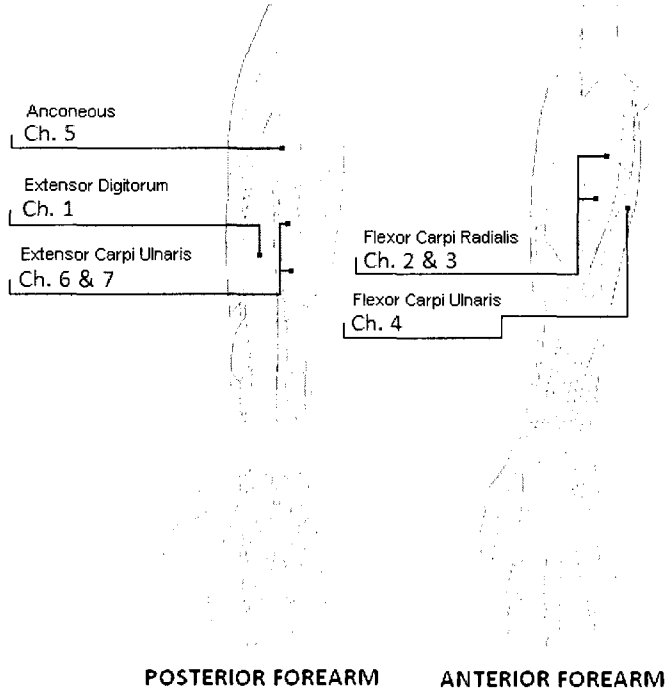

Figure 18. EMG channels location.

On a typical recording session, a subject performed 25 contractions consisting of 5 seconds duration for each of the four classes of motion: abduction, adduction, extension and flexion. The contractions were divided into 5 groups of 5 repetitions of the same contraction each with roughly 3 seconds of resting intervals between repetitions to avoid muscle fatigue. All contractions began with the subject's arm by the side in a comfortable

neutral position. There were not constrains in terms of contraction level; however the subject was asked to be consistent in reproducing the desired motion. Finally, 60 seconds of signals were collected with the forearm upholding and 60 seconds with the forearm resting besides the body. These recordings constituted the Rest class. All the data underwent an analog anti-aliasing low pass filter before being digitized at a sample rate of 960 Hz and quantized with 12-bit resolution. All EMG channels were saved in a single file and exported to Matlab, for each recording trial.

3.3. Signal Conditioning

The raw myoelectric signal acquired is presented in a contaminated form so it needs to be processed for better understanding. The power density spectra of the EMG signal detected at the body surface contains most of its power in the frequency range of 5-500 Hz. However, the frequency components below 10 Hz are unstable and have highly unpredictable fluctuations. In addition, noise associated with motion artifacts and wire sway have low frequencies (<10 Hz). For these reasons, the 7 EMG channels were high-pass filtered with a cutoff frequency of 10 Hz and a notch filter (60 Hz) for suppressing the effect of power line noise. Both filters were designed and implemented under Matlab environment. The high-pass filter was a tenth order Butterworth with less than 3 dB of attenuation in the passband, defined from 10 Hz to the Nyquist frequency (480 Hz), and with at least 60 dB attenuation in the stop-band, defined from 0 to 5 Hz. The notch filter was implemented as a third order band-stop filter with cutoff frequencies selected at 58 Hz and 62 Hz. The motion artifacts, caused mainly by subject's arm movements, are presented in the raw EMG signal as fluctuations of the baseline (Figure 19, top); this effect is removed after signal filtration (Figure 19, bottom).

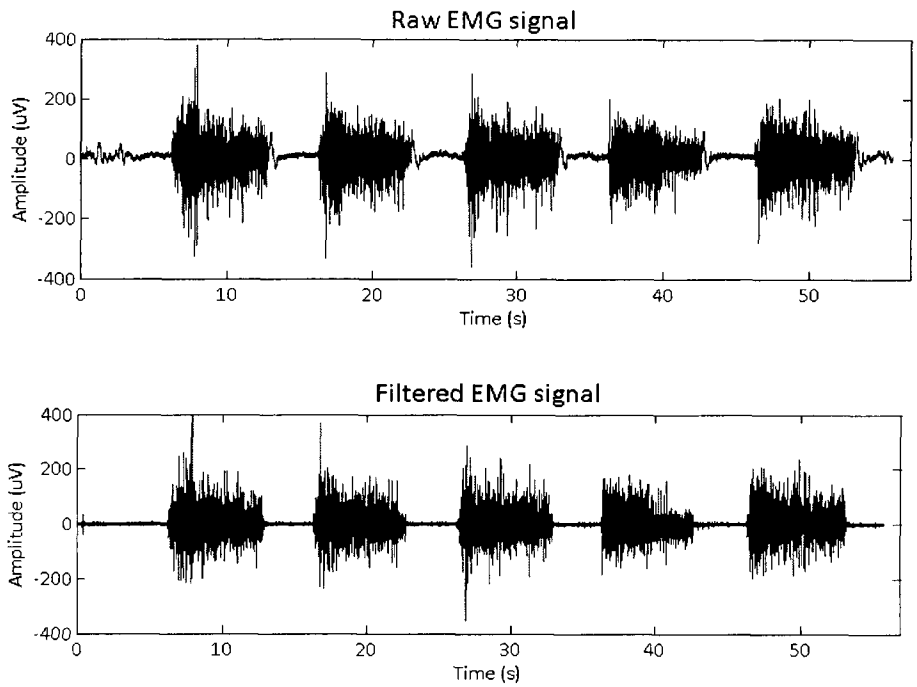

Figure 19. Example of one channel of EMG signal recorded from subject's forearm (top). After both high pass and notch filtering the motion artifacts (low frequency components) are removed (bottom).

3.4. Data Segmentation

As the muscle contractions are separated by rest intervals, it is necessary to isolate them in order to extract a relevant set of features. The protocol of recordings stated that every 5 seconds of contraction must be separated by 3 seconds of rest. However, this timing depended on the delay between the contract/release instruction and the subject's response. Consequently, an algorithm was designed to determine the onset of the muscle contraction. The most representative of the seven channels was selected based on the contraction/rest amplitude ratio. The amplitude of the selected channel was filtered as explained in Section 3.3 (Figure 20, top) and then squared (Figure 20, center). A moving average (MA) filter with a 150 sample window length was used to remove the high frequency components of the resulting signal. A threshold was set and plotted over the

smoothed signal, and an algorithm determined the onset and the end of the muscle contraction (Figure 20, bottom). The threshold value depended on the amplitude of the smoothed signal and was selected to be around 10% of the peak. This procedure was performed on all recorded signals and resulted in five sets of 5 seconds of muscle contraction.

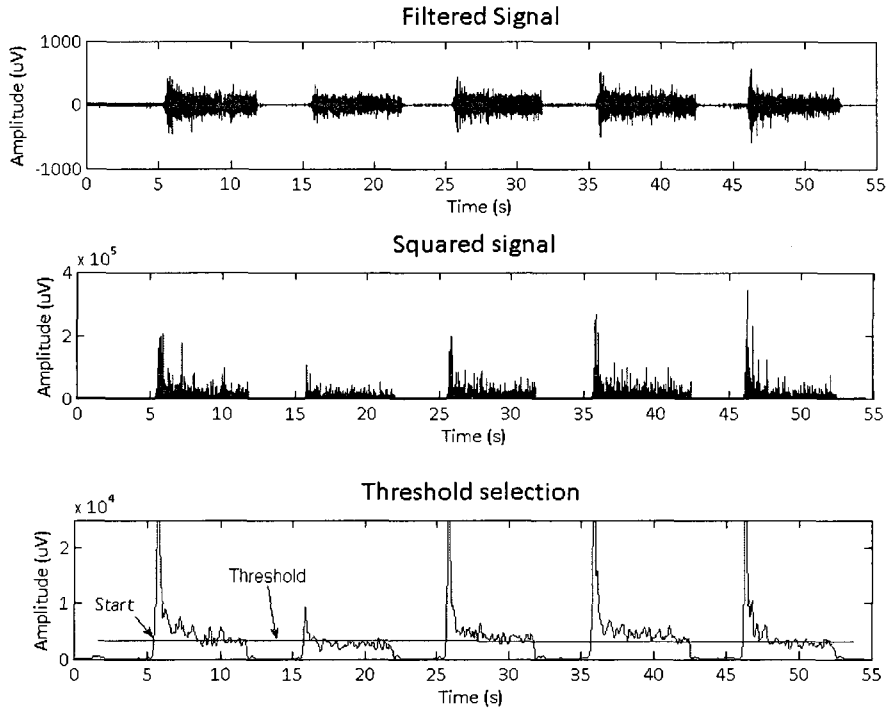

Figure 20. Example of the movement's isolation. The amplitude of the filtered signal (top) is squared to increase the difference between contraction and rest (middle). A threshold is set to determine the approximate location for the muscle contraction onset (bottom).

In order to realize a real-time myoelectric control, the 5-seconds repetitions must be windowed into smaller segments so a fast feature extraction and signal classification can be performed. The width of the analysis window is a critical parameter. The lower limit for the window width is restricted by the low statistical variance of the features

extracted from small windows that yield lower classification accuracy. The upper limit is given by the time required for acquiring and processing the signal in order to obtain the final decision. Englehart *et al.* found that analysis windows of around 128 ms and 256 ms led to acceptable classification accuracy values and allowed the system to be more responsive than shorter window's lengths [21]. In this study, the EMG signals for each wrist motion were partitioned into 256-point segments corresponding to 267 ms of contraction. The number of segments created depended on the number of points of the original signal representing the movement. In most cases, 20 segments were obtained for each 5s interval of muscle contraction. Figure 21 illustrates the segmentation procedure.

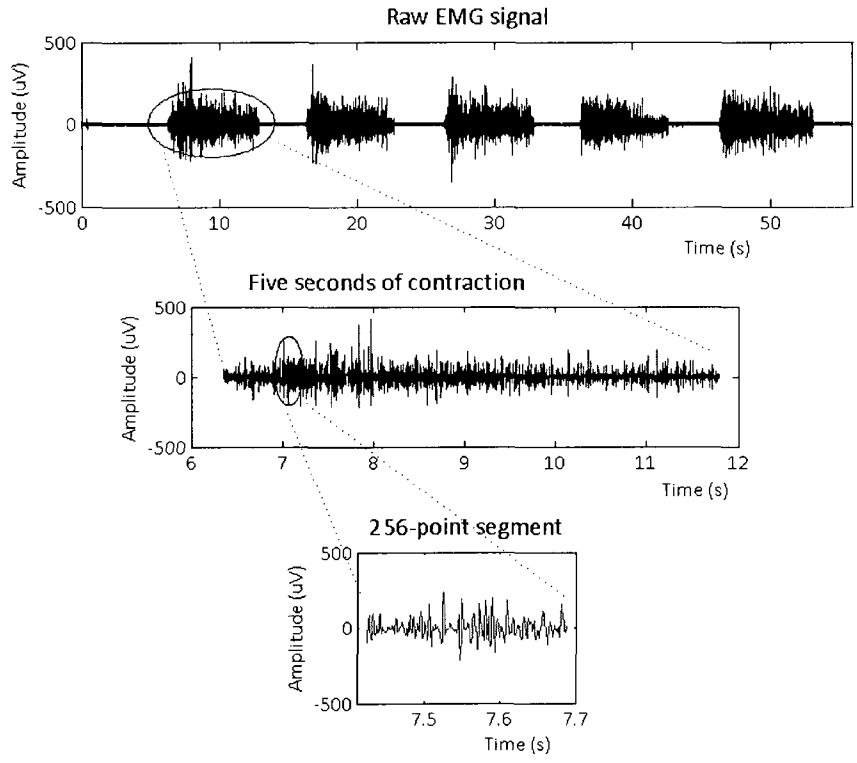

Figure 21. Example of the signal segmentation procedure. Approximately five seconds of muscle contractions are divided into 20 segments of 256 data points. Each segment represents 266 ms of muscle contraction.

3.5. Normalization

During a sustained voluntary contraction, the amplitude of the myoelectric signal decreases progressively [107]. For this reason, the amplitude varied in the EMG segments created from 5 seconds of sustained contraction, as shown in the two windows at the top of Figure 22. The amplitude range of the EMG signal is wider at the beginning of the contraction (left hand side) than near the end of the contraction (right hand side). To overcome this inconsistency, the signal amplitude was normalized within a fixed range of [-1, 1] in all channels. All segment points were scaled with the maximum amplitude value observed. The bottom part of Figure 22 shows the normalized segments for the beginning and the end of a specific wrist motion.

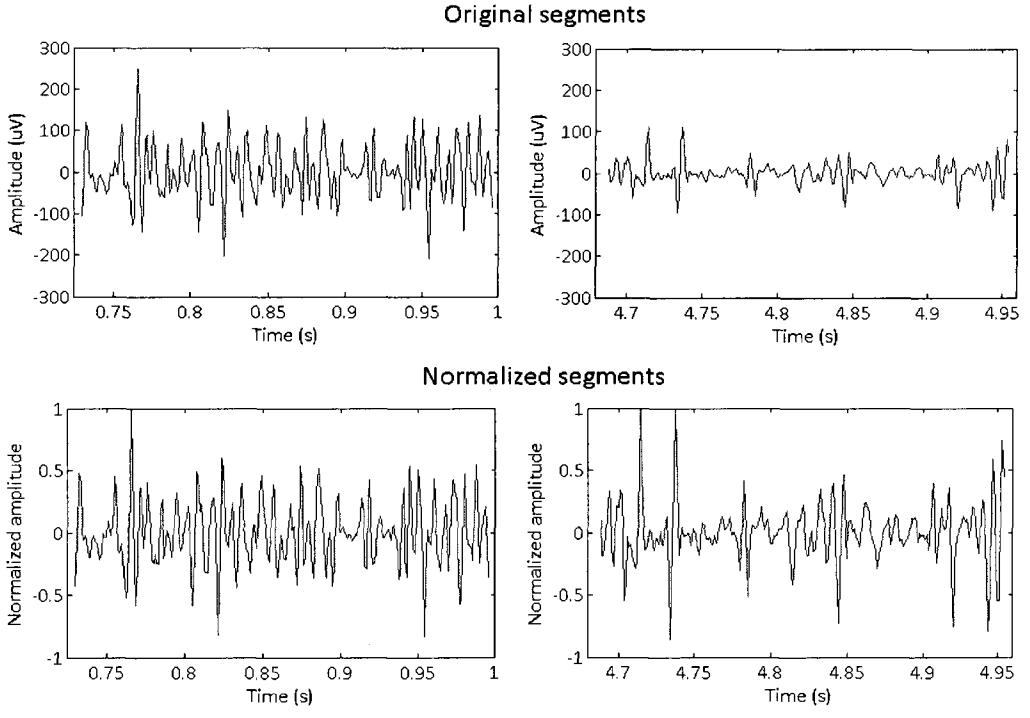

Figure 22. Example of the EMG signal normalization procedure. Each segment's amplitude normalized to fall between the [-1,1] interval.

This amplitude adjustment was the final step of the initial processing for this work. The techniques for feature extraction and signal classification explained in successive chapters were applied over the normalized 256-points windows presented in this chapter.

CHAPTER 4

WAVELET DECOMPOSITION OF EMG SIGNALS

The multichannel EMG signals recorded contain information that can be used for motion classification. A mathematical transformation is needed to extract the relevant information for the discrimination task. This transformation generates a feature space which dimension depends on the nature and the number of the extracted features. The amplitude modulation of a single channel maps the EMG in a one-dimensional feature space but does not yield to an acceptable classification performance. Acceptable performance can be achieved only by extracting more than one feature from the data.

Time-frequency or time-scale features are nonparametric representations of the data that are independent of a possible error in the model choice. The non-stationary nature of the myoelectric signals increases the difficulty of choosing the right model, so the use of time-frequency representations as the nonparametric method for EMG feature extraction represents a good approach.

This chapter presents the rationale for the selection of the discrete wavelet transform (DWT) over traditional Fourier representations. The application of the DWT to extract features from the EMG signal is explained in the last section.

4.1. The Fourier Approach

Most of the mathematical transforms assume that the statistical properties of the signal under analysis do not change in time; they are *stationary*. The Fourier transform (FT) is probably the most popular transformation used for spectral analysis. It is widely known from Fourier theory that any signal can be expressed as a sum of sine and cosine functions. The FT transforms the signal $x(t)$ from its original time domain to a signal in the frequency domain $x(f)$ by calculating the integral:

$$x(f) = \int x(t)e^{-j2\pi ft}dt \qquad \textbf{(1)}$$

This can be considered as a scalar product between $x(t)$ and a family of monochromatic waves of frequency f. The result, $x(f)$, describes which frequency components are present in the original signal. The FT can also be applied to *non-stationary* signals such as biological signals (EMG, EEG, and ECG). However, the interpretation may be imprecise because the FT has only limited ability to localize the spectral components in time. Figure 23.a illustrates a myoelectric signal corresponding to several seconds of wrist flexion. It was sampled at 960 Hz and filtered using both bandpass (20-450 Hz cutoff) and notch (60 Hz) filters. The power spectrum indicates that the major frequency components of the signal are in the range of 50-200 Hz (Figure 23.b). The problem in this case is that they may not be present all the time or that their amplitude may be different at different times.

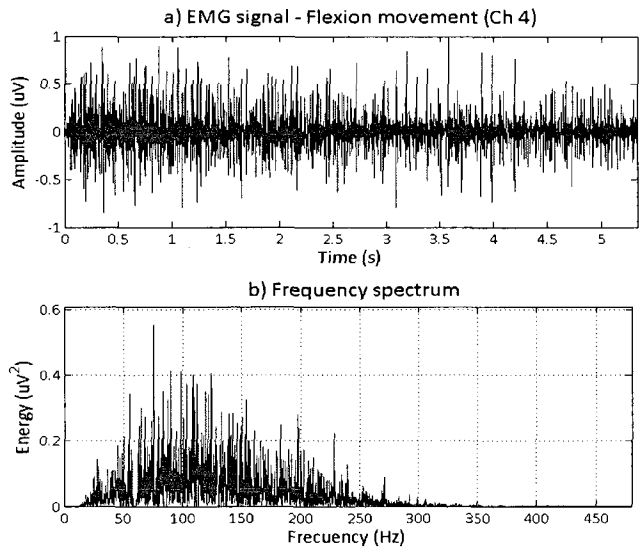

Figure 23. a) Single channel EMG signal during wrist flexion. b) The power spectrum of the MES shows the frequency component present but without time resolution.

Therefore, the main disadvantage of the Fourier expansion is the lack of time resolution, meaning that all the frequency components of the signal are well determined but without indication on when they are present. On the other hand, a time domain analysis describes the signal by its temporal features but without frequency information. To correct this deficiency, Gabor proposed a new method of signal description, intermediate between the two extremes of time analysis and spectral analysis [151]. He adapted the FT to analyze only a small time-interval of the signal at a time, a technique called windowing. The resultant technique maps the signal into a two-dimensional function of time and frequency and is called Short-Time Fourier Transform (STFT).

$$STFT_x(t,f) = \int [x(u)h^*(u-t)]e^{-j2\pi fu}du \qquad \textbf{(2)}$$

Here the signal is assumed to be stationary inside the window $h(t)$ which is centered at the current analysis time t. The FT is the calculated to find the frequency component of the clipped signal. The idea behind these time-frequency joints

representations is to analyze different parts of the signal separately with the aim at giving more information about when and where different frequency components occur. However, the product between the time resolution (Δt) and the frequency resolution (Δf) is limited by a lower bound given by the Heisenberg's uncertainty principle

$$\Delta t * \Delta f \geq 1/4\pi \quad \textbf{(3)}$$

This principle means that the frequency information cannot be determined for a given time instant so they have to be investigated over a time interval defined by the size of the analysis window. Narrow windows give good frequency resolution but poor time resolution. Wider windows give superior time resolution but with reduced frequency resolution and the risk of losing the stationary condition. Although the STFT has many useful properties and can be computed very fast, it is constrained because the size of each cell in the time-frequency plane must be fixed. Figure 24 shows the partition of the time-frequency plane for time, frequency and time-frequency analysis.

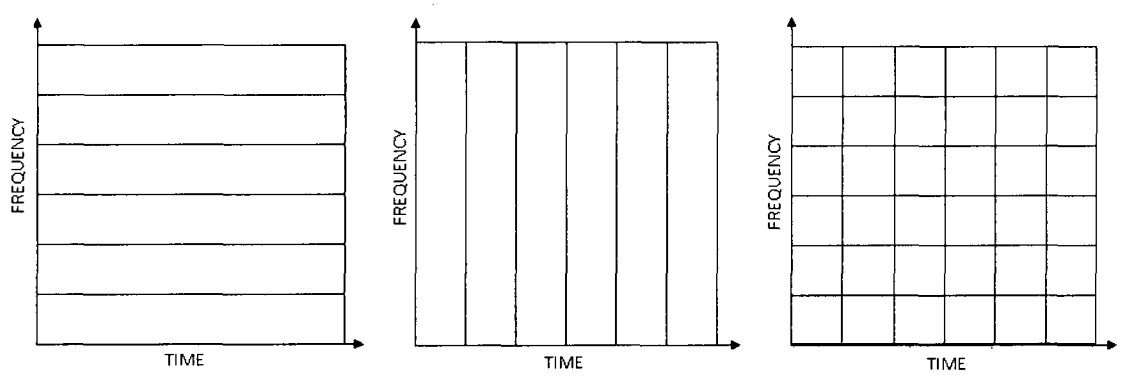

Figure 24. Three different representations of a signal depending on the analysis performed. Spectral analysis gives high frequency resolution but no temporal resolution (left). Temporal analysis gives time but not frequency resolution (center). The STFT solved that problem by partitioning the time-frequency plane into cells that have a fixed time and frequency resolution which depends on the size of the analysis window (right).

The fixed resolution of the STFT can represent a problem when dealing with EMG signals. The usable energy of the surface MES is limited to the 10-500 Hz frequency band, with the dominant energy being in the 50-150 Hz range. In addition, the spectral components are generated at different times and propagate along the muscle fiber. This non-stationary nature of the myoelectric signal indicates that the information is present not only in the frequency domain but also in the time domain. Therefore, a more flexible approach than the STFT is required so the size of the analysis window can be changed to obtain a variable time-frequency resolution.

4.2. The Wavelet Transform

The most significant characteristic of the wavelet transform is that the time resolution and the frequency resolution are not fixed in the time-frequency space. The wavelet transform was introduced as a unifying theory at the beginning of the 1980s by Morlet *et al.*, who used it to evaluate seismic data [152]. Daubechies [153] and Mallat [154] were the first researchers who linked the wavelet theory to the processing of discrete signals. Since then, various types of wavelet transforms have been developed, and many other applications have been found. Wavelet transform has proven to be an efficient method for biological signal compression [155], signal denoising [156] and feature extraction [157, 158].

The continuous wavelet transform (CWT) utilizes basis functions, called wavelets, which have time widths adapted to each frequency band. It is defined as:

$$CWT_x(\tau, s) = \frac{1}{\sqrt{s}} \int_{-\infty}^{\infty} x(t) \psi^* \left(\frac{t - \tau}{s} \right) dt \qquad \textbf{(4)}$$

The CWT correlates the signal $x(t)$ and the translated and scaled versions of a prototype window $\psi(t)$, which is called the *mother wavelet*. The term $1/\sqrt{s}$ is introduced to normalize the energy for all the values of the scale parameter s. The translation term, τ, indicates the location of the window as it is shifted along the signal and the term s is the scale parameter defined as the inverse of the frequency term $(1/f)$. Small values of the scale parameter $(0 < s < 1)$ contract the mother wavelets which highlight the high frequency components of the signal, whereas $s > 1$ expand the basis function and stress the low frequency components. Figure 25 illustrates a simple mother wavelet at different translations and scales. For small scales, poor frequency resolution (Δf) but high time resolution (Δt) is observed; as the scale increases, the wavelet basis is stretched and signal is analyzed with better frequency resolution but poorer time resolution.

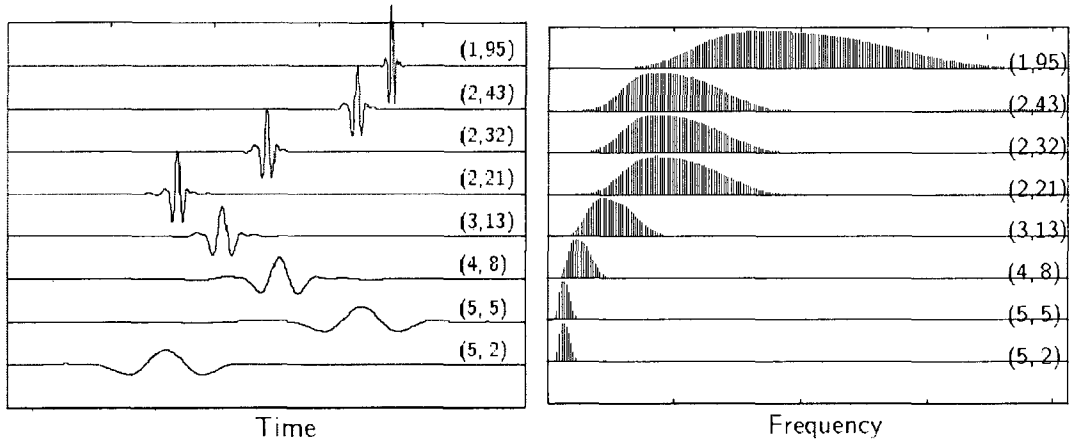

Figure 25. Example of a mother wavelet at different locations and scales in the time domain (left) and in the frequency domain (right). The values in parenthesis (s, τ) indicate the scale and shift values, respectively. [159].

The time and frequency resolution for the STFT generated a regular grid in the time-frequency plane. In the case of wavelet transform, it can be demonstrated that for a

scaled-shifted mother wavelet $\psi_{s,\tau}(t)$, both time and frequency resolutions depends on the scale parameter s as [159]:

$$\Delta f' = \frac{1}{s} \times \Delta f \quad ; \quad \Delta t' = s \times \Delta t \tag{5}$$

This relationship clearly shows that at low scales values (high frequencies), a cell in the time-frequency plane is tall and narrow and for greater scales (low frequencies), the cell is width and short [159] (Figure 26).

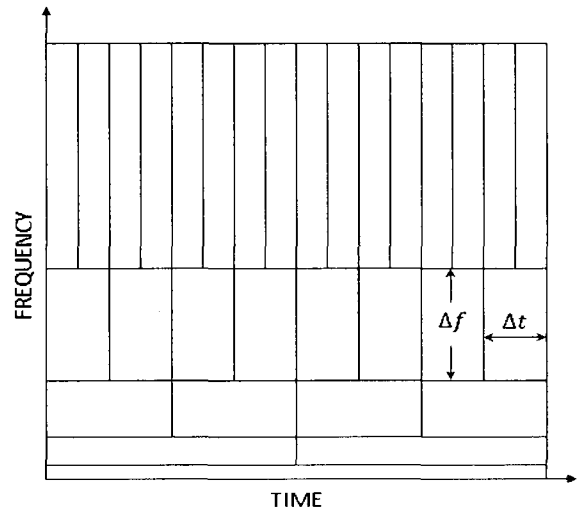

Figure 26. Partitioning of the time-frequency plane when wavelet transform is used to analyze a discrete signal. Good frequency resolution and poor time resolution is observed at low frequencies and poor frequency resolution but good time resolution is obtained at low frequencies.

As in the case of the STFT the time-frequency localization of each wavelet function is subject to the Heisenberg uncertainty principle bound:

$$\Delta f' \times \Delta t' = \Delta f \times \Delta t \geq \frac{1}{4\pi} \tag{6}$$

A family of wavelet functions is obtained by dilatations and translations of the mother wavelet. They constitute a set of orthonormal basis that can generate any function

in the space of square-integrable functions $L^2(\Re)$. In addition, the wavelet $\psi(t)$ is a symmetric function of zero average and a bandpass in nature. A fundamental property indicates a constant relationship between the bandwidth Δf and the center frequency f of the passband as:

$$c = \Delta f / f \tag{7}$$

This relationship has led to a view of wavelet functions as filter banks with a constant relative passband.

The CWT was applied to the EMG signal introduced in Figure 23.a. The absolute value of the wavelet coefficients are plot for the time and scale parameters (Figure 27). The time axis directly indicates the position of the mother wavelet in time, while the scale parameter is inversely related with the normalized frequency. CWT allows the spectral components of the signal to be described at different times. The portion of the graph for the scale range of 4 to 22 (48 to 240 Hz) showed that this components are present during the entire contraction time with different amplitudes. The portion with higher scales ($s > 22$) indicated the presence of frequency components ($f < 48$ Hz) only at the beginning of the contraction.

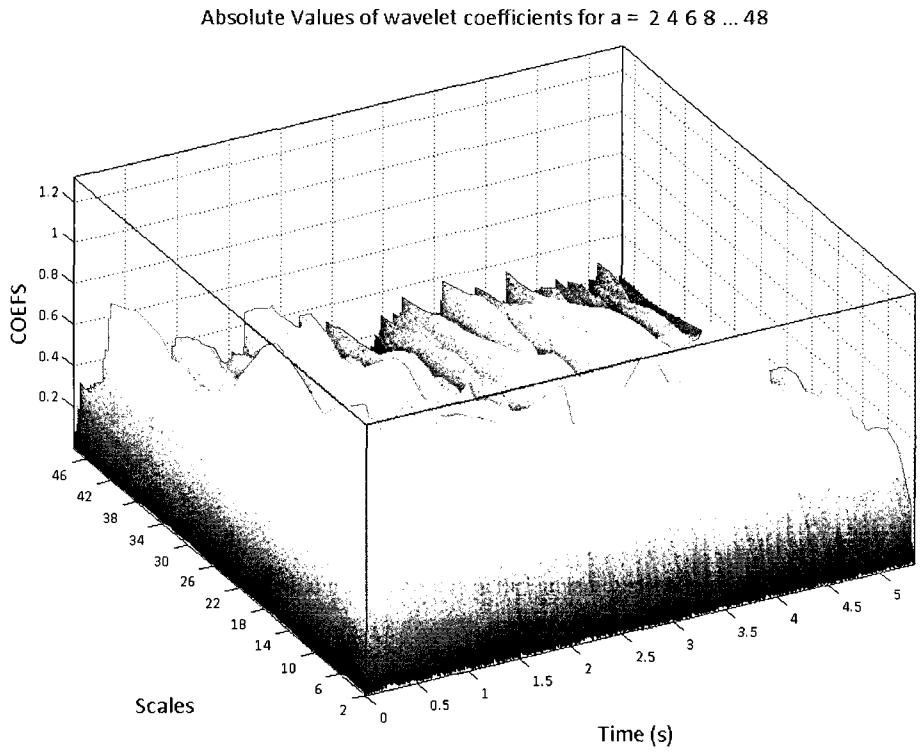

Figure 27. Continuous wavelet transform applied to the signal presented in Figure 23.a. The scale axis corresponds to the 20-480 Hz frequency band. The scale parameter is the inverse of frequency.

The time-frequency resolution approach of the wavelet transform is especially suitable for EMG signals because high frequency components are present during short time periods and low frequency components are observed most of the time [160]. In addition, the mother wavelet functions resemble the motor unit action potentials that represent the gross EMG signal [21]. On the contrary, one of the main drawbacks of the CWT is that the wavelet coefficients obtained after the transformation contain redundant information about the signal, and their calculation requires a significant amount of computation time and resources. To solve that problem and to speed up the computation, filter bank implementations of dyadic wavelets were introduced, as explained in the next section.

4.3. Discrete Wavelet Transform

The wavelet transform of a continuous signal sampled at uniform intervals is computed at discrete scales $s = (s_0)^j$ and translations $\tau = n \cdot (s_0)^{-j}$, where j and n are integers. This sampled version is referred to as the discrete wavelet transform (DWT). The new representation of the mother wavelet $\psi(t)$ is given by Eq. (8).

$$\psi_{n,j}(t) = \frac{1}{\sqrt{s_0^j}} \cdot \psi\left(\frac{t - n \cdot s_0^{-j}}{s_0^j}\right) \tag{8}$$

When analyzing discrete signals, it is usually convenient to choose $s_0 = 2$ so that the sampling of the frequency axis corresponds to a dyadic sampling. The dyadic form of the wavelets is more computationally efficient than the CWT and also the analysis windows achieve the property of mutual orthogonality, which underlies an efficient representation.

A wavelet function is always associated with a partner referred to as the scaling function $\varphi(t)$, which forms a sparse orthonormal basis of $L^2(\Re)$ as wavelet functions do. The set of stretched and translated version of this function,

$$\varphi_{n,j}(t) = \frac{1}{\sqrt{2^j}} \cdot \varphi\left(\frac{t - n \cdot 2^j}{2^j}\right) \tag{9}$$

generates a chain of nested orthogonal subspaces $V_J \subset V_{J-1} \subset \cdots \subset V_1 \subset V_0$, where V_0 is the space of the original signal $x(t)$ and $j = 0,1, \ldots, J$ constitute a set of resolution levels. The scaling function projects $x(t)$ onto the subspaces V_j giving a sequence of successively coarser approximations of $x(t)$ as the resolution levels j go from 0 to J.

In the same way, wavelet basis allows an orthogonal decomposition of any function in $L^2(\Re)$ meaning that a complete description of the signal $x(t)$ can be obtained

from a direct sum of orthogonal subspaces W_j. These new subspaces are defined by the wavelet functions $\{\psi_{n,j}(t)\}$ and they are the complement subspaces of V_j.

The subspaces described by both the wavelet and the scaling functions are related such that:

$$V_{j,0} = V_{j-1} \oplus W_{j-1} \quad \text{for} \quad j = 0,1,\ldots,J \tag{10}$$

The subspace W_{j-1} contains the information needed to go from the approximation level V_{j-1} to a finer level V_j. This information is called a detail and is obtained by the projection of $x(t)$ onto W_{j-1}.

The approximation and detail components of the original signal $x(t)$ at a specific scale $s = 2^j$ are represented by coefficients computed as:

$$A[n] = \langle x(t), \varphi_{n,j}(t) \rangle \quad ; \quad D[n] = \langle x(t), \psi_{n,j}(t) \rangle \tag{11}$$

The projection of $x(t)$ giving the approximation coefficients is a *lowpass* operation in nature, whereas the projection giving the detail coefficients is a *bandpass* operation. Therefore, the low frequency components of $x(t)$ are defined by the scaling function $\varphi(t)$ and the complementary high frequency band is obtained by the wavelet functions $\psi_{n,j}(t)$.

The wavelet transform decomposes the original discrete signal into successive approximation $A[n] \in V_j$ and detail $D[n] \in W_j$ signals (Figure 28). After the first level of decomposition ($j = 1$), the detail coefficients are kept and the approximation signal is subject to a new decomposition ($j = 2$). This procedure continues until the final level J is reached. The result of the DWT is a set of wavelet coefficients corresponding to J levels of detail coefficients and the approximation signal at the lowest level J:

$$\{D_1[n], D_2[n], \ldots, D_J[n], A_J[n]\} \tag{12}$$

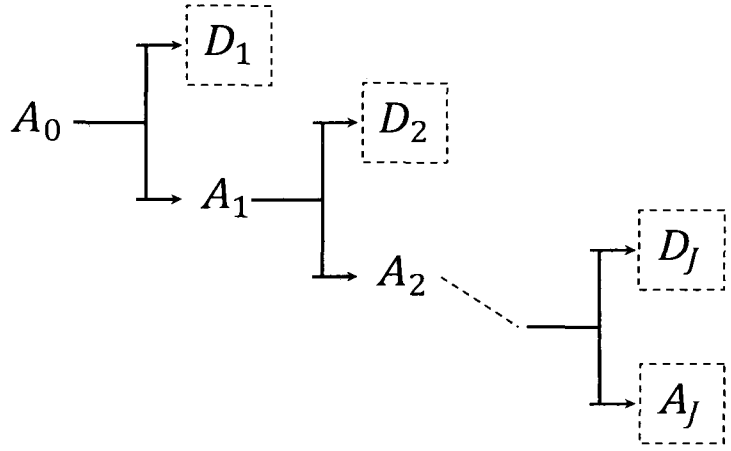

Figure 28. Wavelet decomposition of the original signal A_0 into sub-bands represented by approximation (A_j) and detail (D_j) coefficients.

To avoid the discretization of the wavelet and scaling functions, the DWT is approximated by *digital filter banks* (Figure 29). The *N*-sample original signal $x[n]$ is passed through two complementary filters g and h, where $g(k)$ is the highpass filter and $h(k)$ is the low pass filter. The output of $h(k)$ is a smoothed version of the original signal and therefore it is the approximation signal, whereas the output of $g(k)$ contain the details of the input signal. These two signals have the same number of samples than $x[n]$ meaning that the information is doubled. The filtered sequences are then sub-sampled by a factor of 2 to solve that problem. Next, the vector of the lower frequency band is filtered in the same way to obtain a new approximation signal and a second level of detail coefficients. This process can be repeated $J = \log_2 N$ times in order to obtain a full wavelet decomposition of the input signal $x[n]$. Such analysis in which the signal is divided into a set of frequency bands was developed by Mallat et al. and is called *multiresolution analysis* (MRA) [161].

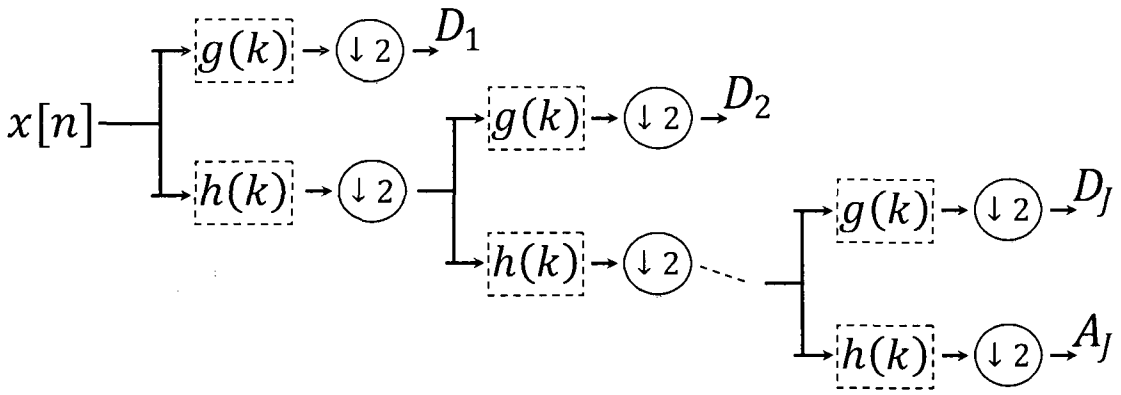

Figure 29. Illustration of the multiresolution analysis performed as successive lowpass and highpass filtering of the approximation signals.

In order to illustrate the procedure, multiresolution analysis was performed on the signal presented in Figure 23.a. ($N = 5120$). The original MES was decomposed into its detail and approximation signals using Daubechies-1 mother wavelet (Figure 30). The decomposition was stopped at the seventh level ($J = 7$) to facilitate the representation. The detail coefficients of the higher level (D1) capture the high frequency components of the original signal. Progressively lower components are caught by coefficients in the lower levels. The approximation signal (A7) is caused by the lowpass filtering of the signal at level $J = 7$. The use of dyadic wavelets reduces length of each successive detail level by a factor of 2.

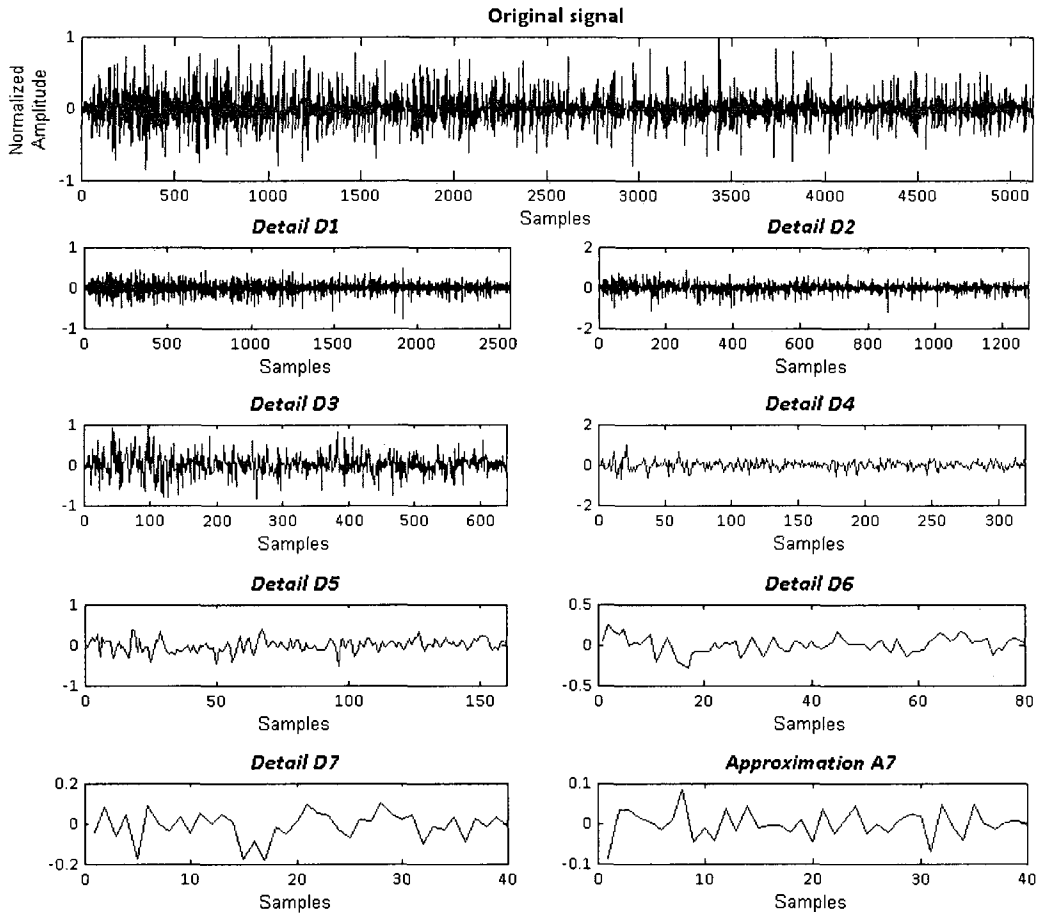

Figure 30. Wavelet decomposition applied to the signal introduced in Figure 23.a. using 'db1.' Seven levels of detail coefficients illustrate the frequency components of the signal. The lower levels catch the high frequency component of the original signal whereas the higher levels the low frequency components.

4.4. Wavelet-Based Feature Extraction From EMG Signals

To extract valuable information contained in the signal, a multiresolution analysis was performed on each 256-samples moving time window segment of muscle contraction after the pre-processing stage (Sections 3.3 to 3.5).

4.4.1. Selection of Wavelet Parameters

Two parameters must be specified when using the WT a) the mother wavelet and b) the depth of decomposition. Coiflet is a family of wavelets created by Daubechies

[162]. They are commonly used to decompose myoelectric signals because it has yielded higher accuracy in signal classification than several other families of different orders. Their ability to resemble the motor unit action potentials, which are the elemental components of the MES, increases their ability to localize the signal energy and to discriminate signals in different classes [82, 100]. For this study in particular, a second order Coiflet was selected as the basis functions to perform a MRA on the EMG dataset (Figure 31).

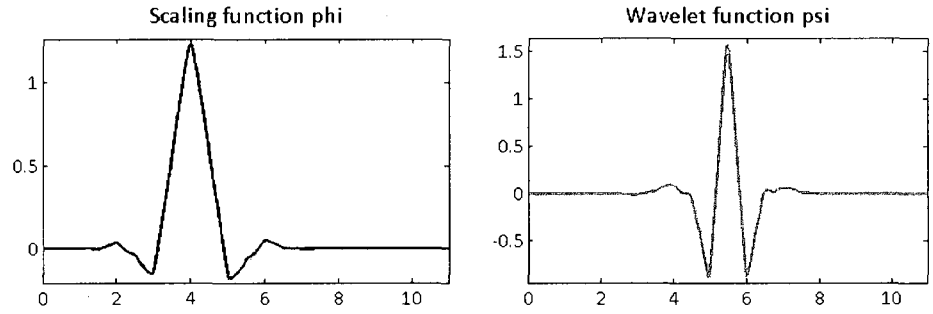

Figure 31. Second order Coiflet scaling and wavelet functions.

The second parameter selected was the depth of the wavelet decomposition. The maximum depth for a signal of length L is given by:

$$J = \log_2 L \tag{13}$$

The full decomposition divides the frequency axis towards zero until no more subdivision can be performed. If decomposition is terminated before the last level, the approximation signal occupies the portion the portion of the frequency axis that was not partitioned. The effect of the depth of decomposition on the performance of the signal classification was studied for myoelectric signals, and it was concluded that full wavelet decomposition yielded the lowest classification error [82, 159].

4.4.2. Feature Extraction

In the data set created for this study, the length of the each MES segment analyzed was $L = 256$, giving a total of 8 levels for a full decomposition. This segmentation provided information from 9 frequency sub-bands: eight details and one approximation. Table 2 presents the frequency components covered by the sub-bands at each resolution level; the deeper the level, the smaller the frequency range. Recalling that the sample frequency of the recorded MES was 960 Hz, the anti-aliasing filter built in the data acquisition system limited the bandwidth of the collected signal to 0 – 480 Hz.

Table 2. Partition of the frequency axis when full wavelet decomposition was performed and the number of wavelet coefficients obtained at each level.

Decomposition level	***Frequency range (Hz)***	***# of coefficients obtained***
$\mathbf{d_1}$	240 – 480	133
$\mathbf{d_2}$	120 – 240	72
$\mathbf{d_3}$	60 – 120	41
$\mathbf{d_4}$	30 – 60	26
$\mathbf{d_5}$	15 – 30	18
$\mathbf{d_6}$	7.5 – 15	14
$\mathbf{d_7}$	3.75 – 7.5	12
$\mathbf{d_8}$	1.875 – 3.75	11
$\mathbf{a_8}$	0 – 1.875	11

The wavelet coefficients corresponding to the first decomposition level ($\mathbf{d_1}$) contains information about the highest frequency components of the signal with poor resolution but good time resolution. As the depth increases the coefficients represent the

signal information about lower frequencies components with higher resolution but loosing time resolution. Figure 32 shows the absolute values of the detail coefficients distributed on the time-frequency plane as a result of full wavelet decomposition applied to a 256-sample segment of EMG signal. The vertical axis indicates the depth of the decomposition, which increases from bottom to top. The horizontal axis is directly related with time ($sample/960 = time(s)$), and it is clear how its resolution is reduced by a factor of 2 as the depth level increases (recall dyadic sampling). On the other hand, the frequency resolution increases by a factor of 2, but it is not represented in the figure for clarity reasons. The top graph shows that the levels 2 to 5 (30 – 240 Hz frequency range) grouped most of the wavelet coefficients with higher amplitude, which suggests that most of the signal information is clustered in that frequency range.

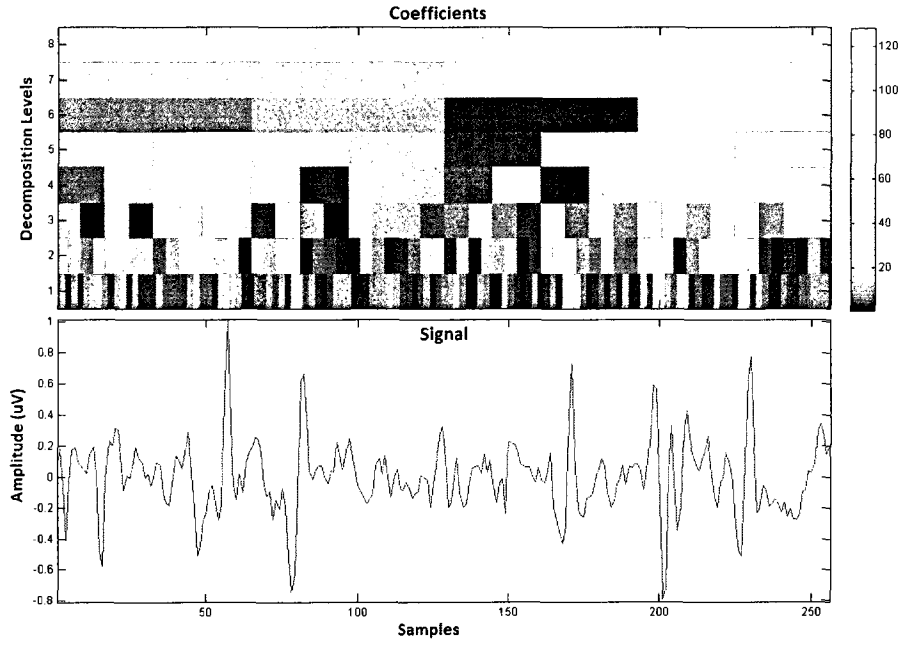

Figure 32. Distribution of the absolute values of the wavelet coefficients on the time-frequency plane obtained after full wavelet decomposition of the 256-sample EMG signal. The highest values are grouped at levels 2 to 5 (30 – 240 Hz frequency range).

Another way to represent the decomposition is by looking at the signals obtained at each level (Figure 33). Recalling that the MRA is performed by successive application of complementary filters to the approximation signals, the detail signals illustrated correspond to the output of the highpass filters whereas the approximation signal represent lowpass output at the deepest level. The signal at detail level 1 ($\mathbf{d_1}$) captures the highest frequency components present in the original EMG segment (240 – 480 Hz frequency range). Lower spectral components are gradually captured at deeper levels as presented in Table 2. The approximation signal ($\mathbf{a_8}$) contains the lowest frequency components (0 – 1.875 Hz).

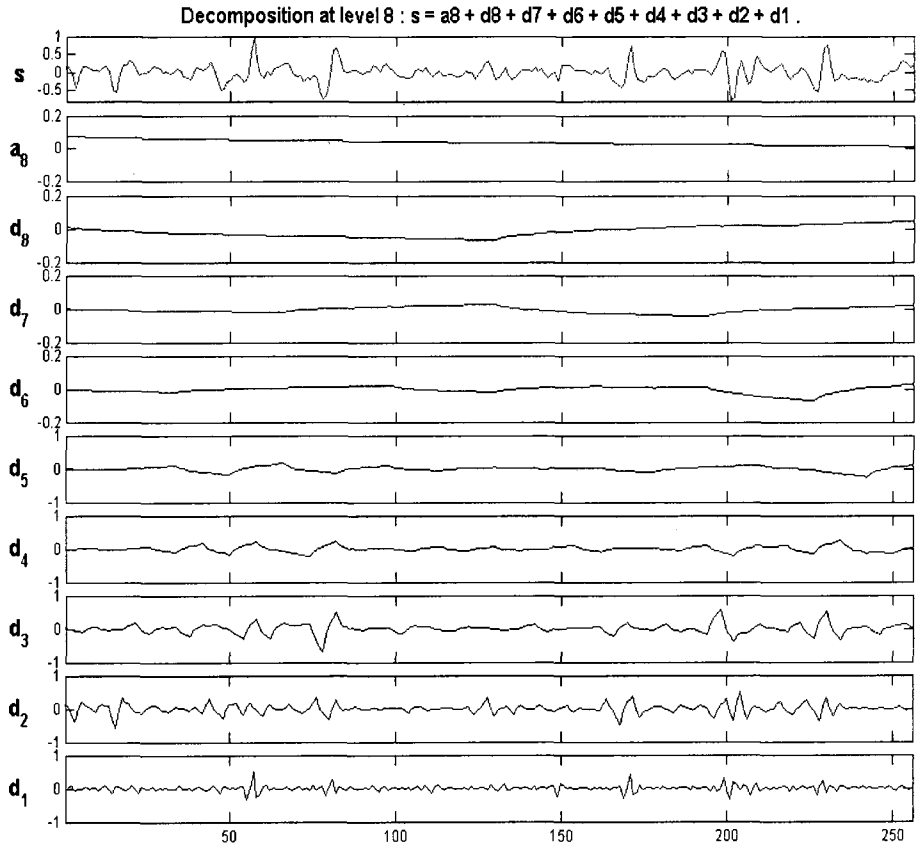

Figure 33. Details signals at each resolution level. They represent the output of the high-pass filters in a multiresolution analysis. The last approximation and the original signals are illustrated at the top. Lower frequencies are captured at deeper resolution levels.

A total of 338 wavelet coefficients were obtained after applying the WT to a single channel of EMG. This number rose up to 2366 after considering all seven channels. If all these coefficients are combined to form a feature vector, the performance of the signal classifier may be affected in terms of accuracy and training and testing times. As the dimensionality (number of features) increases, the data become increasingly sparse and the possible combination of subspaces grows exponentially. This relationship is known as the curse of dimensionality. The result is that an extremely large number of training points are needed to create the model that can lead to a good generalization.

The square of each wavelet coefficient was used instead of the original signed values because the latter are highly irregular and may lead to a poor classifier generalization. The squared values give an indication of the energy contained in the detail and the approximation frequency bands.

In order to reduce the number of features obtained after MRA, the average energy of the wavelet coefficients was calculated at each resolution level:

$$\overline{WT_x} = \begin{cases} \sum_{k=1}^{N_j} \left|d_j(k)\right|^2 & j = 1,2,\dots,J \\ \sum_{k=1}^{N_J} \left|a_J(k)\right|^2 & \end{cases} \tag{14}$$

where d_j and a_J are the detail and approximation coefficients respectively, J is the depth of the decomposition and N_j is the number of coefficients obtained at the jth level. This resulted in a vector containing 9 feature values. As EMG signals were acquired from seven different channels, the final feature vector contained 63 wavelet-based features. It is important to highlight that the time information at each resolution was lost when performing the energy averaging. However, steady-state EMG signals do not have

significant temporal structure and it can be considered as stationary when they are analyzed in time intervals of around 250 ms [82]. It still remains true that the wavelet transformation is the best feature extraction method for this type of signals [82].

Figure 34 illustrates a summary of the feature extraction procedure. The wavelet coefficients obtained after full wavelet decomposition are averaged in order to reduce the number of features per channel. The average energies of nine frequency sub-bands are used as the features of one EMG channel. The features form all seven channels are then combined into a single 63-dimensional feature vector, which represent the EMG signal recorded during 267 ms.

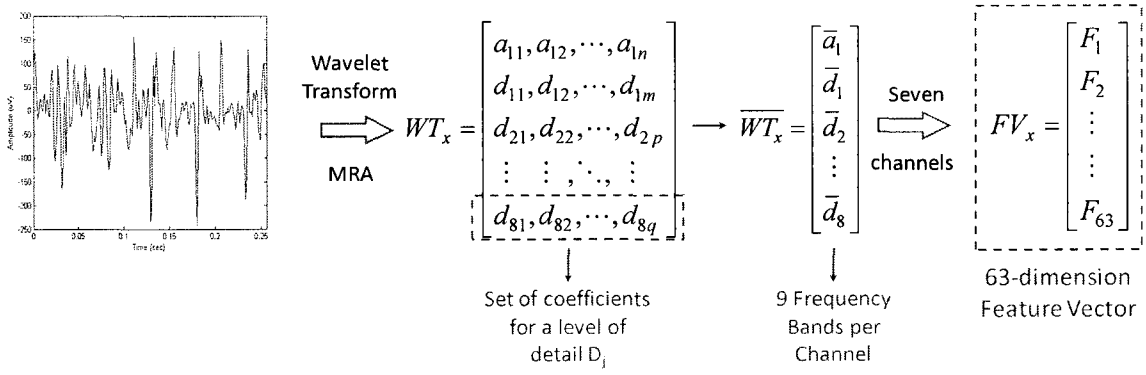

Figure 34. Summary of the feature extraction procedure. MRA was performed on seven channels of EMG signals. The final feature vector represents 267 ms of myoelectric signals.

CHAPTER 5

SUPPORT VECTOR MACHINES SIGNAL CLASSIFICATION

Classification is one of the most important stages affecting the final performance of the myoelectric pattern recognition system. In this stage, the classifier should be able to learn the different muscle contraction patterns selected to actuate the prosthetic device. SVM was chosen as the signal classifier over other techniques because it can generalize complex data. The final model must also be simple enough to meet the real-time constraints. To test the feasibility of the SVM, the classification accuracy on the test set was first computed for the classifiers trained with the data form one recording session. To test the hypothesis that the SVM classifier is able to compensate for variations in the user's myoelectric patterns, displacements of the electrodes from their original location were introduced in the recordings. The patterns obtained in multiple recording sessions were introduced to the training data.

A detailed explanation of the SVM fundamentals is presented at the beginning of this chapter followed by a summary of the most common multiclass classification methods. The methodology section is presented afterwards. The results for the single-session and multi-session classifiers are then outlined. An explanation of the real-time implementation of the myoelectric system is presented before the final discussion section.

5.1. Binary Classification

SVM is a machine learning algorithm that maps the input data into a high dimension feature space, in which the different dynamics are linearly separable by an hyperplane that constitute the decision surface [147] (Figure 35). This new model is represented by the following equation:

$$y(\boldsymbol{x}) = \boldsymbol{w}^T \phi(\boldsymbol{x}) + b \tag{15}$$

where $\boldsymbol{w}$ and b are the parameters of the hyperplane and $\phi(\boldsymbol{x})$ represents the feature space transformation.

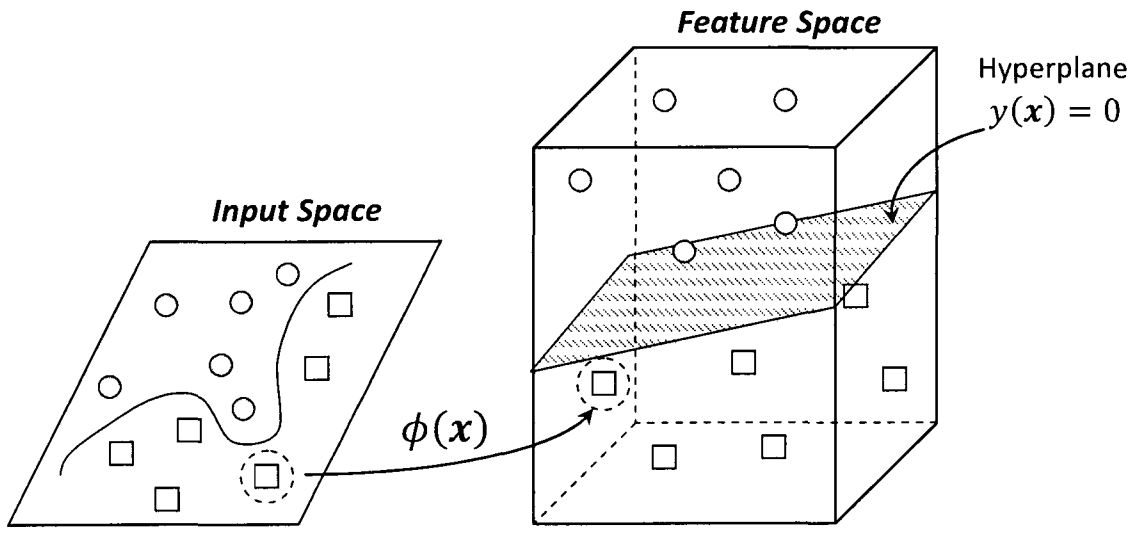

Figure 35. After transforming data to a new feature space, SVM finds a linear decision surface that separates the input data.

5.1.1. Linearly Separable Classes

Considering a two-class classification problem, a data point $\boldsymbol{x}_n$ may have two possible targets ($t_n = \pm 1$). Assuming that the training data is linearly separable in the feature space, the hyperplane created will exactly separate them. Therefore, Equation (15)

will satisfy $y(\boldsymbol{x}_n) > 0$ for points with $t_n = +1$ and $y(\boldsymbol{x}_n) < 0$ for points with $t_n = -1$. Moreover, all points will satisfy the condition:

$$t_n \cdot y(\boldsymbol{x}_n) > 0 \tag{16}$$

Several solutions may be found to separate the classes exactly. The SVM theory attempts to find the solution that gives the smallest generalization error, which means that the model created will correctly categorize a wide variety of new input data [163].

The operation of the SVM is based on the concept of margin. It is defined as the smallest distance between the separating hyperplane (decision boundary) and any of the points (Figure 36). This distance is given by:

$$\frac{t_n \cdot y(\boldsymbol{x}_n)}{\|w\|} = \frac{t_n \cdot (\boldsymbol{w}^T \phi(\boldsymbol{x}_n) + b)}{\|\boldsymbol{w}\|} \tag{17}$$

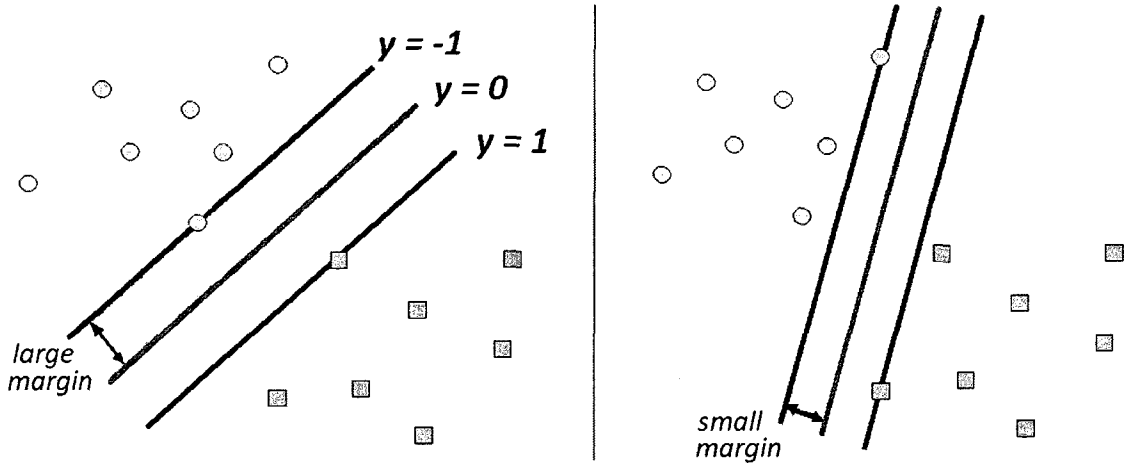

Figure 36. The perpendicular distance between the closest data point and the decision boundary (y=0) is referred to as the margin. SVM finds the maximum margin between classes.

The objective of this approach is to find the optimal parameters $\boldsymbol{w}$ and b that maximize the margin. This is mathematically represented as:

$$\arg\max_{\mathrm{w,b}}\left\{\frac{1}{\|\boldsymbol{w}\|}\min_{n}\left(t_n(\boldsymbol{w}^T\phi(\boldsymbol{x}_n)+b)\right)\right\} \tag{18}$$

To reduce the complexity of this optimization problem, the closest distance of a point to the decision surface is set to 1:

$$t_n\cdot(\boldsymbol{w}^T\phi(\boldsymbol{x}_n)+b)=1 \tag{19}$$

This is based on that the parameters $\boldsymbol{w}$ and b can be scaled by a factor k without changing the distances. Thus, the original problem was converted in an equivalent one that is easier to solve. It requires the maximization of $\|\boldsymbol{w}\|^{-1}$ which is equal to solve the following quadratic optimization problem:

$$\min_{\mathrm{w,b}}\left\{\frac{1}{2}\|\boldsymbol{w}\|^2\right\} \tag{20}$$

subject to the following constrains satisfied for all the N training points:

$$t_n\cdot(\boldsymbol{w}_T\phi(\boldsymbol{x}_n)+b)\geq 1 \qquad n=1,\dots,N \tag{21}$$

The solution is obtained by calculating the Lagrange multipliers $a_n\geq 0$, with one multiplier for each constraint in (21). Thus, each data point is associated with a multiplier. The Lagrangian function is written as:

$$L(\boldsymbol{w},b,\boldsymbol{a})=\frac{1}{2}\|\boldsymbol{w}\|^2-\sum_{n=1}^{N}a_n\{t_n\cdot(\boldsymbol{w}^T\phi(\boldsymbol{x}_n)+b)-1\} \tag{22}$$

where $\boldsymbol{a}=[a_1,a_2,\dots,a_N]^T$. Setting to zero the derivatives of $L(\boldsymbol{w},b,\boldsymbol{a})$ with respect to $\boldsymbol{w}$ and b gives the following new conditions:

$$\frac{\partial L(\boldsymbol{w},b,\boldsymbol{a})}{\partial \boldsymbol{w}}=0 \;\Rightarrow\; \boldsymbol{w}=\sum_{n=1}^{N}a_n t_n\phi(\boldsymbol{x}_n) \tag{23}$$

$$\frac{\partial L(\boldsymbol{w}, b, \boldsymbol{a})}{\partial b} = 0 \;\Rightarrow\; 0 = \sum_{n=1}^{N} a_n t_n \tag{24}$$

A new quadratic optimization problem is obtained when the terms $\boldsymbol{w}$ and b are eliminated from (22) using the conditions (23) and (24). It is a dual representation of the maximum margin problem and it can be written as the maximization of:

$$\tilde{L}(\boldsymbol{a}) = \sum_{n=1}^{N} a_n + \sum_{n=1}^{N} \sum_{m=1}^{M} a_n a_m t_n t_m k(\boldsymbol{x}_n, \boldsymbol{x}_m) \tag{25}$$

subject to the constraints:

$$a_n \geq 0 \quad n = 1,2, \dots, N \tag{26}$$

$$\sum_{n=1}^{N} a_n t_n = 0 \tag{27}$$

The function $k(\boldsymbol{x}_n, \boldsymbol{x}_m)$ is referred to as the kernel function, and it allows the computation of the dot product between the transformed data points without specifying the feature transformation:

$$k(\boldsymbol{x}_n, \boldsymbol{x}_m) = \phi^T(\boldsymbol{x}_n) \cdot \phi(\boldsymbol{x}_m) \tag{28}$$

This type of constrained optimization problem satisfies the Karush-Kuhn-Tucker (KKT) conditions, which imply that every data point in the training set satisfies either $a_n = 0$ or $t_n y(\boldsymbol{x}_n) = 1$. Training points for which $a_n = 0$ are not taken into account for the final model and do not contribute in the classification of new data points. The remaining points satisfy $t_n y(\boldsymbol{x}_n) = 1$ and are used for predicting outputs for new input data. These points define the decision boundary and are called *support vectors*. They are located on the maximum margin hyperplane in feature space (Figure 37).

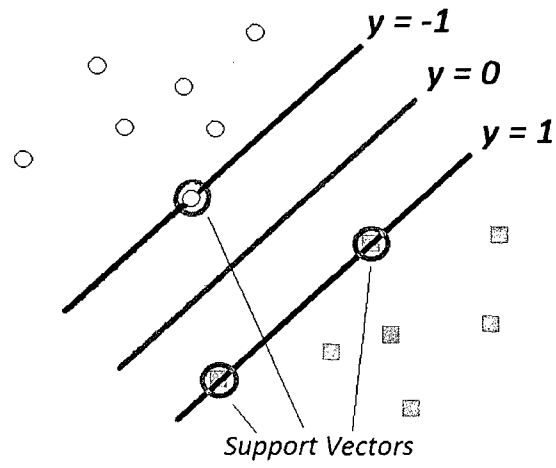

Figure 37. A subset of data points determines the location of the boundary. They are called support vectors.

Once the model is trained, a new data point can be classified by evaluating the sign of $y(\boldsymbol{x})$ in Equation (15). This equation can be rewritten in terms of the Lagrange multipliers obtained (a_n) and the kernel function as:

$$y(\boldsymbol{x}) = \sum_{n=1}^{N} a_n t_n k(\boldsymbol{x}_n, \boldsymbol{x}) + b \tag{29}$$

5.1.2. Overlapping Classes

The training data can be contaminated with a high noise level that causes a large overlap of the classes. In this and other cases of overlapping classes, the solution to the optimization problem may not be reached (hyperplane may not exist). In order to solve this problem, the constraints in (21) have to be relaxed for allowing some training points to be on the wrong side of the decision boundary (soft margin) (Figure 38). It is achieved by introducing a penalty term $\xi_n \geq 0$ for each training point [148]. It is called *slack variable* and its value increase with the distance from the margin boundary. Thus, $\xi_n = 0$ for points on or inside the correct margin; $0 < \xi_n \leq 1$ for points that lie between the

decision boundary and the correct margin and $\xi_n > 1$ for points on the wrong side of the decision boundary (misclassified points).

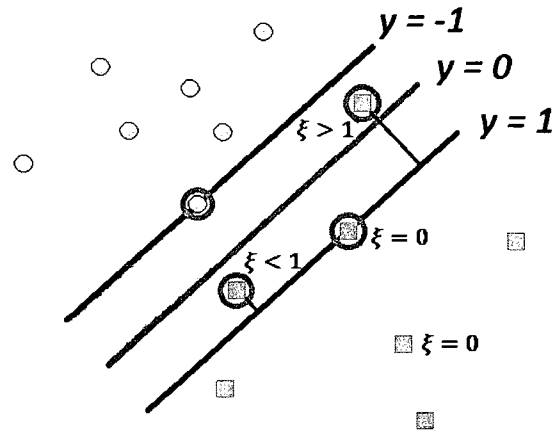

Figure 38. A penalty term is introduced when the data is not linearly separable in the feature space. Data points lying on the wrong side of the decision boundary are support vectors with $\xi > 1$.

The constraints are now changed to:

$$t_n \cdot (\boldsymbol{w}^T \phi(\boldsymbol{x}_n) + b) \geq 1 - \xi_n \tag{30}$$

$$\xi_n \geq 0 \tag{31}$$

The margin is maximized but penalizing those points in the wrong of the margin boundary. The optimization problem becomes:

$$\min_{\boldsymbol{w},b} \left\{ C \cdot \sum_{m=1}^{M} \xi_m + \frac{1}{2} \|\boldsymbol{w}\|^2 \right\} \tag{32}$$

where $C > 0$ is the parameter that controls the tradeoff between the misclassification error and the complexity of the model. In the limit $C \to \infty$, all the training points are correctly classified and the problem becomes the hard margin maximization as in Section 5.1.1. As in the separable case, incorporating the kernel function and rewriting the

problem in terms of Lagrange multipliers leads to the maximization of (25) subject to the constraints:

$$0 < a_n < C \tag{33}$$

$$\sum_{n=1}^{N} a_n t_n = 0 \tag{34}$$

The only difference with the separable case is the introduction of an upper bound for the Lagrange multipliers a_n. Again in this case, a new data point is classified by evaluating the sign of (29).

5.1.3. Quadratic Programming Problem Solution

In a classification problem, training a SVM requires the solution of the quadratic programming (QP) optimization problem presented in (25). The high amount of computation and memory requirements make most of the traditional techniques unpractical, especially for large amount of data. Several algorithms have been designed for decreasing the amount of work and storage by removing the columns of the kernel matrix with Lagrange multipliers equal to zero. Among them, sequential minimal optimization (SMO) [164] is one of the most popular approaches addressed because it is simple and allows fast training speed. It breaks the QP problem into a series of smaller ones that can be solved analytically. The initial goal is to identify the nonzero multipliers and to discard the rest. For various applications, the SMO algorithm scales somewhere between linear and quadratic with the training set size.

In the present work, a pattern recognition system is designed for actuating a prosthetic device in real-time. The classifier is trained offline with data that have been previously collected from the user. Therefore, the training of the classifier does not take

part in the real-time implementation of the whole system so it does not need to be optimized for processing time. Given the advantages presented above the SMO algorithm was used to train all the classifiers analyzed along this project.

5.2. Multiclass Classification

SVM were originally designed to discriminate between two classes. However, several methods have been introduced for combining multiple binary classifiers in order to solve multiclass classification problems.

One of the most common approaches creates a set of K binary classifiers to solve a K-class classification problem. Each model $y_k(\boldsymbol{x})$ is trained considering all data from one class having positive labels and all the data from the remaining classes having negatives labels. This method is referred to as *one-against-all* (OaA) (Figure 39, left). A new point is assigned to the class to which the value of $y_k(\boldsymbol{x})$ obtained was maximum. The main disadvantage of this method is that the training sets are imbalanced and the $y_k(\boldsymbol{x})$ values may not have appropriate scales for different classifiers. In addition, the construction of this type of classifiers may lead to ambiguous regions in the feature space in which an input point may be assigned to multiple classes at the same time (gray regions in Figure 39).

Another method trains $K(K-1)/2$ different binary classifiers on data from only two classes. This approach is called *one-against-one* (OaO) (Figure 39, middle). The class assigned to a new point is decided using a voting strategy. After the point has been evaluated with every classifier, the class having the highest number of votes is selected. As in the case of OaA, this approach may also result in classification ambiguities.

Because the OaO method creates more classifiers, it requires a significantly longer training and testing time than the OaA method for cases with a large number of classes.

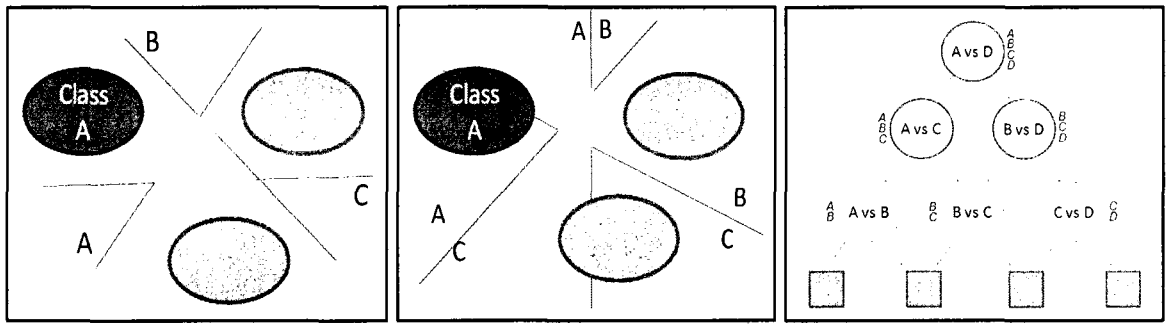

Figure 39. Three multiclass classification approaches using multiple binary SVM classifiers. Left: one-against-all method (OaA); middle: one-against-one method (OaO); right: direct acyclic graph method (DAG).

The decision *directed acyclic graph* (DAG) is another alternative for multiclass classification using SVM proposed in early 2000's [165]. The training stage is the same as the OaO method by solving $K(K-1)/2$ binary SVM's. In the testing phase, a rooted binary directed acyclic graph is used to assign the final class to the new point (Figure 39, right). It has $K(K-1)/2$ internal nodes and K leaves. Each node is associated with a binary classifier and each leaf is associated with a class label. A test point is evaluated at the root node and depending on the result it can go either left or right towards the next level. This process continues until the final leaf indicating the predicted class is reached. The decision path followed by the input point face only $K-1$ classifier evaluations, which makes the testing procedure faster that the OaO method.

A comparison among these methods indicated that the one-against-one and directed acyclic graph methods are more appropriate for practical use [166]. The DAG method overcomes the limitation of the OaO strategy in terms of the evaluation time

needed. It requires less computation time to perform the testing stage, which is an important point for the implementation of the pattern recognition system in real-time. Another advantage of the DAG approach is that for a multiclass classification problem, the bound on the generalization error depends on the number of classes K and not on the dimension of the space.

5.3. EMG Signal Classification Methods

5.3.1. Training and Testing Data Sets

In order to train and test the myoelectric signal classification system, the data collected were divided in two sets. From the five trials recorded during each session, four trials were selected to create the training set and one trial to create the testing set. Each trial collected five 5-s repetitions of a specific wrist motion which led to 100 MES data points. As a result, 400 training points (4 trial x 100 points/trial) and 100 testing points (1 trial x 100 points/trial) were typically obtained. The amount of training data was determined experimentally by gradually increasing the number of trials until the SVM classifier can be appropriately trained.

The data points were obtained following the steps showed in Figure 40. The MES was filtered and segmented into non-overlapping 256-points windows (Section 3.3 and 3.4). The amplitude of the segments was then normalized (Section 3.5) before a discrete wavelet transformation (Section 4.4.2) was applied to extract relevant features. The processing of each segment resulted in a D-dimensional feature vector. It is a single point in the trn/tst matrix and represents 267 ms of myoelectric signal.

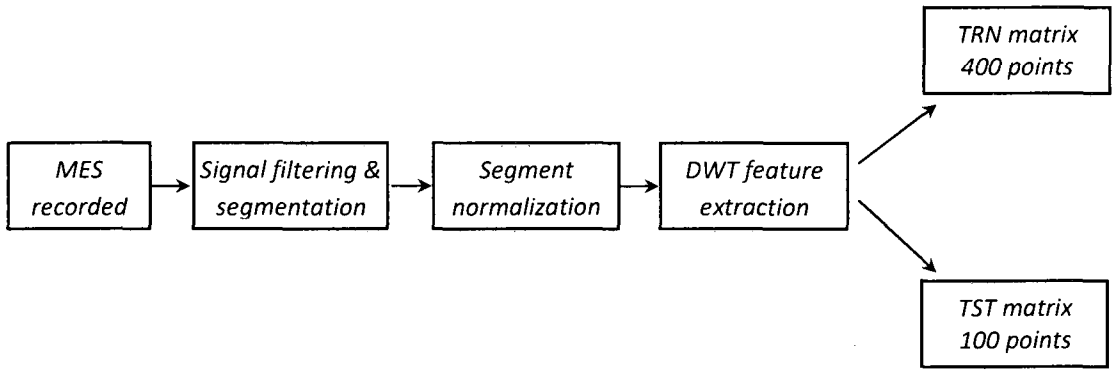

Figure 40. Block diagram representing the steps followed to create the training and testing data sets. Four out of five trials are used for training and the remaining for testing.

Every data point is associated with a class label that depends on the wrist motion that originated that point. The labels assigned to the five classes analyzed in this study are presented in Table 3:

Table 3. Class label assignments

Wrist Motion	***Class #***
Abduction	1
Adduction	2
Extension	3
Flexion	4
Rest	5

After the processing of the MES collected during a recording session, a matrix was prepared to train the SVM classifier. The format of the matrix created is presented in Figure 41. TRN is a *struct*-type variable with two fields: a) *field X* is a DxN matrix (D is the data dimension and N in the total number of training points) that contains the data points used to find the decision boundary and b) *field y* is $1xN$ matrix that has the class

labels associated with each point in the TRN.X matrix. So for example $TRN.y(1,i)$ is the class label for the ith point in $TRN.X(:,i)$.

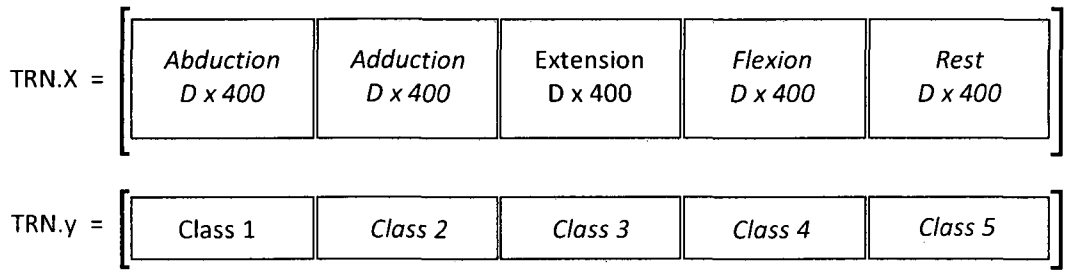

Figure 41. Outline of the training matrix. The TRN.X variable contain the training data and the TRN.y variable the data labels. The dimension D of the matrix depends on the number of wavelet decomposition performed (D=63 for full decomposition).

5.3.2. Training and Testing Algorithms

The reason for choosing that name's nomenclature in the previous section was the pattern recognition toolbox used to create the SVM models. The statistical pattern recognition toolbox (STPRTool) was developed by a group of students at the Czech Technical University in Prague [167]. STPRTool is open source software that contains a collection of pattern recognition methods implemented in Matlab. The toolbox allows the user to use SMO to train SVM models (see Section 5.1.3) and to test new data points by the evaluation of the sign of Equation (29) in Section 5.1. The synopsis and description of the call to the training function is presented in Appendix B.

5.3.3. Decision Directed Acyclic Graph (DAG)

For this study, the DAG method was implemented to classify $K = 5$ movements. In the training stage, one binary classifier is constructed for each pair of movements, leading to a total of 10 binary classifiers. When training each binary classifier, the data corresponding to the two different classes may overlap, therefore, the class separation has

to be performed using the soft margin approach. SMO was used in this pattern recognition system to train the set of classifiers. The kernel function used to map the input data (Radial Basis Function was chosen) as well as the value of the constant C were the parameters required for this algorithm.

In the testing phase, a rooted binary directed acyclic graph was used to determine the movement that originated the input data. As illustrated in Figure 42, our classifier contains 5 leaves and 10 internal nodes. As it is stated in [165], this method is similar to operating it on a list. It starts with all classes at the root node, where the new testing point $\boldsymbol{x}$ is first evaluated against the first and the last classes on the list. The class with the lowest value of the function $y(\boldsymbol{x})$ (Equation (29)) would be eliminated, and a new list is created for the next node. Therefore, the test point will go through an evaluation path containing 4 internal nodes before reaching the leaf that contains only one final class on the list (Figure 42).

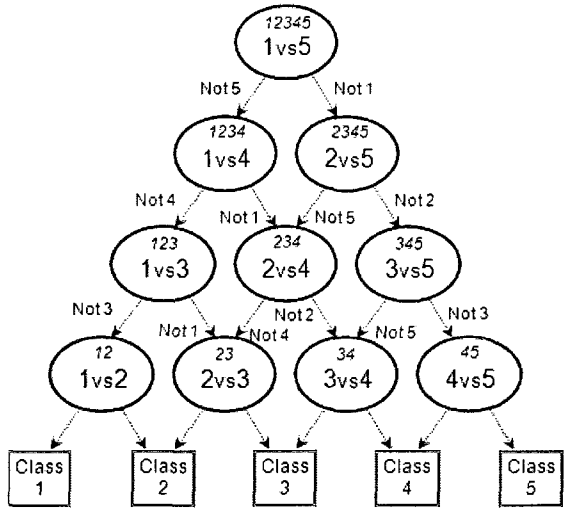

Figure 42. A DAG implementation of the SVM classifier for discriminating five limb motion classes. Inside each decision node, the list state is placed at the top, and the two classes being evaluated are shown at the center. Each node is associated with a binary classifier The final leaf indicates the class predicted for a new test point.

5.4. EMG Signal Classification Results

5.4.1. SVM Parameter Selection

The Gaussian Radial Basis Function (GRBF) is one of the most popular kernels found in the literature and it generally outperforms polynomial kernels when dealing with overlapped class distributions [19, 150, 168, 169]. Its mathematical expression is given by Equation (35).

$$k(\boldsymbol{x}, \boldsymbol{x}_n) = \exp\left(-\frac{1}{2} \cdot \frac{\|\boldsymbol{x}_n - \boldsymbol{x}\|^2}{\sigma^2}\right) \tag{35}$$

The parameter σ is proportional to the kernel width, and in most cases it is determined experimentally. The GRBF kernel was used here to train the SVM models because it can map the input vector into an infinite dimension, increasing the likelihood of obtaining good data separation in the new space.

Besides the kernel parameter σ, the regularization constant C is the only parameter remaining for selection. Therefore, the optimum value for each one was determined by performing a grid search. That is, different combinations of σ and C were used to train multiclass SVM models and the classification performance was then evaluated. The intervals for each of them were selected based on a previous work [170] as:

$$\sigma = \frac{1}{2^{\frac{m+1}{2}}} \qquad \text{for } m = -7, -6, \ldots, 5 \tag{36}$$

$$C = 2^n \qquad \text{for } n = -2, -1, \ldots, 9 \tag{37}$$

As a result, 156 multiclass classifiers were tested using the DAG method. The training set contained 954 data points and the test set comprised 240 samples. These sets were generated using myoelectric signals from three trials of the entire protocol

performed by a single subject. The value of the parameters used to train the model that presented the highest percentage of samples correctly classified (accuracy) were the target of this analysis. Figure 43 illustrates the classification accuracies resulted after testing the entire grid of models. Parameters outside the selected range were not considered because they increased the training time without improving accuracy. The best classification performances were observed at the top-right corner of the graph, suggesting that high accuracy can be achieved when combining wide GRB kernel functions with regularization constants higher than 64. The highest accuracy corresponded to $\sigma = 8$ and $C = 256$ for a classifier 86.67% accurate. These two values were selected for posterior training stages.

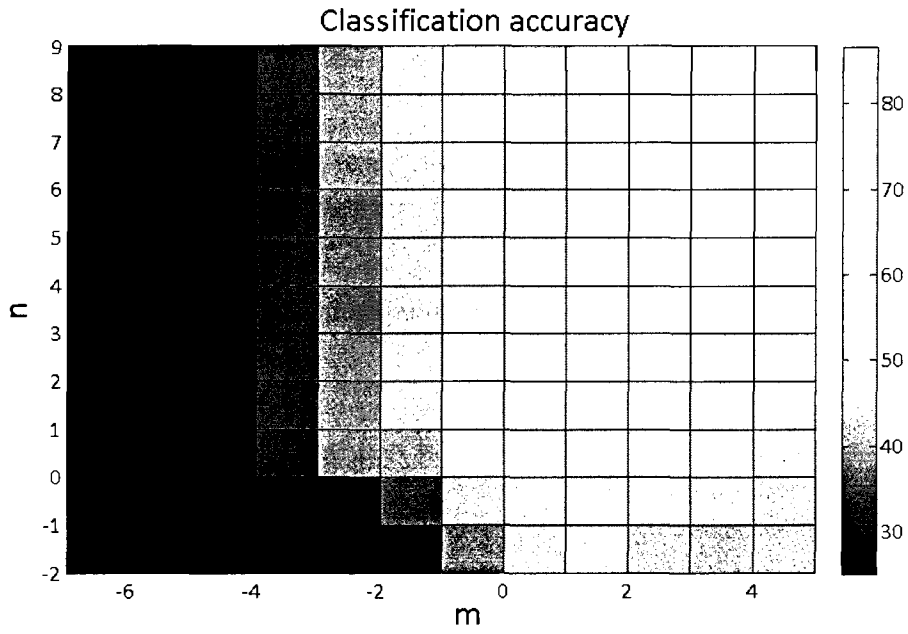

Figure 43. Grid based selection of both the optimal kernel (horizontal axis) and the regularization constant (vertical axis) parameters. The brightest region represents the lowest classification error (higher accuracy).

5.4.2. Offline Classifier Performance

A first look at the performance of the proposed myoelectric control system was taken by training a multiclass classifier for each subject and by determining how well it discriminated the five classes. The dataset used for training was created with data from the first recording session. It contained 400 samples of each class as explained in Section 5.3.1. The parameter C and the value of σ for the GRBF kernel used to create all the SVM models were selected based on the results in Section 5.4.1. The classification accuracies of the test set are illustrated in Figure 44 averaged across the 5 classes. The classifiers for subjects 1, 2, 4, and 5 correctly determined the correct class of the test points more than 93% of the time. The best performance was achieved for subject 1 with an average accuracy of 98.2% ± 1.3%. The test data from subject 6 and 7 presented the lowest classification performance, 85.5% ± 13.3% and 83.5% ± 20.1% respectively.

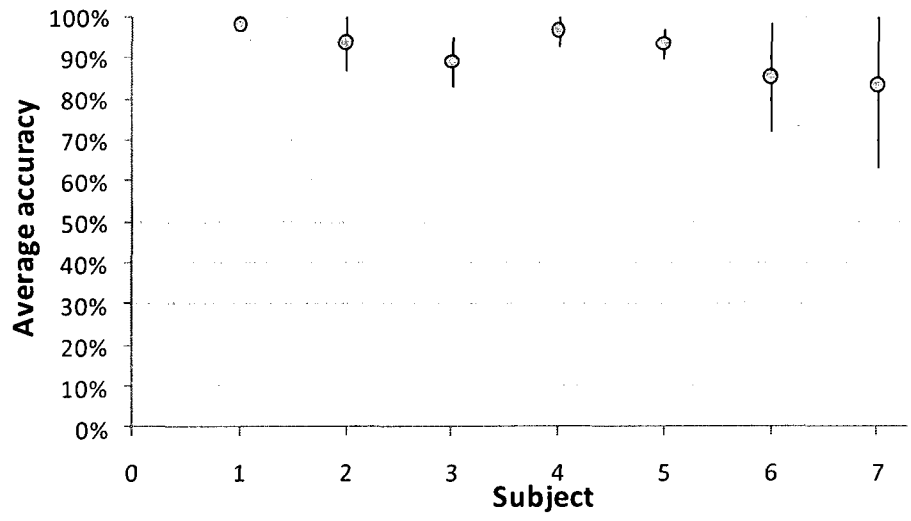

Figure 44. Classification accuracy for each subject averaged across the 5 classes. Subject 1 presented best classification performance with 98.2% ± 1.3%.

The classification performance for each individual class is showed in Figure 45. The accuracy values for subjects 6 and 7 were lower because of the low classification performances for adduction and flexion classes in subject 6 and for abduction and extension classes in subject 7. For both subjects, the classification of the other three classes was more than 90% accurate. The rest class was accurately discriminated with more than 98% of accuracy in all cases. It is an important to have a high accuracy of the rest class because it indicates the suppression of the prosthetic device, hence reducing the amount of inappropriate actuations (< 2% of the time). Among the remaining classes, adduction was correctly classified more that 90% of the time for all subjects except subject 6 (72%). This high performance suggests that the wrist adduction class can be used to activate a critical action of the prosthesis as for example the hand opening or closing. Abduction, extension and flexion classes were classified with and accuracy within 90-100% in five of the seven individuals.

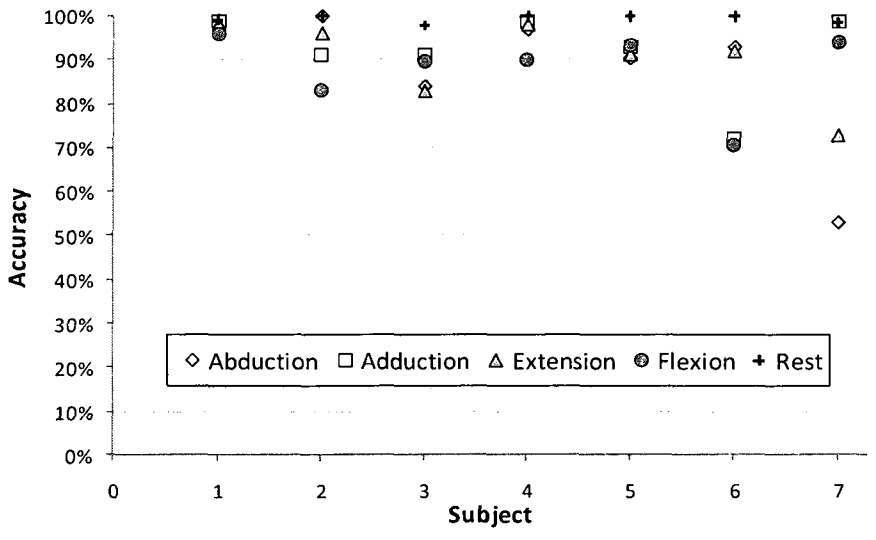

Figure 45. Classification accuracy obtained for each wrist motion. The rest class presented the higher classification accuracies across all subjects.

A confusion matrix was created for each subject to illustrate the results in more detail (Table 4 to Table 10). The rows of these matrices represent the true class whereas the columns indicate the class predicted by the classifier. The perfect classifier performance would lead to off-diagonal elements (miss-predicted points) equal to zero and main diagonal elements (perfectly predicted points) equal to the number of testing points for the corresponding class. The last column is the classification accuracy for the class in the corresponding row. The average classification accuracy is also presented at the bottom-right part of each table to indicate the overall performance of the model. Test points of Subject 1 were correctly predicted most of the time and the few miss-predicted points (9 out of 499 points) were mainly predicted as adduction (4 times) and abduction (3 times) (Table 4). The misclassified points of subject 2 (30/513) were wrongly predicted as abduction points more than half of the time (Table 5). For both subjects, the rest class was classified almost perfectly; there was only one point misclassified as abduction (Subject 1).

Table 4. Confusion matrix subject 1.

SUBJECT 1			PREDICTED CLASS					Class
			Abd	*Add*	*Ext*	*Flex*	*Rest*	*accuracy*
	TRUE CLASS	*Abd*	99	0	0	1	0	*99.00%*
		Add	0	99	0	1	0	*99.00%*
		Ext	0	2	98	0	0	*98.00%*
		Flex	2	2	0	96	0	*96.00%*
		Rest	1	0	0	0	98	*98.99%*
							Avg.	***98.20%***
							St. Dev.	*1.30%*

Table 5. Confusion matrix subject 2.

SUBJECT 2		PREDICTED CLASS					Class
		Abd	Add	Ext	Flex	Rest	accuracy
TRUE CLASS	Abd	99	0	0	0	0	100.00%
	Add	4	91	0	5	0	91.00%
	Ext	3	0	96	1	0	96.00%
	Flex	8	6	3	83	0	83.00%
	Rest	0	0	0	0	114	100.00%
						Avg.	**94.00%**
						St. Dev.	7.18%

The classification of the test points of subject 3 showed that all classes except the rest class were misclassified at least 9% of the time (Table 6). When their true class was incorrectly assigned, abduction points were mostly predicted as extension and vice versa. In the same way, flexion points were predicted as adduction but adduction points were assigned to either extension or flexion classes. Again for this subject, the rest class was almost perfectly discriminated

Table 6. Confusion matrix subject 3.

SUBJECT 3		PREDICTED CLASS					Class
		Abd	Add	Ext	Flex	Rest	accuracy
TRUE CLASS	Abd	84	0	10	5	1	84.00%
	Add	0	91	4	5	0	91.00%
	Ext	16	1	83	0	0	83.00%
	Flex	0	10	0	87	0	89.69%
	Rest	0	0	2	0	96	97.96%
						Avg.	**89.13%**
						St. Dev.	6.03%

A better classification performance was observed in the model trained for subject 4 (Table 7). All the classes were discriminated with more than 97% accuracy except for the wrist flexion class (90%). Misclassified flexion points were only confused with

adduction or abduction points. Rest class was correctly classified all the time and no points were wrongly predicted as rest.

Table 7. Confusion matrix subject 4.

SUBJECT 4		PREDICTED CLASS					Class
		Abd	Add	Ext	Flex	Rest	accuracy
TRUE CLASS	Abd	97	0	0	3	0	97.00%
	Add	0	99	0	1	0	99.00%
	Ext	0	2	98	0	0	98.00%
	Flex	6	4	0	90	0	90.00%
	Rest	0	0	0	0	82	100.00%
						Avg.	**96.80%**
						St. Dev.	3.96%

Another good performance was obtained in the classification of the test points of subject 5 (>90% for all classes) (Table 8). As it happened with test set of subject 1, most of the misclassifications corresponded to adduction pointes predicted as flexion and vice versa. The rest class was perfectly classified.

Table 8. Confusion matrix subject 5.

SUBJECT 5		PREDICTED CLASS					Class
		Abd	Add	Ext	Flex	Rest	accuracy
TRUE CLASS	Abd	85	1	7	1	0	90.43%
	Add	1	93	2	4	0	93.00%
	Ext	7	0	83	1	0	91.21%
	Flex	2	4	0	85	0	93.41%
	Rest	0	0	0	0	70	100.00%
						Avg.	**93.61%**
						St. Dev.	3.78%

The low averaged accuracies found for subjects 6 and 7 had the same cause. Three of the five classes were discriminated with a high accuracy (>92%), whereas the performance of the remaining two classes was radically poor. Adduction patterns of

subject 6 were predicted as flexion 24% of the time, whereas flexion patterns were assigned to adduction another 24% of the time (Table 9). For subject 7, an unexpected accuracy of 53% was obtained for the abduction class, which was because 45% of these points were predicted as belonging to the rest class (Table 10). The 73% of accuracy in the classification of extension patterns also dropped the overall performance of the model. The classification of the rest patterns was perfect for subject 6 and only one point was misclassified as abduction in the test set of subject 7.

Table 9. Confusion matrix subject 6

SUBJECT 6		PREDICTED CLASS					Class
		Abd	Add	Ext	Flex	Rest	accuracy
TRUE CLASS	Abd	93	2	4	0	1	93.00%
	Add	1	72	3	24	0	72.00%
	Ext	4	2	92	2	0	92.00%
	Flex	0	24	5	70	0	70.71%
	Rest	0	0	0	0	79	100.00%
						Avg.	**85.54%**
						St. Dev.	13.32%

Table 10. Confusion matrix subject 7.

SUBJECT 7		PREDICTED CLASS					Class
		Abd	Add	Ext	Flex	Rest	accuracy
TRUE CLASS	Abd	53	2	0	0	45	53.00%
	Add	0	99	1	0	0	99.00%
	Ext	5	15	73	0	7	73.00%
	Flex	1	5	0	94	0	94.00%
	Rest	1	0	0	0	70	98.59%
						Avg.	**83.52%**
						St. Dev.	20.12%

To get an idea of the general classification performance of each motion class, all confusion matrices were combined into a single matrix. The sensitivity (or True Positive rate) was plotted against the specificity (or 1 minus the False Positive rate) for each one

of the discriminated classes of motions (Figure 46). Sensitivity is a measure of how well the classifier assigns the positive class label to a point that is positive. Specificity indicates how likely it is for the classifier to predict a negative class for a point that has a negative class label. These two measures are defined by following the binary confusion matrix given as example (Table 11).

Table 11. Binary confusion matrix used to define different measures

		PREDICTED CLASS	
		p	N
TRUE CLASS	P	*TP*	*FN*
	N	*FP*	*TN*

Sensitivity and specificity are defined as:

$$\text{Sensitivity} = TP \text{ rate} = \frac{TP}{P} \tag{38}$$

$$\text{Specificity} = 1 - FP \text{ rate} = \frac{TN}{FP + TN} \tag{39}$$

As this case is a multiclass classification problem (5 classes of limb motion), one movement was taken as the positive class and all the others as the negative classes. This adaptation was called class reference formulation [171]. One point in the graph represents the classification performance for a specific class averaged across the seven subjects. The closer the point to the top-right corner, the better the classification performance for that specific class. Results in Figure 46 confirmed that the rest class was the best discriminated class with more than 97% of sensitivity and specificity. Adduction and extension classes were better classified that abduction and flexion classes. All the classes present acceptable specificity (>97%) meaning that a small number of false positives

(points predicted as the positive motion when they belong to other motion) are predicted. On the other hand, the sensitivity of the abduction and flexion classes was low, indicating that the classifier predicted a small number of true positives.

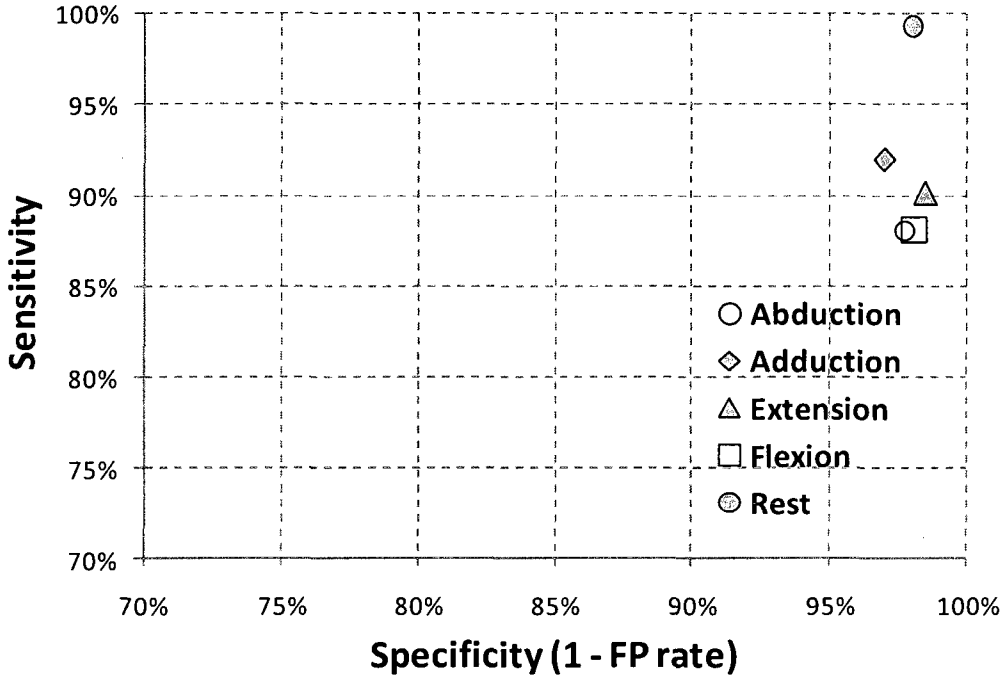

Figure 46. Each point in the sensitivity vs. specificity plot represents the classifier ability to discriminate each class averaged across all subjects.

The good classification performance of the rest class was also supported by the classifier's margins obtained (Table 12). SVM models are trained to maximize the margins between the decision boundary and the closest point of each class (Figure 36). The average margins for all of the models involving the rest class (class 5) at least doubled the margins of the other classifiers, meaning that rest class is well separated from the others. The smallest margin was found in the binary classifier that discriminated adduction and flexion classes (classes 2 and 4, respectively).

Table 12. Margins obtained for each binary classifier.

CLASSIFIER'S MARGINS									
SVM Classifier	SUBJECT							Avg. Margin	St. Dev.
	1	2	3	4	5	6	7		
1-vs-2	0.0064	0.0070	0.0074	0.0083	0.0068	0.0083	0.0107	**0.0078**	0.0015
1-vs-3	0.0072	0.0081	0.0053	0.0094	0.0065	0.0065	0.0074	**0.0072**	0.0013
1-vs-4	0.0066	0.0062	0.0063	0.0075	0.0059	0.0086	0.0098	**0.0073**	0.0014
1-vs-5	0.0169	0.0165	0.0093	0.0163	0.0179	0.0168	0.0129	**0.0152**	0.0030
2-vs-3	0.0064	0.0072	0.0067	0.0088	0.0069	0.0064	0.0078	**0.0071**	0.0009
2-vs-4	0.0050	0.0052	0.0051	0.0050	0.0059	0.0049	0.0063	**0.0053**	0.0005
2-vs-5	0.0195	0.0166	0.0142	0.0159	0.0283	0.0182	0.0216	**0.0192**	0.0047
3-vs-4	0.0061	0.0072	0.0069	0.0085	0.0071	0.0066	0.0090	**0.0073**	0.0010
3-vs-5	0.0184	0.0112	0.0093	0.0170	0.0257	0.0158	0.0194	**0.0167**	0.0054
4-vs-5	0.0183	0.0160	0.0145	0.0195	0.0300	0.0182	0.0223	**0.0198**	0.0051

5.4.3. Electrode Placement Variations

The success of any pattern recognition-based myoelectric system is commonly related to the classification accuracy. Although it is not the only factor affecting the acceptability of prosthetic devices, it plays an important role because accuracy is directly related to the correct interpretation of the intended movement performed for the subject. A signal classifier is trained to learn the nature of the muscle contractions patterns that are repeated at specific electrode locations. However, various factors can change these patterns over time. One of the most important changes is produced by the spatial movement of the electrodes over the skin. Such movement may be caused by misalignment between the socket and the residual limb or a slight change in the electrode position when the prosthesis is used for a long period of time. Therefore, the classifier must accommodate those changes. It was demonstrated that the accuracy of the pattern recognition system decreased when possible shifts in the electrode location are not taken into account [172]. A potential solution is to minimize the effect of electrode placement

variations by training a robust classifier on data collected from the area that covers the displacement range.

To confirm the effect of the spatial changes, preliminary tests were run on the data set collected for the present work. MES from two sessions were used, where the locations of the electrodes were not exactly the same in the two sessions. Even though these variations were not intentionally introduced; slight changes in the position were expected because the original location was not marked on the skin. The multiclass classifier was trained and tested with data from the first and second sessions respectively. The order was then swapped and a new classifier was created. A 5-fold cross-validation was used to show the performance of the classifier for data from the same location and the test set for data from different location. The classifier of the first session discriminated with an average accuracy of 28% for the test set and 90% for cross-validation. The second model accurately classified 36.5% of the test data and 85% of the cross-validation (Table 13). These results suggest that small changes in electrode placement strongly affect the accuracy of the classifier.

Table 13. Classification accuracy results using 5-fold cross-validation and a test set.

	Train with 1st session		**Train with 2nd session**	
Fold	Same session	Different session	Same session	Different session
1	89.09%	28.59%	84.92%	37.11%
2	89.09%	26.68%	85.71%	35.56%
3	90.37%	27.83%	83.75%	37.84%
4	90.83%	28.03%	85.75%	36.47%
5	89.91%	27.63%	86.15%	35.65%
Avg.	***89.86%***	***27.75%***	***85.26%***	***36.53%***
St Dev	*0.65%*	*0.53%*	*0.93%*	*0.92%*

Both data sets were then merged into a single training set to create a new classifier. The results of a 5-fold cross-validation showed an average accuracy of approximately 80% (Table 14). This accuracy suggests that an improvement in the robustness of the classifier has been made when incorporating data from different sessions. However, an additional test set from a new recording session would be necessary to confirm that behavior. The set would comprise new spatial changes that were not included in the two-session model and would indicate whether accuracy was significantly improved.

Table 14. Cross-validation results for classifiers trained with data from two sessions

Train data 1st & 2nd session	
Fold	Accuracy
1	77.67%
2	82.55%
3	81.23%
4	79.61%
5	78.13%
Avg.	***79.84%***
St Dev	*1.68%*

A new training strategy was implemented to analyze the performance of the classifier as information of the spatial changes is progressively added to the training set. To simulate the electrode deviations, EMG signals were recorded during consecutive experimental sessions. From one session to another, slight shifts (< 3 cm) in the electrode location were expected when they had been removed and replaced. Following each recording, a classifier is trained and tested with the information from the previous and current sessions, respectively. The first set for every subject is trained in the second

session using all the data recorded on session one. All the data recorded in the current session is used for testing in the DAG method. The same rule is applied for subsequent sessions, the training and testing sets are created with data from previous and current sessions respectively (Figure 47).

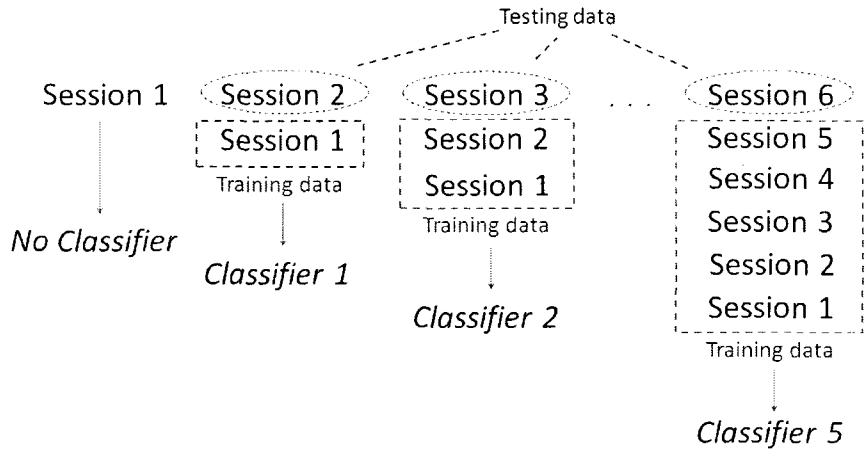

Figure 47. Training strategy designed to diminish the effect of variations in electrode placement. Data is progressively added to the training set by combining different recording sessions. Classifier is tested with data from a new session.

The performance of the classifier sets was evaluated by calculating the numbers of points of the testing set that were correctly classified. This calculation is referred to as the classifier accuracy. Figure 48 illustrates the accuracy of the multi-state classifier after each training session. The values were averaged over six subjects. Because the classifier of a specific session is trained on data from previous ones, the first point of this figure corresponds to session 2. The results indicate that a minimum of three recording sessions are required to achieve accuracy higher than 89%. After training the multiclass classifier with data from two sessions (in recording session #3) the classifier accuracy starts to reach a plateau, so it does not increase considerably after that point ($p>0.05$). Figure 49 illustrates the improvement in accuracy for the classification of each movement. Except

for the Flexion movement, the accuracies of the remaining classes (abduction, adduction, extension and rest) are higher than 85% after only three sessions of recordings.

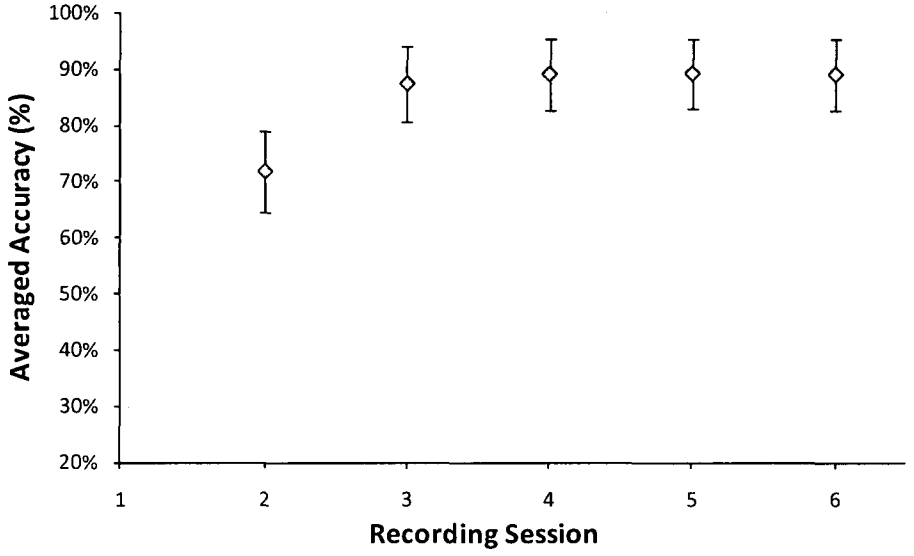

Figure 48. The averaged accuracy obtained for the classifiers trained during different recording sessions. After the fourth session the performance does not increase significantly

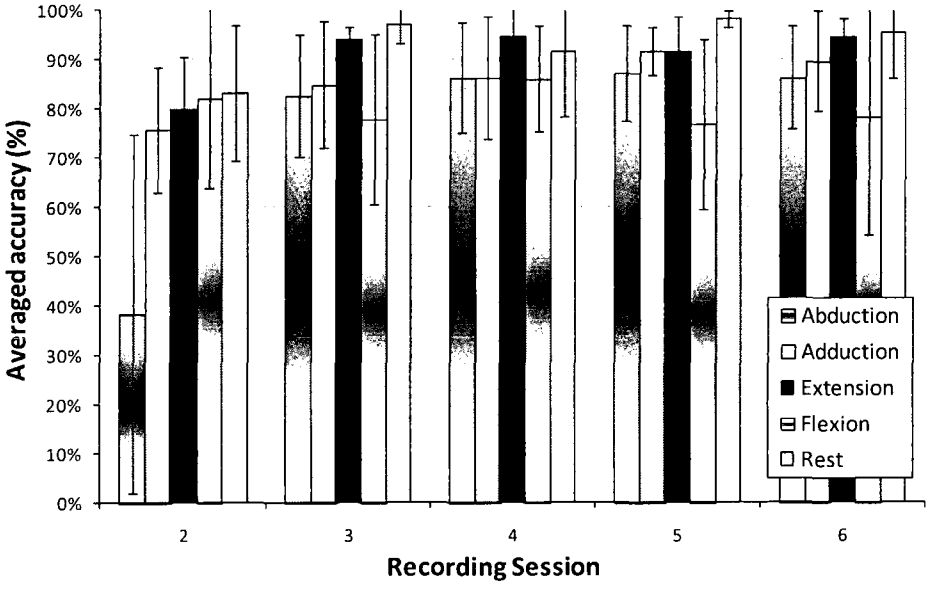

Figure 49. Progress of the movement classification accuracy over the training sessions. Each class was averaged over all subjects

Another way to evaluate the classifier performance is shown in Figure 50. We are interested in both the correct identification for each movement and the potential cost associated with misclassification. The sensitivity (or True Positive rate) is plotted against the specificity (or 1 minus the False Positive rate) for each one of the discriminated movements. As this case is not a binary classification problem, the class reference formulation is used [171]. One movement is taken as the positive class and all the others as the negative classes. For every movement, one point in the 'sensitivity-vs-specificity' graph represents the movement performance for a specific recording session. As a result, five points per class are drawn in the graph. They illustrate the behavior of the movement classification through the training sessions. The points closer to the upper-right corner represent higher accuracy in the discrimination of movements than points closer to the bottom-left corner. The results illustrated in Figure 7 indicate that the multi-state classifier discriminated both Extension and Rest classes more accurately than Flexion class. Classification of Abduction and Adduction movements presented similar behavior.

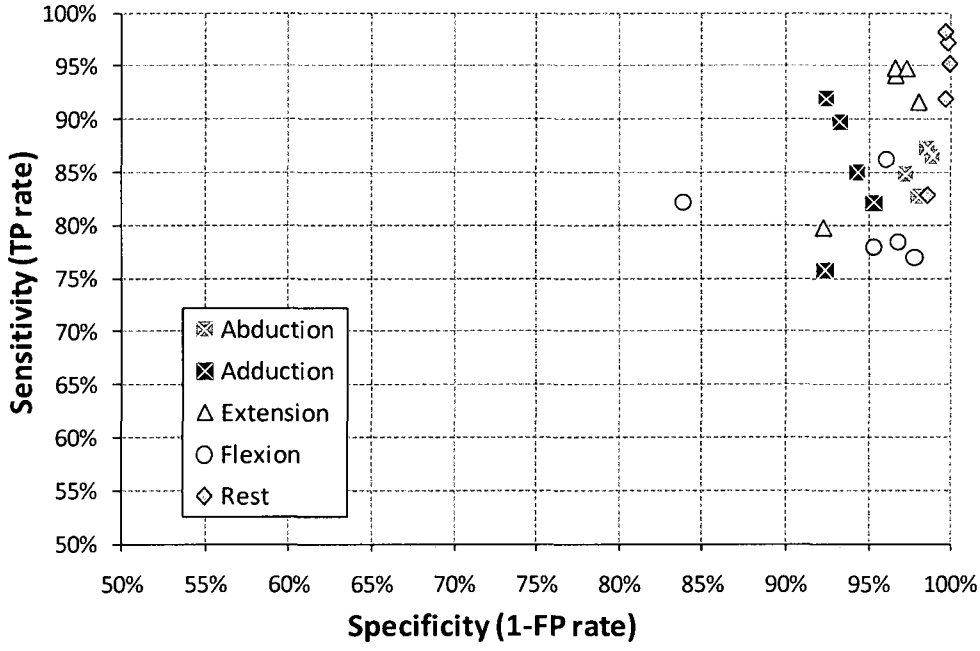

Figure 50. The 'sensitivity-vs.-specificity' plot. Each movement contains five points corresponding to the five training sessions

After a critical number of recordings, the pattern recognition system was able to adapt to the shifts in the electrode placement, meaning that the classification accuracy will not be significantly affected by the addition of new training data ($p>0.05$). As a result, the prosthetic device can be commanded accurately despite of possible electrode placement variations.

5.5. Real-Time Implementation

The myoelectric pattern recognition system presented in this work was implemented in real-time using National Instruments' LabVIEW development system. The main objective of this task was to assess the performance of the entire system in terms of its response time. This evaluation was extremely important to decide whether the system was suitable for real-time control.

5.5.1. Methods

The system response time is considered as the delay between the initiation of a command (onset of muscle contraction) and moment of the prosthetic actuation. Real-time constraints impose a maximum of 300 ms as the acceptable delay for controlling the device, which includes the acquisition of the MES data, the computation of features, the signal classification, and the generation of the control command. Several lengths for the MES window were tested by Englehart *et al.* to analyze their effect on the classification accuracy of the system [82]. An analysis window of 256 ms contained enough information to accurately estimate the motion state of the hand.

Two main approaches have been used to create a real-time continuous myoelectric signal classifier. The simplest approach uses adjacent, non-overlapped windows of length T_A (Figure 51). This approach generates one class decision (D_n) for each window. The time required to compute the signal features and the classification is called the processing delay (T_D). If the data can be processed while new signals are acquired, the interval between decisions is limited by, and equal to, the window length. Because the processing delay is generally shorter than T_A, processing power is available that could be exploited to provide more frequent decision updates.

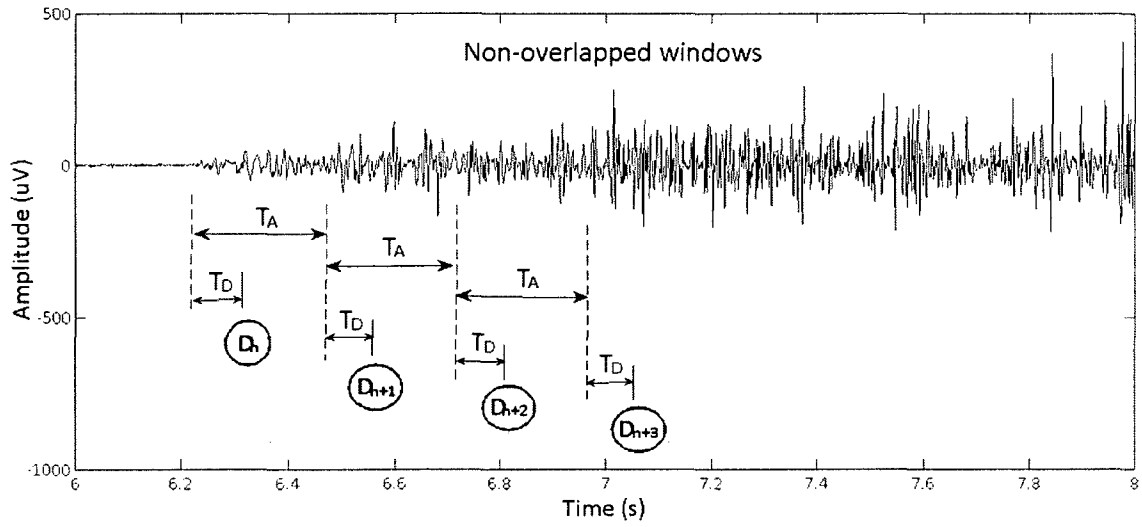

Figure 51. Signal classification scheme that uses non-overlapped widows of myoelectric signals. The class decisions are separated by one window length, T_A.

Another approach uses overlapped windows that generate a dense stream of class decisions for myoelectric control [21] (Figure 52). The sliding window is shifted by a time interval, T_i, which must be long enough to allow the processing of the segment (T_D) but must not be longer than the length of the segment, T_A, (Figure 52). In the optimal scenario, the processing of each analysis widow would start as soon as the previous decision was generated. As a result, the decisions are separated by intervals equal to the processing delay ($T_i = T_D$) and they correspond to the most recent T_A milliseconds of signal. This scenario fully uses the computational capacity of the system because the segmented signal is processed while it is being acquired.

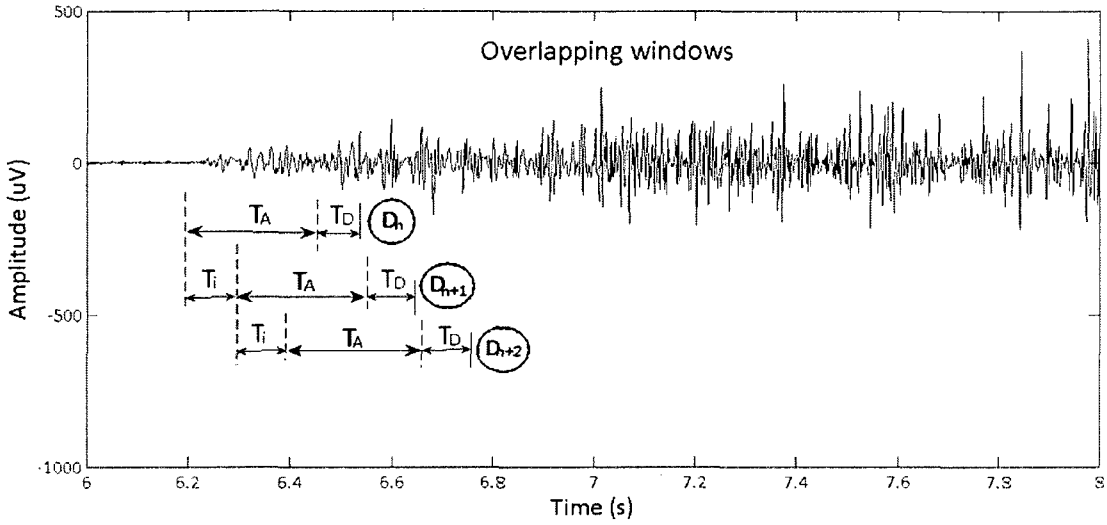

Figure 52. Overlapped windows signal classification scheme. The decision stream is more dense than in the in the non-overlapped windows scheme and each decision is separated by T_i milliseconds.

The real-time myoelectric control interface was developed in LabVIEW, based on the overlapped window approach. The algorithm implemented can be divided into three main parts: a) signal acquisition, b) signal processing, and c) signal classification or class decision (Figure 53).

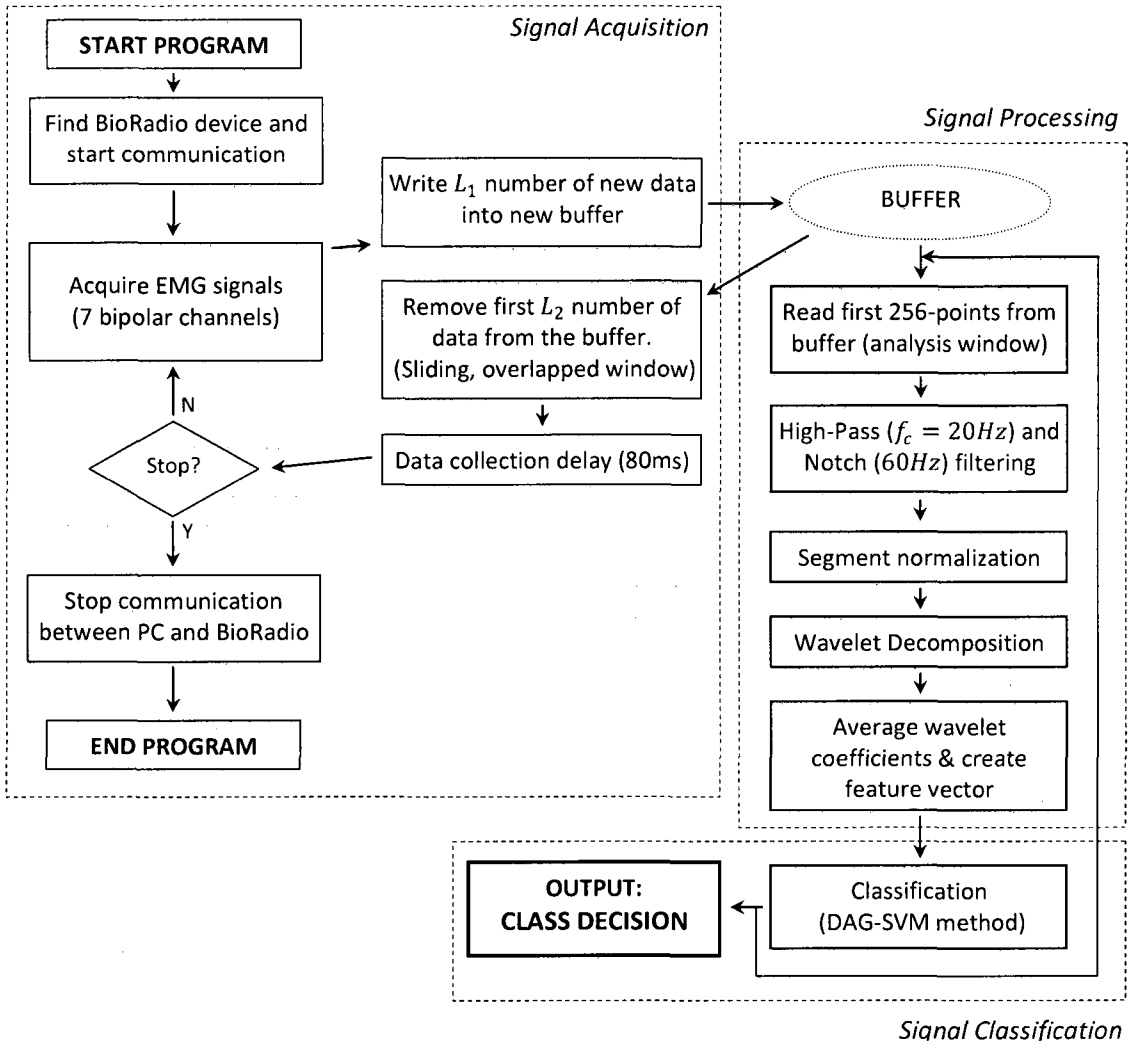

Figure 53. Block diagram of the real-time myoelectric patter recognition scheme implemented in LabVIEW. The signal is acquired (read from PC's port) and stored in an internal buffer for computation of the feature vector and classification. Before new data is acquired, the oldest data points are removed from the internal buffer.

Signal Acquisition

The signal was acquired with the BioRadio 150 wireless system (CleveMed, Inc) as explained in Section 3.2. A software DLL interface was developed by CleveMed, Inc to allow the communication and control of the BioRadio 150 through LabVIEW-based applications. The basis communication involves six main steps.

1) *Finding the attached device*: Indentify the attached receiver

2) *Starting base communication:* Start the communication between the PC and the BioRadio Computer Unit (embedded in the receiver). Create a software device object.

3) *Starting acquisition:* Start the communication between the Computer Unit and the User Unit (transmitter).

4) *Acquiring data*: Read and interpret data from the port buffer. Acquire transmission statistics (missing packets of data as well as good and bad packets).

5) *Stopping acquisition*: Stop the communication between transmitter and receiver.

6) *Stopping base communication*: Stop communication between PC and receiver, and destroy the software device object.

Steps 1 to 3 are performed only once at the beginning of the acquisition, and steps 5 and 6 only once at the end to conclude the communication. Regarding to the step 4, the software collects the data from the PC's communication port where the Computer Unit has deposited them. The time interval between port's readings can be controlled from the software interface and it was set to 80 ms as the default time. The data read from the PC's port were piled up into an internal buffer where L new data points are accumulated at the end. The first 256 points of that new buffer are read on each cycle to obtain the analysis window. Before performing the next reading from the PC's port, the older L data points are removed from the internal buffer to create the overlapped windows. The value of L depends on the data acquisition delay selected. When 80 ms is set as the delay time, L is

approximately equal to 80. The internal buffer must first be filled until the number of points increased up to more than 256 points so the first analysis window can be created.

Signal Processing

All the task of the signal processing stage were coded in Matlab and implemented as an embedded script node in the LabVIEW software. After the analysis window was read, both the high-pass and notch filters were applied to the acquired segment. As the signal was sampled at 960 Hz, the 256-point time window represented a total of 266 ms of muscle contraction. The extraction of the features by wavelet decomposition followed the amplitude normalization. The final task consisted in the averaging of the wavelet coefficients at each decomposition level to create the feature vector.

Signal Classification

In the signal classification stage, the input feature vector was assigned to the one of the five classes using the DAG-SVM framework explained in Section 5.3.3. This class output is associated with an action of the prosthetic device, which would be executed by the control system.

5.5.2. Results

The real-time algorithm was evaluated on subject 2. Seven bipolar electrodes were placed over the right forearm in according to the recording protocol. The subject was asked to place the arm in a relaxed position before starting. In the evaluation trial, the person sequentially performed 6 seconds of the four wrist movements separated by rest intervals: abduction, adduction, extension and flexion. The algorithm used the pre-trained SVM model to classify the segments while the EMG signal was being acquired. Two models from subject 2 were used: one created with data from the first four recording

sessions (three trials) and one with data from the first five sessions (three trials) (see Section 5.4.3). Two models were chosen because the four-session model presented the best accuracy in the experiments reported in Section 5.4.3 and the five-session classifier contained all the trained data.

For each class decision, the time required for acquisition, processing and classification was computed (processing and classification were combined into a single value). For both SVM models, the total time averaged less that 20 ms, that is, from the onset of the muscle contraction to the time when the final decision is made (Table 15). This number would leave more than 250 ms for the control system to actuate the device when the decision stream is as dense as possible ($T_D = T_i$). For this particular case, the decisions were separated by T_i = 80 ms, the default setting for the data collection delay. However, this number could be adjusted for further experiments.

Table 15. The total system response time includes the acquisition time plus the signal processing and classification times. Four-session classifier was used in trials 1-3 and five-session classifiers in trials 4-6.

Time (ms)	*TRIAL*						Avg. time (ms)
	1	*2*	*3*	*4*	*5*	*6*	
Acquisition	0.163	0.141	0.154	0.160	0.147	0.151	0.153
Processing + Classification	17.715	17.912	18.085	19.949	17.606	17.621	18.148
						Total system response time(ms)	**18.301**

The classification accuracies were lower than expected, especially for the abduction class (Table 16). The accuracies of all classes dropped from those obtained in the electrode displacement experiments (Section 5.4.3). The most critical parts were found near the transition intervals, when the contraction types were changed (Figure 54).

Table 16. Real-time classification accuracies obtained after 6 different trials. Rest was the best discriminated class.

CLASSIFICATION ACCURACY					
	class 1	*class 2*	*class 3*	*class 4*	*class 5*
Trial 1	76.92%	90.00%	86.27%	88.24%	92.26%
Trial 2	84.00%	60.00%	98.00%	83.67%	91.47%
Trial 3	54.55%	85.19%	72.22%	85.19%	95.76%
Trial 4	62.96%	69.23%	84.31%	66.07%	84.49%
Trial 5	60.38%	58.82%	80.39%	73.08%	89.62%
Trial 6	48.08%	72.55%	85.19%	70.37%	90.98%
Average	**64.48%**	**72.63%**	**84.40%**	**77.77%**	**90.76%**
St Dev	13.58%	12.81%	8.41%	9.09%	3.70%

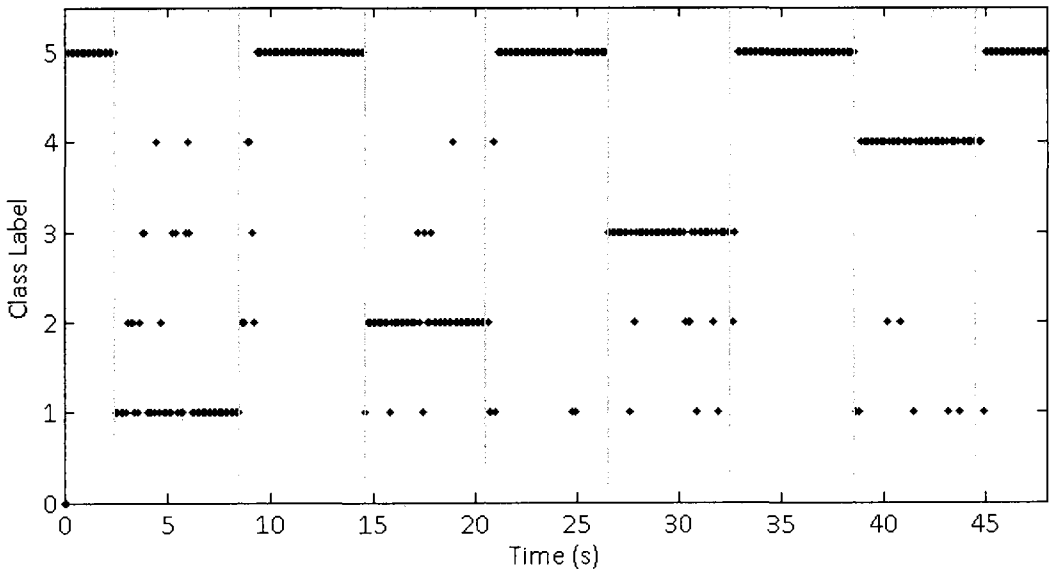

Figure 54. Class decisions obtained after processing the signal in real-time (Trial 1). Abduction, adduction, extension and flexion contractions are separated by rest intervals. Abduction presented the least accuracy and the rest class was the most accurately discriminated.

5.6. Discussion

Offline classification

The SVM models were evaluated on seven different subjects. The RBF kernel selection was based on the results of previous studies, and its parameter sigma (σ) was determined experimentally. Because the data points corresponding to the five classes overlapped in the original feature space, the soft margin approach was used to train the classifiers (the regularization constant parameter C was also determined experimentally). The classification accuracies obtained were satisfactory; test points were correctly discriminated 91.5% of the time. This value was averaged across all subjects and it is comparable with the results obtained by other researchers [16, 140, 150]. The 15% difference between the poorest classification performance (Subject 7, 83.5 %) and the best performance (Subject 2, 98.2%) may be a consequence of the SVM parameter selection. Before creating the models, the purpose was to generalize the training phase by using the same set of parameters for all subjects. Although the results were promising, the high variability suggested that the classifier parameters could not be generalized but needed to be optimized individually for every subject. This optimization combined with an optimization of the wavelet parameters may lead to a customized pattern recognition system that authentically represents user's intent.

The classifier's ability to discriminate each class was presented in Figure 46 (page 90). The high specificity for all classes meant that the classifiers generated few false positives. The rest class presented the best performance because it was well separated from the other classes, as indicated by the margins of the points to the decision boundary (Table 12). The classification accuracies of classes 1 through 4 differed for every subject.

Adduction presented the best averaged performance (92%) but was poorly discriminated by the classifiers of subject 6. Abduction and extension classes were well-classified for subject 6 but not for subject 7. In contrast, adduction and flexion classes were well classified for subject 7, but they were poorly discriminated for subject 6. The classifier of subject 2 discriminated all the classes with more than 90% accuracy, except the flexion class (83%). These results suggest another possible customization of the myoelectric control system. The class that activates the actions of the prosthesis can be adapted according to the classification performances for each class. The classes with higher classification accuracies may be used to actuate the most critical functions of the prosthesis.

Pattern variations caused by electrode displacements

The training strategy proposed in Section 5.4.3 attempted to simulate the variations in electrode placement by recording EMG signals during consecutive sessions. The strategy was examined because small shifts in electrode position were expected. The performance of the multiclass classifiers was illustrated in Figure 48. It showed an improvement in the classification accuracy that asymptotically approaches 90%. After a critical number of recording sessions, the classifier accuracy started to reach a plateau, meaning that inclusions of new training data did not significantly improve the performance of the multi-state classifier ($p>0.05$). This study showed that an average of three sessions was needed to achieve classification accuracy higher than 89%. This value may be increased by combining an additional algorithm able to determine the best combination of the averaged wavelet features for this application. PCA for

dimensionality has been shown to work effectively in combination with wavelet transform [115, 123]. The inclusion of PCA with SVM will be examined in Chapter 6.

The extension and rest classes were classified with high accuracy (>90%) from early sessions, as illustrated in Figure 49, meaning that only a small data set was required. However, additional data recorded for the flexion movement did not directly translate to a high flexion classification accuracy. The accuracy could be improved by increasing the number of repetitions performed during each recording session. As outlined in Figure 50, all movements can be distinguished with high specificity. The specificity-vs.-sensitivity data for the flexion movement was saturated at a lower level than the other classes, meaning that the classifier was more likely to reject false flexion points than to accept true flexion points. Abduction and adduction were classified with good accuracy (>85%) when the multiclass classifier was trained with data from more than three recording sessions.

The results obtained for the implemented pattern recognition system supported the hypothesis that the proposed training strategy allows the classifier to adapt to the changes produced by alterations in the electrode location. This adaptation will permit the amputee to manipulate the prosthetic device effectively, even when the socket is placed incorrectly on the residual limb or is moved from its original location after long term use.

Real-time implementation

The real-time constraint on the myoelectric control system forces the controller delay to be as small as possible. An acceptable delay between the onset of the contraction and the prosthesis motion is 300 ms. The pattern recognition scheme proposed was able to record, process and classify the controlling signal in less than 20 ms on a 1.99 GHz

Pentium 4-based workstation. This result is comparable with results obtained by other researchers. The short the delay can be used advantageously in two ways. First, a myoelectric system with fast response time can be created since the processing time is low when compared with the perceivable delay. Second, the class decisions can be post-processed to improve accuracy. The decision can then be based on a sequence of successive output states instead of a single time window. The class with the greatest number of occurrences is selected as the output class. This scheme may prevent the misclassifications produced during the transitions from one contraction to another, but will increase the system response time.

CHAPTER 6

FEATURE PROJECTION FRAMEWORK

The main purpose of the work presented in this chapter was the implementation of a feature projection framework based on PCA, with the aim to expedite the processing time and improve the classification accuracy of the myoelectric control system. PCA is a standard, non-parametric method for extracting relevant information from confusing, complex data sets to reduce them to a lower dimension. The PCA algorithm was found to work effectively in combination with wavelet transform as a potential mean to reduce the EMG feature space dimensionality prior to the signal classifier [115, 124, 137]. These results led to the hypothesis that the implementation of a PCA feature projection framework would gather the relevant discriminatory information from the original features set, improving the classification accuracy of the SVM classifier. In addition, a reduction in the dimensionality of the new feature set would expedite the processing time in the decision stage.

This chapter begins with a brief introduction to the PCA method and the way that the new feature space is obtained. The two feature-projection frameworks evaluated are presented next. The results are expressed in terms of classification accuracy and processing time at the end of the chapter.

6.1. Principal Component Analysis

PCA refers to the orthogonal projection of multivariate data into a new coordinate system (feature space) such that the variance of the projected data is maximized [131] (Figure 55). This new feature space is defined by the eigenvectors corresponding to the eigenvalues of the covariance matrix of the data set. So, for a D-dimensional data set containing L number of observations the covariance matrix is defined as:

$$\boldsymbol{S} = \frac{1}{L} \cdot \sum_{l=1}^{L} (\boldsymbol{x}_l - \bar{\boldsymbol{x}}) \cdot (\boldsymbol{x}_l - \bar{\boldsymbol{x}})^T \tag{40}$$

where $\boldsymbol{S}$ is a D x D matrix and $\bar{\boldsymbol{x}}$ is the mean vector given by the following equation:

$$\bar{\boldsymbol{x}} = \frac{1}{L} \sum_{l=1}^{L} \boldsymbol{x}_l \tag{41}$$

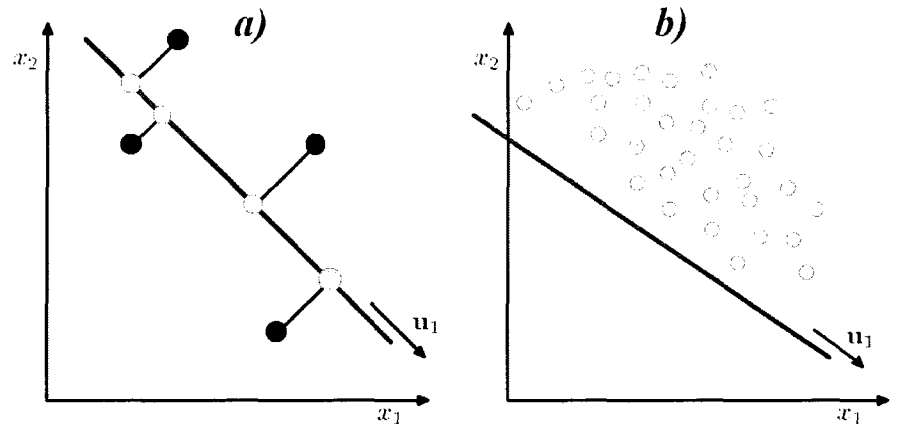

Figure 55. a) Orthogonal projection of the multivariate data into a new dimension. b) PCA maximizes the variance of the projected data

The principal components are presented in terms of D-dimensional unit vectors $\boldsymbol{u}_m$ ($\boldsymbol{u}^T \cdot \boldsymbol{u}$) so a single vector in the data set is projected to the first component as ($\boldsymbol{u}^T \cdot \boldsymbol{x}$), resulting in a scalar vale. The variance of the projected data is given by:

$$\frac{1}{L} \cdot \sum_{l=1}^{L} \{\boldsymbol{u}_1{}^T \cdot \boldsymbol{x}_l - \boldsymbol{u}_1{}^T \cdot \bar{\boldsymbol{x}}\} = \boldsymbol{u}_1{}^T \cdot \boldsymbol{S} \cdot \boldsymbol{u}_1 \tag{42}$$

The goal of PCA is to maximize (42) subjected to the constraint $\boldsymbol{u}_1{}^T \cdot \boldsymbol{u}_1 = 1$. This is done by finding the eigenvectors of $\boldsymbol{S}$:

$$\boldsymbol{u}_1{}^T \cdot \boldsymbol{S} \cdot \boldsymbol{u}_1 = \lambda_1 \tag{43}$$

As a result, the variance will be at its maximum when choosing the eigenvector $\boldsymbol{u}_1$ corresponding to the largest eigenvalue λ_1. The vector $\boldsymbol{u}_1$ is the first principal component.

Therefore PCA can be used to reduce the dimension of the original data (from D to M). Thus, the optimal M-dimensional linear projection that maximizes the variance of the projected data is given by the eigenvectors $\boldsymbol{u}_1, \boldsymbol{u}_2, \ldots, \boldsymbol{u}_M$ of the covariance matrix $\boldsymbol{S}$ corresponding to the M largest eigenvalues $\lambda_1, \lambda_2, \ldots, \lambda_M$.

6.2. Feature Projection Methodology

6.2.1. Datasets

The feature set obtained in Section 4.4.2 was used to evaluate two feature projection frameworks. The full wavelet decomposition of the original EMG segment provided information from 9 frequency bands per channel. Seven recording channels were combined, resulting in a feature vector of dimensionality $D_8 = 63$. The complete dataset contained 400 training samples and 100 testing samples (typically) of each of the five classes.

A second dataset of reduced dimension was created not only to analyze the performance of the PCA projection framework but also to compare its performance with the original dataset. Since the MES was high-pass filtered, the sub-bands corresponding

to the lower frequencies may have information that is not relevant (last four frequency intervals in (Table 2). This second feature set was created by performing 4 levels of wavelet decomposition, which provided information from 5 frequency sub-bands. The number of wavelet coefficients obtained for each sub-band was reduced by taking the average energy for each recording channel. Finally, the five DWT features of each channel were aggregated into a 35-dimension embedding feature vector for D_4.

PCA was applied to both D_8 and D_4 dimensional wavelet feature sets in order to find a new coordinate system for projecting the data. The resultant orthogonal coordinates are organized in such a way that the first coordinate contains the highest variance of the training data and the last coordinate the smallest variance. Figure 56 illustrates a general scheme of the PCA implementation. Samples from each class are merged into a training matrix. After all the points are projected to the new space, the first M most significant dimensions are used to train the model.

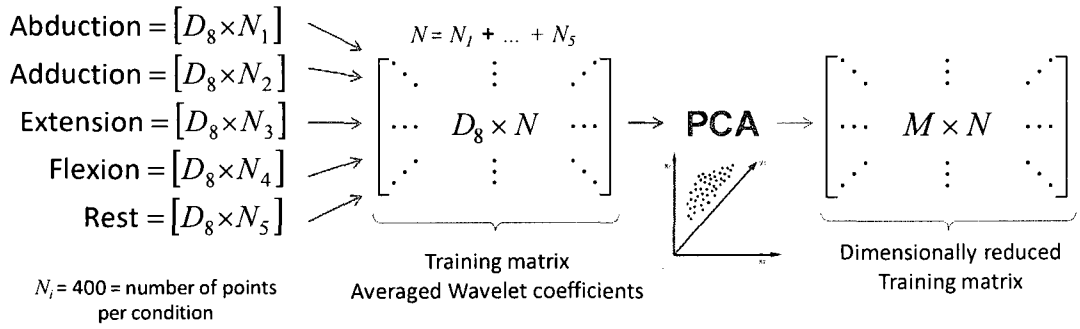

Figure 56. Representation of the feature projection method. The original feature set is projected to a new feature space using PCA. The first M most significant dimensions are used to train the SVM classifier

Since the solution for the multiclass classification problem is approached by training multiple binary classifiers, two different methods involving PCA are

implemented for projecting the data before the training stage and their performances are compared in terms of both classification accuracy and processing time. These two methods are presented in the next two Sections.

6.2.2. One PCA

In the one PCA method, a single feature space is associated with the DAG signal classification tree that contains the ten binary classifiers (Figure 57). All data is merged into a single training matrix consisting of 2000 data points (5 classes, 400 points per class). After the new feature space is found, each point in the training set is linearly projected before training the entire set of binary classifiers. As a result, a point in the testing set is projected to the same feature space before going through the decision path in the classification tree.

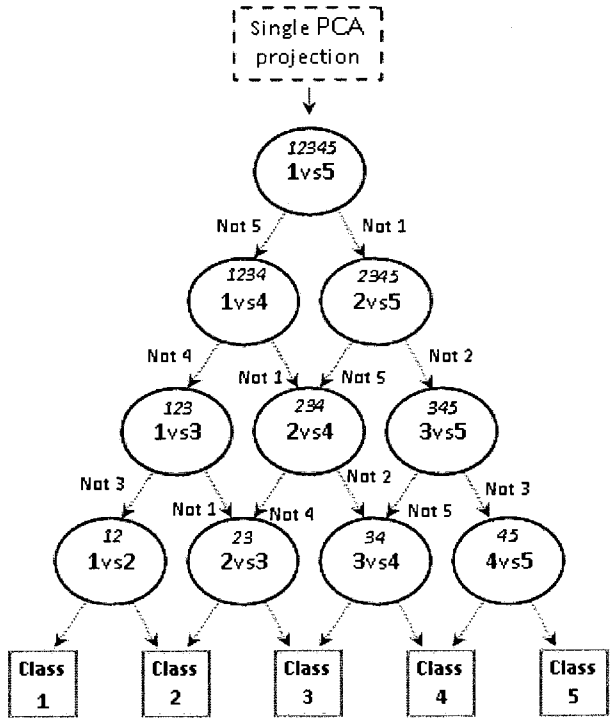

Figure 57. One PCA (oPCA) method project the input point into a new feature space before making the class decision through the DAG graph.

6.2.3. Multiple PCA

In the multiple PCA method, one feature space is associated with each binary decision node (Figure 58). Each space is found by combining the data points corresponding to two of the classes and applying PCA. As a result, a point in the validation set is projected to the corresponding feature space before entering each decision node.

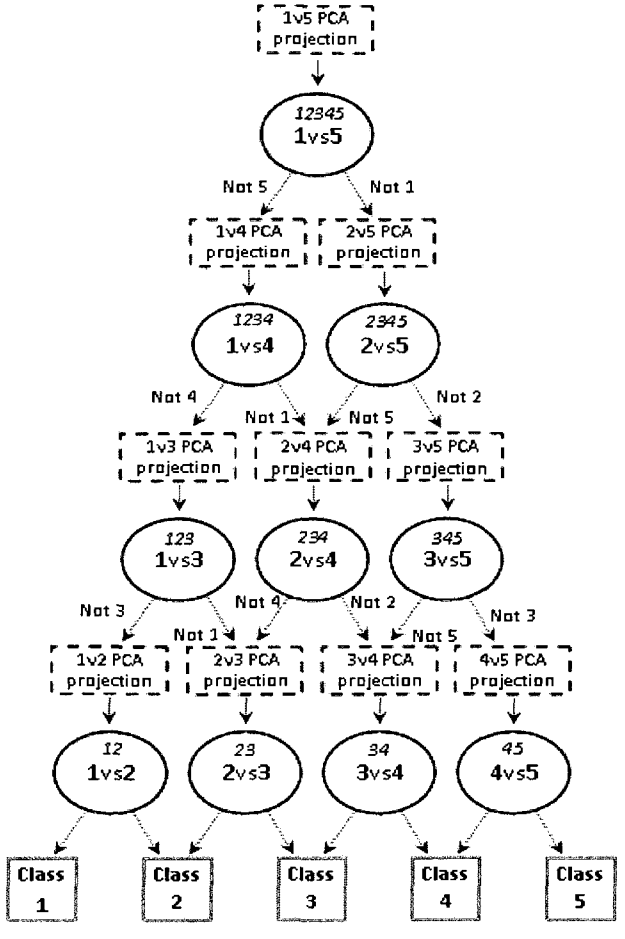

Figure 58. Multiple PCA (mPCA) method projects the input point into a new feature space before reaching each node of the decision path.

From this point forward, the single PCA projection method will be referred to as oPCA and the multiple PCA projection method will be called mPCA. Data from the second recording session (randomly chosen) was used to evaluate the performance of the classifier trained with the projected features as well as to decide on the appropriate reduced dimension M for both oPCA and mPCA feature sets that does not jeopardize the performance of the myoelectric pattern recognition system. Finally, in order to incorporate potential variations of the electrode placement at the recording sites, EMG data collected during six different sessions was progressively added to the training set. Consequently, one SVM classifier was trained on each session using data from all previous sessions which were projected into the new feature space by either oPCA or mPCA. The improvement in classification accuracy was evaluated as more data were added to the training set as well as the time required for classifying a single instance. For each feature projection framework, one set of classifiers were trained using the feature vectors projected but not reduced in dimension and another using the feature vectors subjected to dimensionality reduction. The classification accuracy for the SVM classifier, trained with the features in the wavelet domain and without projection, was denoted as the baseline

6.3. Feature Projection Results

6.3.1. Finding the Best Reduced Dimension

The feature projection frameworks implemented in this study were compared to determine the appropriate number of dimension that could be reduced without risking both the classification accuracy and processing time of the decision-making stage. Accuracy was defined as the number of correctly classified points over the total number

of points in the test set. The processing time included the time required to classify the test point using either the oPCA framework (Figure 57) or the mPCA framework (Figure 58).

When oPCA and mPCA were applied to the original D_8 vector, no significant difference in accuracy was found, whereas a greater delay was found when using mPCA. Figure 59 and Figure 60 illustrate the classification and processing time results of the testing stage for different dimensions. The reduction in the dimension of the training vectors obtained with oPCA and mPCA methods was associated with a reduction in the classification accuracy (Figure 59). In both cases, the best fit for the data was given by a logarithmic function ($R^2 = 0.985$ for oPCA and $R^2 = 0.9803$ for mPCA). On the other hand, one-way ANOVA in combination with multiple comparison test indicated that more time was required for classifying a single instance using mPCA than either oPCA or DWT features ($p < 0.05$) (Figure 60). Between oPCA and DWT features, the processing time for DWT was significantly lower in most dimensions beyond 18 ($p < 0.05$).

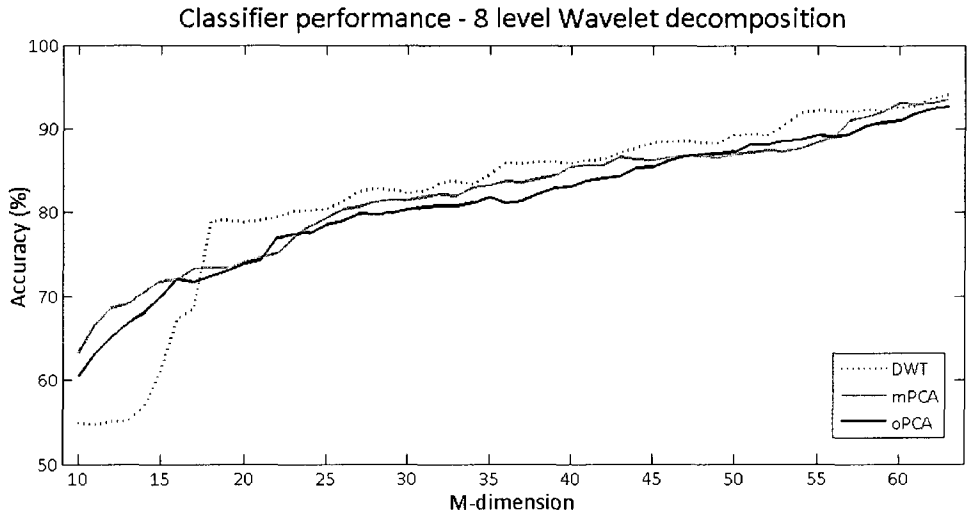

Figure 59. Classification accuracies averaged across all subjects. The classifiers were trained with 8-levels wavelet features that were projected using either oPCA or mPCA methods. The dashed line represents the baseline results. No significant difference in the accuracy values was found for all M dimensions

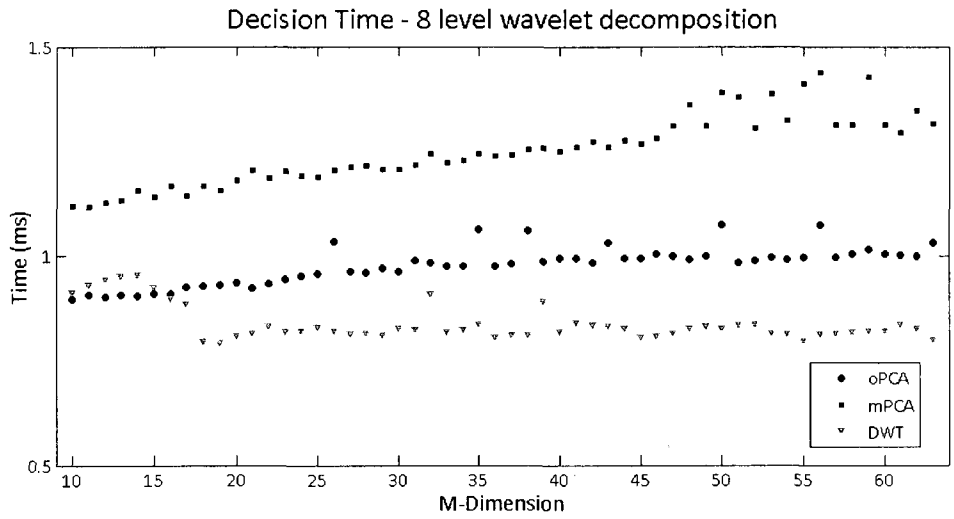

Figure 60. Average time required for the processing of a single data point in the decision stage using 8-levels wavelet features. The baseline time (DWT features) is the lower than the mPCA time in most of the dimensions (One-way ANOVA, $p < 0.05$).

Similar results were observed when oPCA and mPCA where applied to the feature vector D_4. No significant differences in accuracy were found between the two projection methods and between each one of them and the baseline (Figure 61). The reduction in the dimension was also accompanied by a reduction in the classification accuracy (best fit: logarithmic function, $R^2 = 0.9589$ for oPCA and $R^2 = 0.9794$ for mPCA). Regarding to the processing time, oPCA features and DWT features presented equivalent results ($p < 0.05$) but the time required to classify mPCA features was higher than for classifying baseline features (Figure 62). Between mPCA and oPCA features, the processing time was higher for the former than for the latter in most of the dimensions (One-way ANOVA, $p < 0.05$).

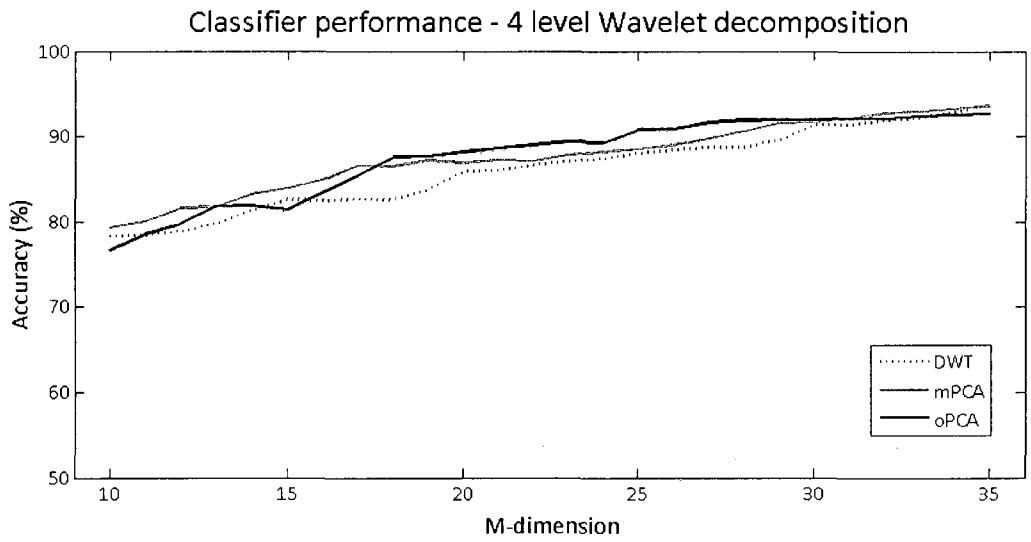

Figure 61. Classification accuracies obtained for the classifiers trained with 4-levels wavelet features and projected using either oPCA or mPCA methods. No significant difference was found along all M dimensions

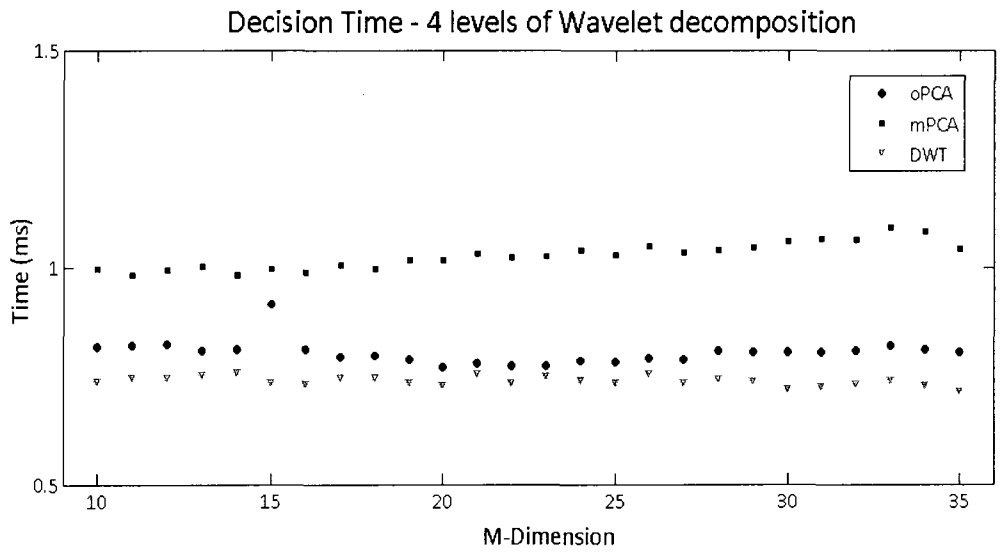

Figure 62. Average time required for the processing of a single data point in the decision stage using 4-levels wavelet features. No significant difference was found between the baseline time (DWT features) and oPCA times. Baseline time is the lower than the mPCA time in dimensions beyond 16 (One-way ANOVA, $p < 0.05$).

To determine the number of dimensions that can potentially be reduced, the classification accuracy for every dimension was statistically compared with the classification accuracy of the non-reduced vector (D_8 or D_4). For 8-levels wavelet decomposition, a maximum of 16% and 12% in data dimension can be reduced without significant drop in the accuracy using oPCA and mPCA, respectively ($p > 0.05$ in both cases for a t-test). A more interesting result was found when combining the 4-levels wavelet decomposition feature vector and the oPCA method. Up to 49% of data dimension can be reduced without considerable drop in the classification accuracy (t-test, $p > 0.05$), which suggested that 18 dimensions could be used to train the SVM model. Table 17 summarizes the dimensionality reductions that are suitable for each method (rows) and for each feature extraction technique (second and third big columns).

Table 17. Reduced dimension implemented the electrode displacement experiment

REDUCED DIMENSION SELECTED				
Feat. Proj. framework	**4 levels** From D_4=35 to	% of dim. Reduction	**8 levels** From D_8=63 to	% of dim. Reduction
oPCA	*18*	48%	*53*	16%
mPCA	*24*	32%	*55*	12%

The classification accuracies obtained for the feature vectors D_8 and D_4 that were projected using both frameworks but not dimensionally reduced were also compared (Table 18). No statistical differences were found in the oPCA framework as well as in the mPCA framework and the baseline (no feature projection). These results may indicate that dimensionality the original D_8 feature vector (Section 4.4.2) could be reduced

stopping the wavelet decomposition at the fourth level instead of going to the deepest level (level 8). The processing time is significantly reduced between D_8 and D_4 in both of the PCA frameworks and in the baseline scheme.

Table 18. Classification accuracies for the baseline and the two PCA frameworks

AVERAGE CLASSIFICATION ACCURACY		
Framework	**4 levels *(M=D₄=35)***	**8 levels *(M=D₈=63)***
DWT (baseline)	93.84% (± 3.64%)	94.092% (± 3.75%)
oPCA	92.67% (± 4.77%)	92.645% (± 3.17%)
mPCA	93.60% (± 4.04%)	93.459% (± 3.88%)

6.3.2. PCA and the Electrode Displacement Effect

Based on the results observed in the previous Section, the performances of the classifiers were examined using the reduced dimensions as presented in Table 17. The main goal was to evaluate the improvement of classification accuracies and processing times of the SMV models as more data were added to the training set. These results suggested whether the PCA projection methods would cause a significant improvement in the performance of the pattern recognition-based myoelectric control system proposed in this study.

The oPCA and mPCA methods applied to the D_8 feature vector were compared with the baseline. For oPCA, classification accuracies for both the reduced ($M = 53$) and the original ($D_8 = 63$) feature vectors showed the same trend as the baseline (Figure 63). There was a sudden increase in accuracy when the data from the second session were

incorporated into the training set. This suggests that the variability introduced by data from sessions 1 and 2 was captured by the SVM classifier. For the mPCA method, the classifier performance was steadily improving as more data were added to the training set (Figure 64). The projected feature vector without dimensionality reduction (D_8) presented an almost identical behavior to the baseline. After the second session of recordings, the session-to-session increment in accuracy was not significant $(p > 0.05)$ for both the reduced ($M = 55$) and the non-reduced ($D_8 = 63$) feature vectors. The dimensionality reduction performed by any the two frameworks did not significantly improve in the classifier performance $(p>0.05)$.

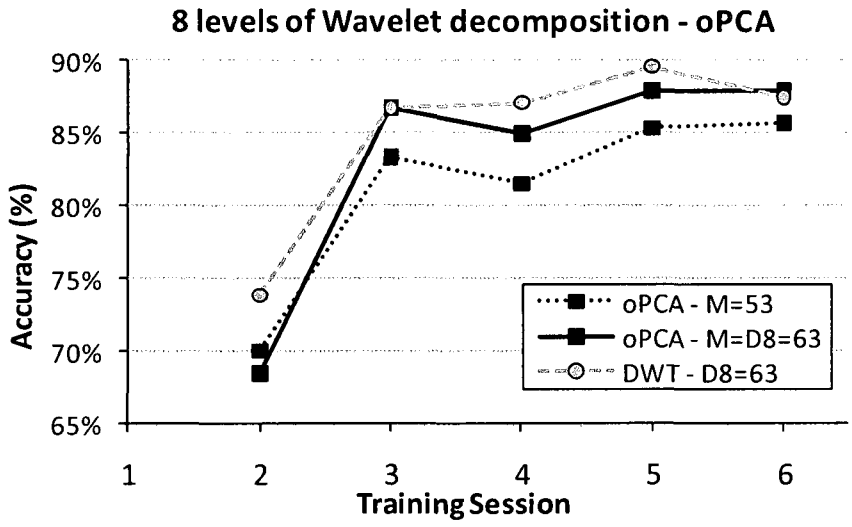

Figure 63. Classification accuracy on the test set averaged across 6 subjects. The training set contained features from 8 wavelet decomposition levels and projected using oPCA. The best performance was achieved when the features were not reduced in dimension.

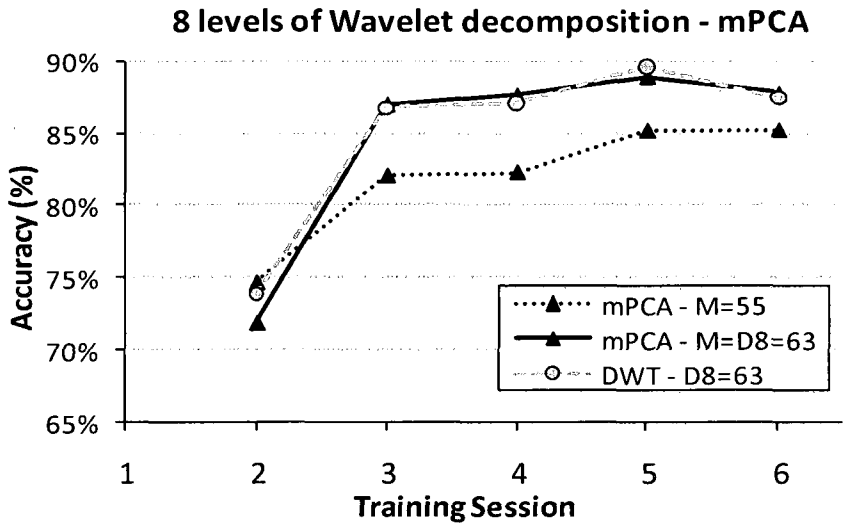

Figure 64. Classification accuracy on the test set averaged across 6 subjects. The training set contained features from 8 wavelet decomposition levels and projected using mPCA. An increasing trend was observed when data from different sessions was added to the training set. The best performance was achieved when the features were not reduced in dimension.

Similar results were observed when comparing oPCA and mPCA with the baseline for a 4-levels decomposition (Figure 65 and Figure 66). After the training set was projected onto the new feature space using oPCA, the classification accuracy indicated a better performance without feature reduction ($D_4 = 35$) than with reduced features (Figure 65). There was a significant increment in accuracy $(p < 0.05)$ when data from the second session was added to the training set but no significant change afterwards $(p > 0.05)$. On the other hand, classification accuracies for mPCA are similar to oPCA (Figure 66). The original feature set resulted in higher accuracy than the reduced set. In both frameworks, there were not major differences in the performances of the SVM classifiers when compared with the baseline.

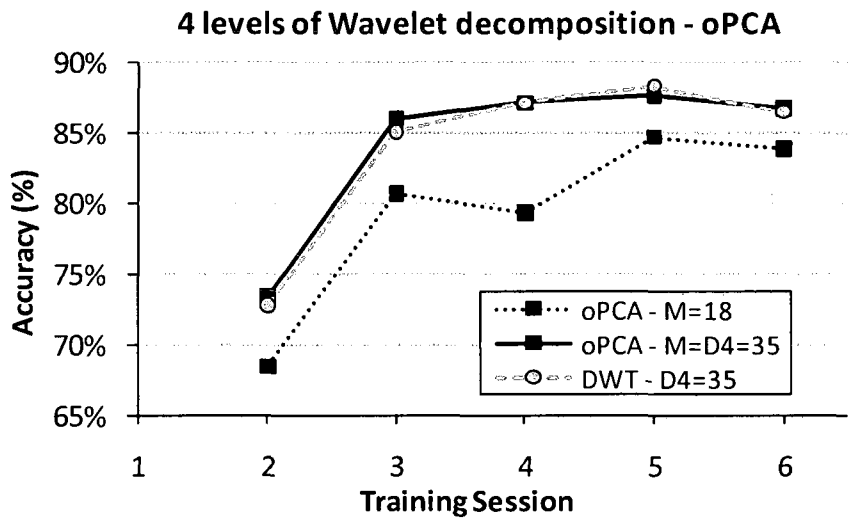

Figure 65. The signal classification accuracy was evaluated when the features from 4 levels of wavelet decomposition from each recording session were added to the training set. The projection and dimensionality reduction of the features using oPCA framework did not significantly improve the performance of the baseline classifier

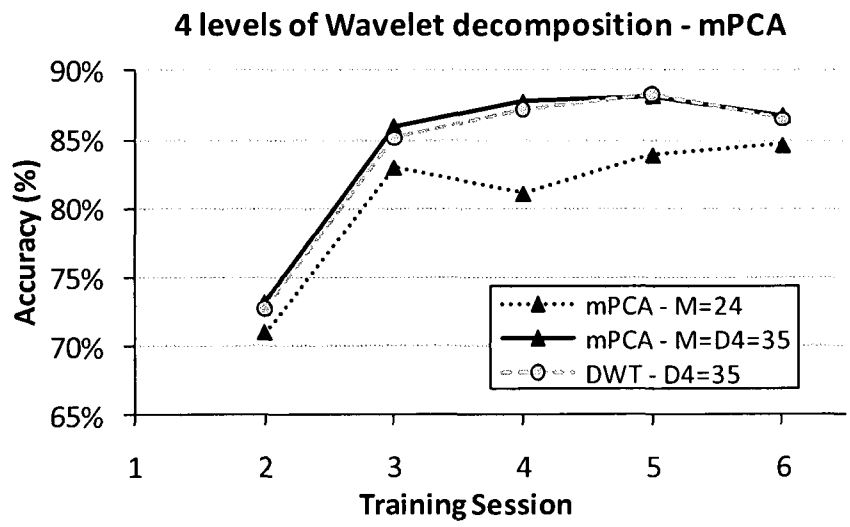

Figure 66. Improvement in the average classification accuracy when the features from 4 levels of wavelet decomposition from each recording session were added to the training set. The mPCA feature projection framework did not improve the performance of the baseline classifier.

The time required for classifying a single trial when its features were projected with either oPCA or mPCA were compared in order to determine their feasibility for real-time implementation. Results for 8-level and 4-level wavelet decomposition features are illustrated in Figure 67 and Figure 68, respectively. The processing time for a single trial without feature projection is presented as the baseline. For D_8 features, the time it took to classify the baseline features was lower than it took to classify oPCA or mPCA features (Figure 67). In addition, less time was needed to classify test data without dimensionality reduction. A possible reason for this behavior was that the complexity of the SVM model (number of support vectors) increased after the training stage when lower dimensionality was used. This result suggested that there was a tradeoff between the number of dimensions reduced and the model complexity. For D_4 features, no major differences in the decision time were obtained in all cases (Figure 68). The PCA feature projection frameworks implemented did not expedite the final processing time.

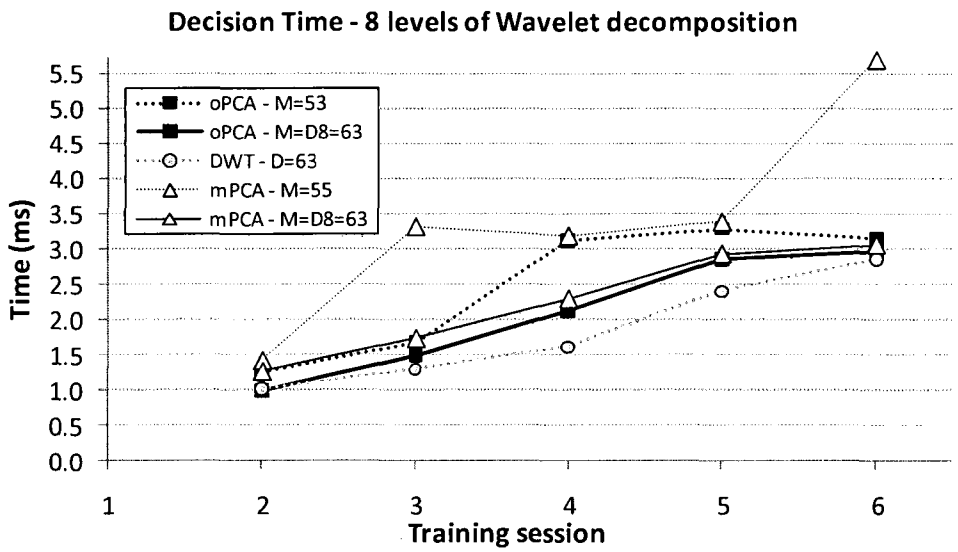

Figure 67. Time required to classify a single data point containing information from an 8-level wavelet decomposition. In both feature projection frameworks, oPCA and mPCA, the reduction in the dimension increased the processing time.

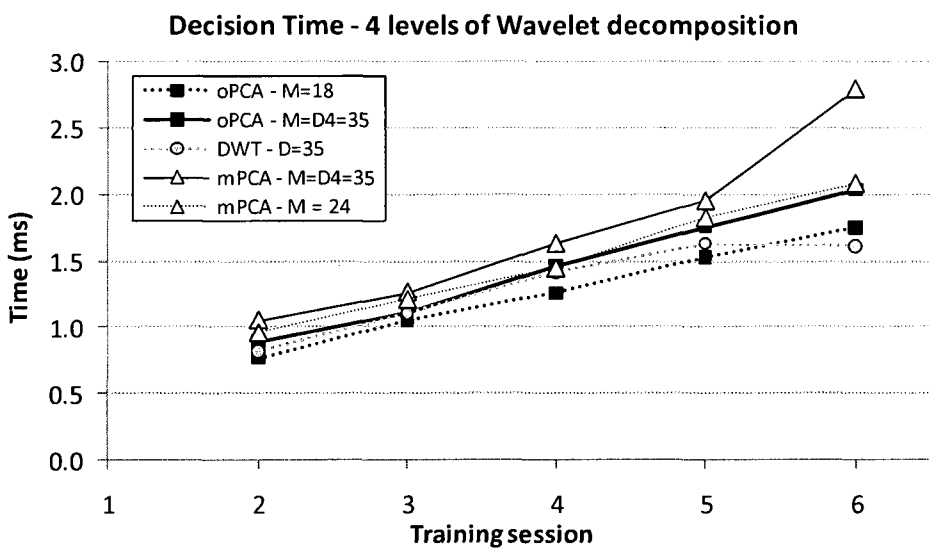

Figure 68. Time required to classify a new vector containing information from 4 levels of wavelet decomposition. A linear trend is observed when the features are projected and reduced on both PCA frameworks.

6.3.3. Four vs. Eight Levels of Wavelet Decomposition

The classification results for the two sets of features obtained using 4 and 8 levels of wavelet decomposition were evaluated. The performances of both methods were similar without dimensionality reduction. After the testing stage, the dimension of the training set was gradually decreased and a new classifier was trained. This procedure was repeated until the averaged accuracy dropped below an acceptable level (i.e. < 80%). Figure 69 illustrates the baseline classification results. For the classifiers trained with 8 levels of wavelet decomposition ($D_8 = 63$), the accuracy presented a slower trend for $M > 18$ with a considerably drop for $M < 18$. On the other hand, the behavior of the classifier trained with 4 levels of decomposition ($D_4 = 35$) was approximately linear for the entire range.

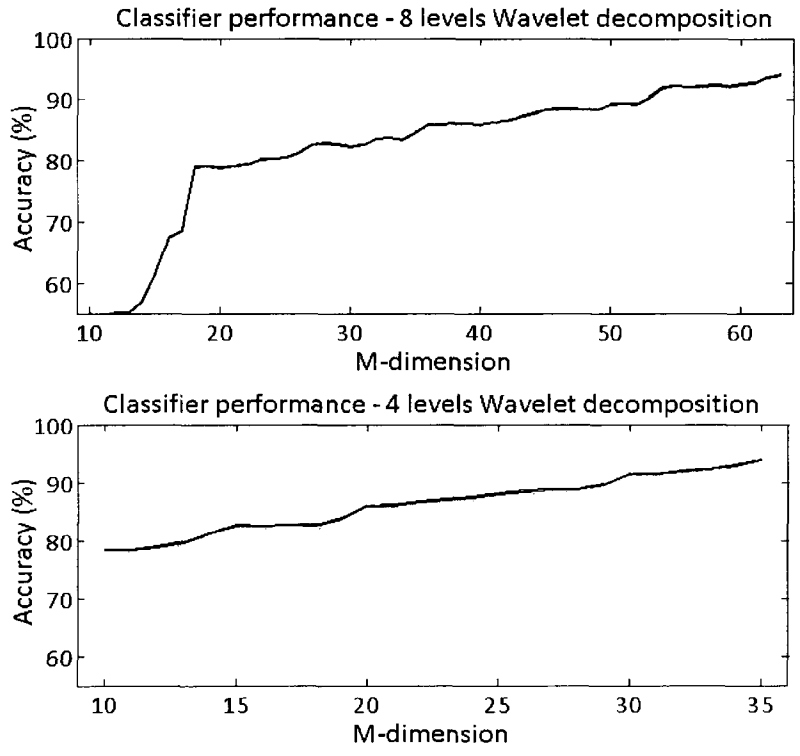

Figure 69. Averaged accuracies obtained on the test data, when the classifiers were trained using 8 (top) and 4 (bottom) levels of wavelet decomposition.

An interesting result was observed when the dimensions of the feature vectors were not reduced. No significant differences were present in the performance of the classifiers trained with $D_8 = 63$ and $D_4 = 35$ ($p > 0.05$). The average classification accuracy was 94.09% for the D_8 feature vector and 93.84% for D_4. However, the dimension reduction of the 8-level training vectors from $D_8 = 63$ to $M = 35$ significantly reduced the classification accuracy. These results suggested that wavelet decomposition beyond the fourth level is unnecessary because it does not significantly improve the classification.

6.4. Discussion

Uncorrelated features from either oPCA or mPCA methods did not improve the discriminatory power. This result is supported by a lack of statistically significant improvement in the performance of the SVM classifier when using any PCA framework. Moreover, the classification accuracy was reduced when the dimension of the projected features was reduced. This behavior may be related to the location of the recording channels. The muscles in the forearm are closely spaced, so a signal recorded from the surface may have contributions from more than one muscle. When a contraction is produced, the spatial propagation of the action potentials may lead to correlated signals at different recording sites. A previous study used PCA to remove the correlation present on the raw MES recorded from electrodes circumferentially located around the apex of the forearm muscle bulge and showed an improvement in the classification accuracy [102]. In the present study, the electrode locations were meticulously selected so that the recordings were not strongly dependent on each other. As a result, the redundant

information collected and decoded by wavelet transformation was reduced; no significant improvement can be made using the PCA frameworks.

A one-way ANOVA test was performed at each reduced dimension to compare the computation times (Figure 60 and Figure 62). A significant difference was observed between mPCA and the baseline, regardless of decomposition level at sufficiently high feature dimensions $(p < 0.05)$. Internal processes of the computer may have delayed the computation and caused the outliers. For 4-level wavelet features, D_4, no significant difference was found between the processing times of oPCA and the baseline $(p > 0.05)$, except for an outlier at $M = 15$. For 8-level features, D_8, computation time for the baseline, beyond 18 feature dimensions, is faster than that of the oPCA $(p < 0.05)$. The mPCA has a longer delay, most likely because it calculates a new projection at each decision node in the DAG path, whereas the oPCA calculates the projection only once. In addition, the processing time for classifying a single point was not significantly decreased when the dimensionality of the data was reduced.

Finally, both PCA frameworks were applied on wavelet features representing data from different recording sessions for evaluating the classifier performance. It was shown in Section 5.4.3 that the SVM classifier achieved 90% accuracy after three training sessions when using features obtained with 8-levels wavelet decomposition [95]. The dimensionality reduction of the D_8 feature vector did not significantly change the classification performance. The accuracy was lower for the reduced feature vectors and the processing time was slower. The same results were observed for the reduced D_4 feature vector, which did not significantly change the processing time. These results suggest that oPCA and mPCA did not improve the ability of SVM to capture the

variations in the EMG patterns. Both oPCA and mPCA projection of D_8 or D_4, without reducing their dimensions, improved the classification accuracy in the recording sessions to a level that was almost identical to the baseline accuracy. The processing times were also extremely close to the baseline time for both feature vectors. These results suggest that the effect of electrode placement variations can be generalized.

The experiments performed to evaluate the potential implementation of two PCA methods showed that these frameworks did not significantly improve the performance of the baseline classifier. Additionally, the reduction in dimension of D_8 from 63 to 53 (35 to 18 for D_4) in the case of oPCA, and from 63 to 55 (35 to 24 for D_4) in the case of mPCA, was not significant.

An interesting result from these experiments that was not related to PCA presented an alternative method to reduce the dimensionality of the feature vector. The performance of the myoelectric pattern recognition system using 8-level wavelet features can be improved by decoding information from the raw MES using 4-level wavelet decomposition. The 4-level decomposition would require less computation time without significantly reducing the classification accuracies obtained for both feature vectors. The similar accuracy for 4-level and 8-level decompositions arises because the wavelet coefficients corresponding to the levels 5 to 8 did not add useful information to the feature vector. The frequency band represented by the approximation coefficients after 4 resolution levels is 0-30 Hz. This frequency is not relevant, as most of the information of the muscle contractions selected for this application exceeds 30 Hz. The classification process using D_4 was less computationally intensive than using D_8, making it more suitable for real-time implementation.

CHAPTER 7

CONCLUSION AND FUTURE WORK

7.1. Conclusion

A myoelectric control system that classifies a user's intention to actuate different functions of a prosthetic hand has been developed and tested. A pattern recognition-based controller was chosen over a conventional controller because it allows multifunction control (more that 2 degrees of freedom) to be performed without the constraint of independent muscle sites. By discriminating different muscle contraction patterns, the prosthetic device can be actuated in a more intuitive manner.

Surface EMG signals were classified with an SVM implemented, as a DAG that used 63-dimension wavelet features from seven channels. Single session results obtained from seven able-body subjects have showed that classification could be up to 98.2% accurate. This value was similar to results from other studies [16, 140, 150]. However, these models did not accommodate small changes in the user's patterns over time, which caused a significant drop in the classification accuracy. To increase the robustness of the models, EMG data from different recording sessions were incorporated to the training dataset to account for the variations in the user's signal patterns. The high generalizability of the SVM captured most of the variability in the data after the second recording session and produced an average 90% classification accuracy for new data points. A plateau in the classification accuracy was reached after the third session. Even though the accuracy

dropped with respect to the single-session classifiers, the results were promising since the new training strategy yielded a more robust classifier. The real-time processing of the whole control system introduced a delay of only 20 ms, which was much lower that the acceptable delay of 300 ms. This time is counted from the onset of the muscle contraction until the final class decision is made. The small processing time allows several class decisions to be combined to improve the performance of the system.

Two PCA feature projection frameworks were implemented in an attempt to improve the classification accuracy and to expedite the processing time. In both cases, the features embedded in the wavelet domain were linearly projected into a new coordinate system for further dimensionality reduction. These frameworks did not introduce significant improvement in the classification accuracies when compared with the baseline study. In addition, both frameworks introduced additional delays that contributed to prolonging the overall processing time. These results suggested that carefully selected EMG channels are highly uncorrelated; hence, there is no need for PCA.

The results from this work show that a myoelectric pattern recognition-based control system that uses an SVM classifier applied to time-frequency features can be used to discriminate a set of limb motions for prosthetic applications.

7.2. Ongoing and Future Work

7.2.1. Current Tests on Amputees

Even though the proposed control system was able to classify five limb motions of normally-limbed subjects, its ability to discriminate the activation patterns of amputees' muscles remains to be tested. Classification tests are being performed in the laboratory to demonstrate the feasibility of the control system in amputees. Two very-

short below elbow congenital amputees were recruited for signal recording. As the recording locations selected for normally-limbed subject were not available in these cases, the seven bipolar channels were located according to the available musculature. For subject 8, electrodes were circumferentially located around the upper arm, and for subject 9, they were also circumferentially located but around the residual forearm. Figure 70 illustrates the layout of the cross-sectional and lateral views of the electrode placement for both cases. The recording channels were uniformly distributed on the recording region.

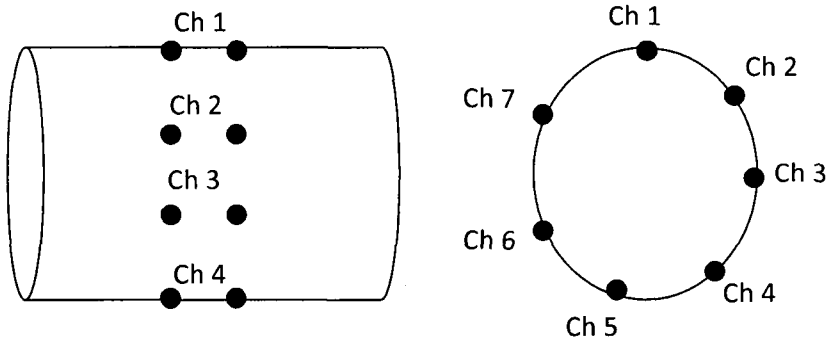

Figure 70. Left: analogy for the lateral view of a residual limb used to illustrate the distribution of the bipolar channels. Right: analogy for the cross sectional view of the residual limb. Seven bipolar channels were distributed with equidistant separation among them.

The methodology followed to obtain the training set was the same as in able-bodied subjects. The signals recorded were segmented into non-overlapping 256-point windows, and the DWT was applied to each segment to obtain the feature vectors. SVM classifiers were tested to discriminate five different classes of motion. Preliminary results showed an averaged accuracy of 92% for a classifier created with single-session data. The performance of classifiers trained with multi-session data is being assessed.

Successful results on those classifications would produce an important advance to the final implementation of the myoelectric pattern recognition-based control system.

7.2.2. Future Improvements for Clinical Trials

Although the classification accuracy obtained in this work was acceptable (around 90%), there is an obvious motivation to increase that value as much as possible. The usability of the myoelectric control system would be enhanced by increasing the accuracy. However, it is important to perform clinical trials to find a threshold for this classification accuracy that is acceptable for prosthetic actuation. Several steps need to be accomplished before the pattern recognition system can be tested on the field:

- *Implement the real-time post-processing strategy.* In the real-time scheme presented in Section 5.5.1, every class decision represented an output of the system. This strategy is susceptible to short-time involuntary contractions that should not be considered for classification. To create a more robust real-time processing strategy, the class decisions would be made based on a sequence of successive output states. The class with greatest number of occurrences would represent the output of the system. This new strategy would also reduce the misclassification rate produced in the areas where changes of muscle contraction types are produced.
- *Implement the myoelectric control system in a microcontroller.* Clinical trials would investigate the performance of the control system over days or months. While these tests are being performed, the subjects involved must be able to continue with their daily living activities. Even though the initial recording sessions and the classifier training can be performed in the lab, all pattern

recognition stages (signal acquisition, processing and classification) must be embedded into a single external device. A feasible option is a digital signal processor (DSP), which is a specialized microprocessor that is optimized for fast computation of mathematical operations. The DSP can digitize analog EMG signals and perform all the operations involved in the pattern recognition scheme to produce the class output necessary to activate the prosthesis. The DSP can include the SVM classifier and store the support vectors and their corresponding class labels. Each data point is classified through the necessary matrix operations that compute the function $y(\boldsymbol{x})$ from Equation (29) (page 72).

One of the most important constraints is related to the physical dimensions of the board designed for the DSP. It should be small enough to be embedded inside a socket specially designed for the trials.

- *Design a prosthesis socket that can hold seven bipolar channels.* The final step towards the clinical tests of the proposed work is the design of the prosthetic socket. The seven bipolar electrodes and the electrical wires must be strategically distributed on it to allow the recording of activity of specific muscles. The DSP device may also be located on the socket or embedded in the hand prototype. The socket has to be custom made to pick up the signals from the appropriate locations so a successful classification can be achieved. In addition, this customization would create a better fit between the residual limb and the prosthetic device allowing as much function of the residual limb as possible.

To conclude, one of the principal limitations of this type of control system is the lack of robustness in processing the input myoelectric signal to select the output action. The ability of SVM to generalize was important to capture the variations in the muscle contraction patterns over time caused by electrode displacements. However, these variations may also be caused by either electrophysiological changes (muscle fatigue) or electrode conductivity changes (perspiration). An important improvement for this work would take those factors into account to design a myoelectric patter recognition system that adapt to most of the changes on the user's patterns over time.

APPENDIX A

EMG DATA ACQUISITION PROTOCOL

This appendix presents the protocol designed to record Electromyographic (EMG) signals from the surface of the skin. It was approved by the IRB for implementation.

Materials

- Disposable Ag-AgCl surface electrodes.
- CleveMed BioRadio 150 wireless programmable Data Acquisition System (DAQ), with the following specifications:
  - RF band: 902-928 MHz (ISM band) or 2.4-2.484 GHz.
  - Transmission range: ~100 feet.
  - Number of channels: 8 configurable channels (external sensors) and 4 embedded channels.
  - Resolution: 8, 12, 16 bits.
  - Sampling rate: 128 - 960 samples per second per channel (configurable).
- Matlab and LabVIEW software installed in either a Desktop or a Laptop computer.
- Abrasive skin gel for skin cleaning purpose.
- Conductive gel.

Procedure

EMG signals were recorded from 7 locations over the skin's surface using disposable Ag-AgCl electrodes. The subject was asked to perform four different isometric muscle contractions. The procedure required for the data collection is presented in the following subsections:

1. Movement Selection

The following four movements of the wrist were asked of the subject to perform:

- Wrist abduction (radial deviation of the wrist).
- Wrist adduction (ulnar deviation of the wrist).
- Wrist extension.
- Wrist flexion.

In addition to them, the subject was asked to maintain the forearm in a relaxed position besides his/her body as well as to uphold the forearm during a certain period of time.

2. Skin Preparation

- The skin was cleaned with an abrasive skin gel. It was applied to the electrode site by using a gauze pad and by rubbing the gel into the skin surface. The excess of gel was removed using clean gauze.
- A small amount of conductive gel was applied to the electrode site in order to improve signal conductivity of the electrode–skin interface
- After the skin was prepared, the next step was to positioning the patient in the starting posture. It allowed determining the proper site of the electrode on the muscle. For these recordings, the subject was seated on a chair with the arm resting besides the body. Then he/she performed different movements with the wrist and fingers to identify the muscles.

3. Electrode Placement

General considerations

The surface EMG (sEMG) sensor location is defined by the SENIAM project [173] (Surface Electromyography for the Non-Invasive Assessment of Muscles) as the position of the center of two bipolar electrodes on the muscle. For this protocol, because unipolar electrodes were readily available, a pair of them was placed to obtain a bipolar recording. The recommendations given by the SENIAM project were as follows:

- The electrode size in the direction of the muscle fiber has to be less than 10 mm.
- The inter-electrode distance, defined as the center-to-center distance between the conductive surfaces of two electrodes, has to be around 20 mm.
- The bipolar electrodes must be oriented parallel to the muscle fibers.
- The reference electrode must be placed in one of the standard locations. In this case, it was placed on the wrist at the styloid process of the ulna (bone end).

Seven electrode locations were used for this experiment. They were distributed along the following forearm muscles: Extensor Carpi Radialis, Extensor Digitorum, Anconeous, Flexor Carpi Radialis and Flexor Carpi Ulnaris (Figure 71).

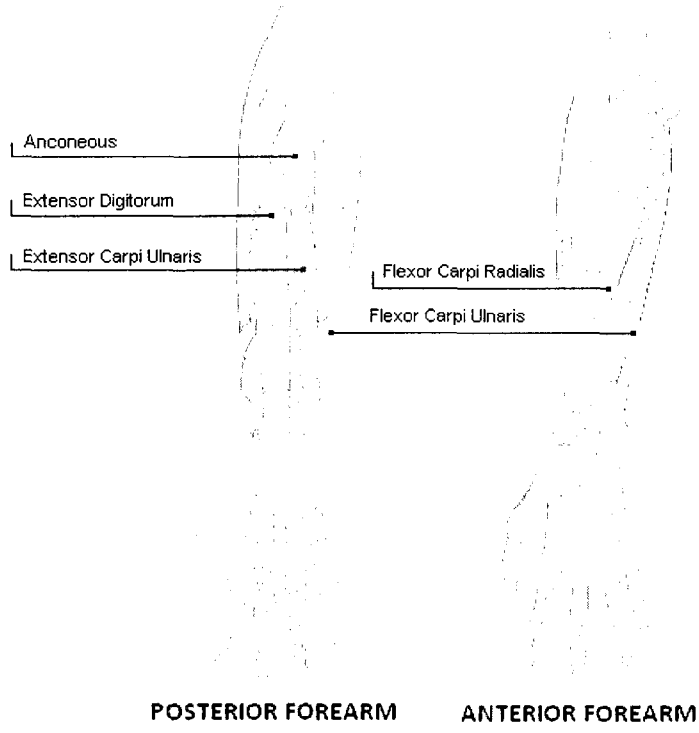

Figure 71. Location of the forearm muscles selected for EMG signal recording.

Channel identification

To identify the sensor location and to place the electrodes, the subject performed different actions, which are explained in the next paragraphs.

Channel 1 - Extensor Digitorum: To identify this muscle, the subject was asked to sequentially extend and flex the index, middle, ring and small fingers. A muscle activity can be detected in the posterior forearm, which corresponds mostly to the Extensor Digitorum muscle. After the muscle was found, pair of electrodes was placed at 40% of the line extended from the elbow to the wrist articulation.

Channel 2 & 3 - Flexor Carpi Radialis: The subject was asked to perform wrist flexion while applying pressure to the hand in the direction of the wrist extension. That action caused a contraction of the Flexor Carpi Radialis that can be detected by placing

the hand over the surface of the anterior part of the forearm. Two pair of electrodes were placed on this muscle, one at 25% of the origin of the muscle (medial epicondyle of the Humerus) and at 50% of the origin.

Channel 4 - Flexor Carpi Ulnaris: The same movement performed to identify the Flexor Carpi Radialis muscle was done for finding the electrode location for this muscle. A pair of electrodes was placed at around 40% of the line extended from the origin of the muscle to the end. It corresponded with the thickest cross section of the muscle

Channel 5 - Anconeous: The subject to both flex and extend the forearm at the elbow, continuously. That movement activated the Anconeous muscle, which can be detected by placing the hand over the surface of the skin close to the bone end of the ulna at the elbow.

Channel 6 & 7 - Extensor Carpi Ulnaris: After the ulna bone was identified, the subject was asked to perform an ulnar deviation of the wrist. Along with others muscles, that movement activated the muscle needed. It can be perceived by placing the hand over the forearm just above the ulna. Two electrode locations were used for this muscle. One was placed at around 30% of the line from the elbow to the wrist articulation. The other location was placed at around 60% of the same line.

4. Recording Process

The next steps were followed to set up the data acquisition system:

I. The BioRadio software was started and the Wireless Transmitter turned on.

II. After the 'Start' button was clicked, the connection between the Computer Unit and the Wireless Transmitter was checked.

III. The '*Config*' button was pressed to set up the data collection parameters. A new window pop up, and the following values were set:

- Sample Frequency: 960 samples per second
- Resolution: 12 bits.
- The boxes of the first seven channels were selected and AC voltage with a range of $\pm 1.5mV$ was set. All the other boxes were leaved unchecked.
- Click in the 'Program' icon and then close the window.

IV. On the '*DSP Settings*,' a High-Pass Filter was added for each one of the channels by clicking on the arrows on the DSP Method column. The filter was set to 2 and the cutoff frequency as 2.125 Hz. A Notch Filter (60 Hz) was also included for each one of the channels. After that, the DSP Filtering knob was switched to the 'on' position in the main window.

V. In the last step, a file was created to save the data that will be collected. After clicking on the 'Save Data' icon, the name of the new file and the folder location were selected. The file was saved as comma separated values ('.csv' extension). As a convention, the files corresponding to one subject were saved in a single folder called Subject#_date (e.g. if recorded from subject 3 on October 13th of 2008, then the folder was named S3_20081013). Inside that folder, the name of the file had the following format. Subjec#_Movement_Trial# (e.g. if collecting the second trial of recordings from subject 3 and he/she was performing the Adduction of the wrist, then the file should be called 'S3_Add_2.csv').

The entire protocol was divided in several subsections (trials). In each one of those, the subject was asked to perform isometric contractions, also called static contractions. It means that the subject started the specified movement and maintained it for the time required. That generated steady state EMG signals, which then were processed according to the needs. It is important to mention that there was no restriction regarding to the strength of the muscle contraction, the subject performed the movement as naturally as possible.

In each subsection of the protocol, EMG signals of one kind of movement were collected. The order of them was the following:

1. Wrist Abduction (Abd).
2. Wrist Adduction (Add).
3. Wrist Extension (Ext).
4. Wrist Flexion (Flex).
5. Relaxed position (Rest).
6. Uphold the forearm (RestUp).

The protocol of recording was the same for the first four movements and it was repeated as many times as needed depending on the amount of data required in the processing stage. The time between repetitions of the protocol was around 1 minute. The steps followed for recording signals when performing the first four movements is explained below:

a) The subject was sat on a chair with the arms in rest position beside the body.
b) The transmitter-receiver connection of the data acquisition system was started.
c) Three to four seconds were given before the contraction.

d) The subject was asked to perform the specific movement and to maintain the contraction for six seconds

e) The subject was asked to release the current contraction.

f) Steps c) to e) were repeated four more times.

Thus, the resultant signal contained 5 repetitions of the muscle contraction of six seconds length and spaced by three to four seconds intervals. It was saved in a file, which name followed the convention already explained.

For the rest data collection, the protocol was simpler. For the movement 5)

a) The subject was sat on a chair with the arms in rest position beside the body.

b) The transmitter-receiver connection of the data acquisition system was started.

c) 60 seconds of data were collected while the subject stayed in the rest position.

For the movement 6)

a) The subject was sat on a chair with the arms in rest position beside the body.

b) The subject was asked to lift the forearm at the shoulder's level and to maintain the contraction for at least 60 seconds.

c) 60 seconds of data were collected.

After collecting data from these two movements, the protocol was run again in order to increase the data available for further processing.

Security information

1. Instruments and measures to insure protection of confidentiality, anonymity

The researchers take great caution in maintaining a high level of confidentiality or anonymity of the research data. All documents will be handled only by the principal investigator and will be stored in a secure environment. All files will be coded with group

labels and numbers. Data files of any kind will not contain any personal information of the subject. Subject's identity will not be disclosed to any third parties. Only aggregate data will be presented for the public (articles, presentation, et al.)

2. Risk/Alternative treatments

Before a patient is accepted for EMG signal recording, it was necessary to perform an allergic test in order to determine any allergic reaction to the electrode or to the gel used to measure the signals.

Although the risk of micro shots is very low, it should be taken into account in order to ensure subject safety.

The muscle fatigue was considerate in the design of the recording time of this protocol.

3. Safeguards of physical and emotional well-being

Prior to the recording procedure, the researchers will inform the subjects in full details, the risk involved with the measurements. All information collected from the study will be held strictly confidential. No one will be allowed access to the recorded data except the authorized personnel.

APPENDIX B

MATLAB ALGORITHMS

The algorithms used in this dissertation have been included in an attached optical media. It also contains a database with the EMG signals recorded from the seven subjects studied. Al algorithms were implemented in Matlab (The MathWorks, Inc).

- For preprocess the raw signals and for the feature extraction stage:

Main program: '*EMG_Processing.m*'

Sub-programs used in the main program: '*hpf_emg.m*'; '*ploteo.m*'; '*start_end.m*'; '*onset.m*'; '*segmentation.m*'; '*normalization.m*' and '*wavelet_decomposition.m*'.

Main program synopsis: Program that initially takes the raw EMG signal from a single trial and perform the preprocess steps outlined in Sections 3.3 to 3.5. The program calls different sub-programs to filter, segment and normalize the data. The last step is the wavelet feature extraction that is carried out using the 'wavelet_decomposition.m' algorithm. The number of levels of decomposition was set to eight but it can be modified to perform different levels.

- For training and testing the SVM classifier:

The statistical pattern recognition toolbox (STPRTool) is an external Matlab toolbox that was used in this dissertation. Some machine learning functions, implemented in the selected toolbox, were embedded in a Matlab code developed for training and testing.

Training program: '*nclass_DAGSVM_trn.m*'

Testing program: '*nclass_DAGSVM_tst.m*', '*accuracy.m*'

Programs synopsis: The training algorithm takes the dataset containing patterns corresponding to the five classes. The data of one class is paired with data from other class and the corresponding binary classifier is trained. A set of ten binary classifiers is

created each time the program is run. The testing algorithm takes the model created and classify all the data points inputted using the DAG scheme. It also calculated the confusion matrix and the accuracy of the classification.

A detailed description of the call to the STPRTool functions is presented in the following paragraphs.

$SVMmodel = smo(TRN, options);$

The function smo is the STPRTool implementation of the Sequential Minimal Optimizer algorithm to train binary SVM classifiers with soft margin. The inputs to the function are the *struct*-type variables: TRN and $options$. The TRN input contains the sample MES patterns used to create the models with the following outline (see Figure 41 for reference):

TRN.X = training data points (DxN, D = dimension feature vector, N = # of training points)

TRN.y = labels for each data point in the *TRN*.X matrix ($1xN$).

The $options$ input groups the control parameters in the following fields:

$options.$ker = Kernel identifier. 'rbf' for Gaussian Radial Basis function

$options.$arg = Arguments for the kernel function selected.

$option.C$ = Regularization constant (see Section 5.1.2).

The output of this function is another *struct*-type variable that includes the following important fields:

$SVMmodel.Alpha$ = Values of the Lagrangian multipliers $[nsv\ x\ 1]$.

$SVMmodel.b$ = Value of the bias $[1\ x\ 1]$.

$SVMmodel.sv.X$ = Support Vectors used to predict class labels of new points.

$SVMmodel.nsv$ = Number of support vectors $[1\ x\ 1]$.

$SVMmodel.margin$ = Margin of the found classifier $[1\ x\ 1]$.

$SVMmodel.cputime$ = CPU time used to get the model $[1\ x\ 1]$.

The testing of new data points is carried out using the function $svmclass$, which classifies each point into one of two outputs using Equation (29). The call to this function is done as follows:

$y = svmclass(TST.X, SVMmodel)$

The inputs to this function are the *struct*-type variable $TST.X$ that contains the test data and the variable $SVMmodel$, which is the output on the smo function. The output is the vector y that has the predicted labels (for the ith point $y(i) = 1$ or $y(i) = 2$). The '*nclass_DAGSVM_tst.m*' algorithm makes successive calls to the $svmclass$ function to implement the DAG multiclass classification scheme.

- For the experiments involving PCA:

The number of SVM classifiers trained increased significantly because a set of 10 binary classifiers was created at each feature dimension (10 to 63) and for each PCA framework (oPCA and mPCA). To expedite the training stage, Weka data mining software was used and run from Matlab [174]. This software is coded in Java environment and it is well suited for developing machine learning schemes.

PCA frameworks: '*dataForClassifiers_oPCA.m*';

'*dataForClassifiers_mPCA.m*'

Dim. reduction: '*findBestDimensionDWT.m*';

'*findBestDimensionOnePCA.m*';

'*findBestDimensionMultPCA.m*';

'*wekaTrainSMOClassifier*';

'*wekaClassifySMO_multiPCA.m*';

'*wekaClassifySMO_DAG.m*'

Programs synopsis: The PCA frameworks programs take the wavelet features obtained previously. In both cases, the new feature space is found and the wavelet features are projected into the new coordinates. The dimensionality reduction programs train one set of classifiers for each dimension using the *smo* algorithm included in Weka. The classification uses different files, depending on the PCA framework used. These algorithms can be slightly modified to process the wavelet features obtained after 4 levels of wavelet decomposition.

APPENDIX C

REAL-TIME ALGORITHM IN LABVIEW

The LabVIEW algorithms used in this dissertation for the real-time implementation of the myoelectric pattern recognition system are included in the optical media attached. The main program was designed for acquiring, processing and classifying EMG signals. A screen shot of the latest version of front panel designed is illustrated in Figure 72. The seven channels of signal being acquired are plotted in the charts showed in the left-hand side of the figure. The time delay and the class decision output are displayed in the right-center side of the front panel. The rest of the indicators display information related with the device configuration, link status and for debugging purposes.

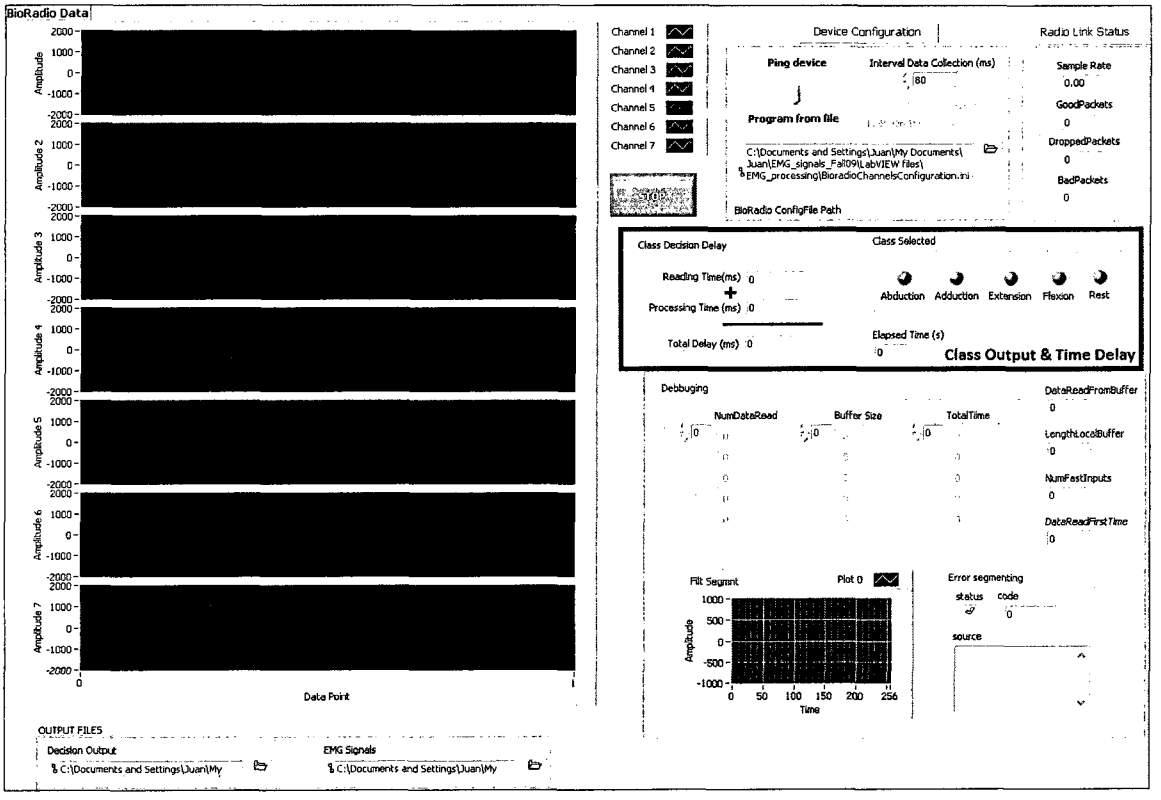

Figure 72. LabVIEW front panel of the real-time myoelectric pattern recognition system implemented in this dissertation.

National Instruments' LabVIEW programs are known as Virtual Instruments (VI's) because they simulate real instruments. Several VI's can be combined to create new VI's. In this dissertation, VI's provided by CleveMed Inc were used to allow the communication and control of the BioRadio 150 data acquisition system through a LabVIEW virtual instrument. This main program used those VI's in combination with other custom VI's to perform the three principal tasks previously mentioned: acquisition, processing and classification.

Main VI: '*BioRadio_EMGProcessing.vi*'

Sub-VI's for starting acquisition: '*BioRadio_FindAndChooseReceiver.vi*'

'*BioRadio_StartBaseComm.vi*'

'*BioRadio_Start.vi*'

'*BioRadio_Read.vi*'

Sub-VI's for stopping acquisition: '*BioRadio_Stop.vi*'

'*BioRadio_StopBaseComm.vi*'

Sub-VI's for processing: '*onLineProcessing.vi*'

Sub-VI's for classification: '*onLineProcessing.vi*' and '*classIndicator.vi*'

Programs synopsis: The main VI contained all sub-VIs. The signal recording is initialized by using the sub-VIs for starting acquisition. As more data is read, a Matlab script embedded in the main VI stores them in a buffer and creates the analysis segments. These segments are sent to the processing and classification sub-VI, which has another Matlab script embedded. On this script, the segmented signal is filtered and normalized before the wavelet is decomposed. The final class decision is made using the classifier previously trained offline. These processes are timed to display the processing delay for

each segment in the front panel. The *classIndicator.vi* program takes that decision and activates a green light in the front panel that corresponds to the selected class. Figure 73 shows the set up of a typical recording session.

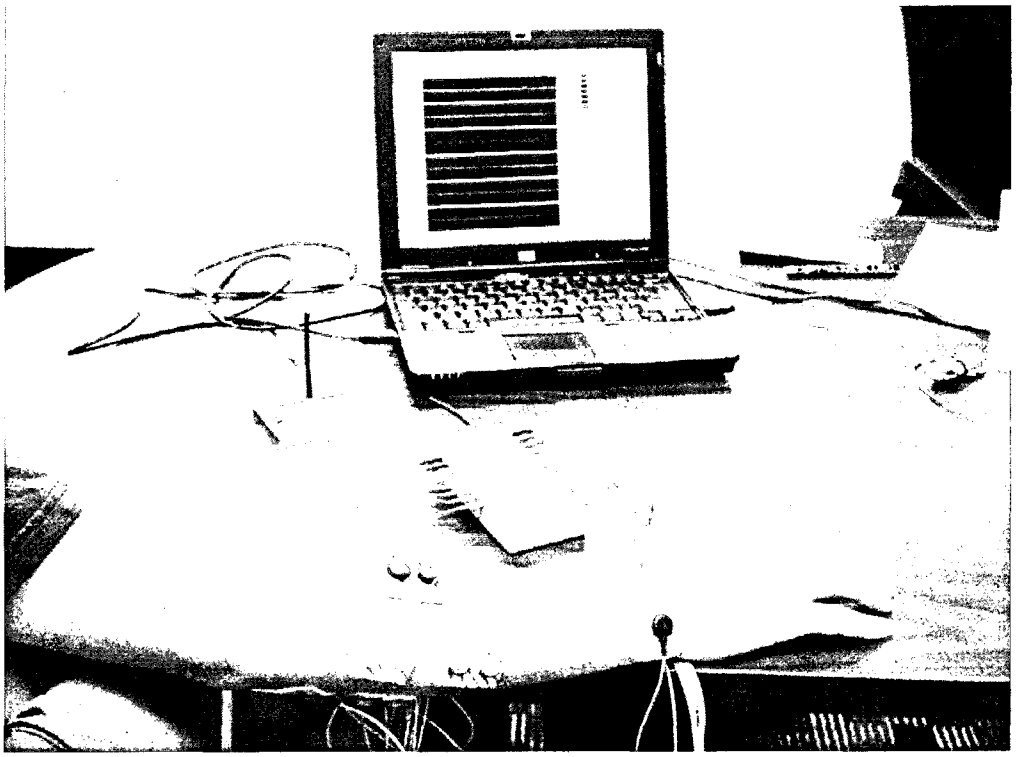

Figure 73. Illustration of the complete set up used for recording, processing and classifying EMG signals in real-time. Electrodes placed on the subject forearm are connected to the wireless transmitter. The receiver communicates with the computer through the LabVIEW application.

REFERENCES

[1] K. Ziegler-Graham, E. J. MacKenzie, P. L. Ephraim, T. G. Travison, and R. Brookmeyer, "Estimating the Prevalence of Limb Loss in the United States: 2005 to 2050," *Archives of Physical Medicine and Rehabilitation,* vol. 89, pp. 422-429, 2008.

[2] T. R. Dillingham, L. E. Pezzin, and E. J. MacKenzie, "Limb amputation and limb deficiency: Epidemiology and recent trends in the United States," *Southern Medical Journal,* vol. 95, pp. 875-883, 2002.

[3] K. A. Raichle, M. A. Hanley, I. Molton, N. J. Kadel, K. Campbell, E. Phelps, D. Ehde, and D. G. Smith, "Prosthesis use in persons with lower- and upper-limb amputation," *Journal of Rehabilitation Research and Development,* vol. 45, pp. 961-972, 2008.

[4] R. F. Baumgartner, "Guest Editorial: Upper extremity amputation and prosthetics," *Journal of Rehabilitation Research and Development,* vol. 38, 2001.

[5] E. Biddiss and T. Chau, "Upper limb prosthesis use and abandonment: A survey of the last 25 years," *Prosthetics and Orthotics International,* vol. 31, pp. 236-257, 2007.

[6] G. H. Kejlaa, "Consumer concerns and the functional value of prostheses to upper limb amputees," *Prosthetics and Orthotics International,* vol. 17, pp. 157-163, 1993.

[7] M. A. Oskoei and H. Hu, "Myoelectric control systems-A survey," *Biomedical Signal Processing and Control,* vol. 2, pp. 275-294, 2007.

[8] P. Parker, K. Englehart, and B. Hudgins, "Control of Powered Upper Limb Prostheses," in *Electromyography: Physiology, Engineering, and Non-Invasive Applications*, R. Merletti and P. Parker, Eds. New York, NY: Wiley-IEEE Press, 2004, pp. 453-475.

[9] P. Parker, K. Englehart, and B. Hudgins, "Myoelectric signal processing for control of powered limb prostheses," *Journal of Electromyography and Kinesiology,* vol. 16, pp. 541-548, 2006.

[10] C. Castellini and P. Van Der Smagt, "Surface EMG in advanced hand prosthetics," *Biological Cybernetics,* vol. 100, pp. 35-47, 2009.

[11] M. Zecca, S. Micera, M. C. Carrozza, and P. Dario, "Control of multifunctional prosthetic hands by processing the electromyographic signal," *Critical Reviews in Biomedical Engineering,* vol. 30, pp. 459-485, 2002.

[12] D. Graupe, J. Salahi, and K. H. Kohn, "Multifunctional prosthesis and orthosis control via microcomputer identification of temporal pattern differences in single-site myoelectric signals," *Journal of Biomedical Engineering,* vol. 4, pp. 17-22, 1982.

[13] G. Li, A. E. Schultz, and T. A. Kuiken, "Quantifying pattern recognition- based myoelectric control of multifunctional transradial prostheses," *IEEE Transactions on Neural Systems and Rehabilitation Engineering,* vol. 18, pp. 185-192, 2010.

[14] L. J. Hargrove, E. J. Scheme, K. B. Englehart, and B. S. Hudgins, "Multiple binary classifications via linear discriminant analysis for improved controllability of a powered prosthesis," *IEEE Transactions on Neural Systems and Rehabilitation Engineering,* vol. 18, pp. 49-57, 2010.

[15] C. Martelloni, J. Carpaneto, and S. Micera, "Classification of upper arm EMG signals during object-specific grasp," in *30th Annual International Conference of the IEEE Engineering in Medicine and Biology Society, EMBS 2008.*, 2008, pp. 5061-5064.

[16] F. V. G. Tenore, A. Ramos, A. Fahmy, S. Acharya, R. Etienne-Cummings, and N. V. Thakor, "Decoding of individuated finger movements using surface electromyography," *IEEE Transactions on Biomedical Engineering,* vol. 56, pp. 1427-1434, 2009.

[17] J. U. Chu, I. Moon, Y. J. Lee, S. K. Kim, and M. S. Mun, "A supervised feature-projection-based real-time EMG pattern recognition for multifunction myoelectric hand control," *IEEE/ASME Transactions on Mechatronics,* vol. 12, pp. 282-290, 2007.

[18] X. Hu, Z. Wang, and X. Ren, "Classification of surface EMG signal using relative wavelet packet energy," *Computer Methods and Programs in Biomedicine,* vol. 79, pp. 189-195, 2005.

[19] Y. H. Liu, H. P. Huang, and C. H. Weng, "Recognition of electromyographic signals using cascaded kernel learning machine," *IEEE/ASME Transactions on Mechatronics,* vol. 12, pp. 253-264, 2007.

[20] D. Tkach, H. Huang, and T. A. Kuiken, "Study of stability of time-domain features for electromyographic pattern recognition," *Journal of NeuroEngineering and Rehabilitation,* vol. 7, 2010.

[21] K. Englehart and B. Hudgins, "A robust, real-time control scheme for multifunction myoelectric control," *IEEE Transactions on Biomedical Engineering,* vol. 50, pp. 848-854, 2003.

[22] T. Moritani, D. Stegeman, and R. Merletti, "Basic physiology and biophysics of EMG signal generation," in *Electromyography: Physiology, Engineering, and Non-Invasive Applications*, R. Merletti and P. Parker, Eds. New York, NY: Wiley-IEEE Press, 2004, pp. 1-25.

[23] C. J. De Luca, "Physiology and Mathematics of Myoelectric Signals," *IEEE Transactions on Biomedical Engineering,* vol. BME-26, pp. 313-325, 1979.

[24] A. C. Guyton and J. E. Hall, "Excitation of skeletal muscle: Neuromuscular transmission and excitation-contraction coupling," in *Textbook of Medical Physiology, 11th edition*: Elsevier Health Sciences, 2005, pp. 87-93.

[25] J. W. Clark Jr, "The origin of biopotentials," in *Medical Instrumentation: Application and Design, 3rd Edition*, J. G. Webster, Ed. New York, NY: John Wiley and Sons, Inc., 1998, pp. 121-182.

[26] M. Knaflitz and G. Balestra, "Computer analysis of the myoelectric signal," *IEEE Micro,* vol. 11, p. 12, 1991.

[27] D. Farina, R. Merletti, and D. F. Stegeman, "Biophysics of the generation of EMG signals," in *Electromyography: Physiology, Engineering, and Non-Invasive Applications*, R. Merletti and P. Parker, Eds. New York, NY: Wiley-IEEE Pres, 2004, pp. 81-107.

[28] R. Merletti and A. Farina, "Analysis of Intramuscular electromyogram signals," *Philosophical Transactions of the Royal Society A: Mathematical, Physical and Engineering Sciences,* vol. 367, pp. 357-368, 2009.

[29] R. S. Lefever, A. P. Xenakis, and C. J. De Luca, "A Procedure for Decomposing the Myoelectric Signal Into Its Constituent Action Potentials-Part II: Execution and Test for Accuracy," *IEEE Transactions on Biomedical Engineering,* vol. BME-29, pp. 158-164, 1982.

[30] R. S. Lefever and C. J. De Luca, "A Procedure for Decomposing the Myoelectric Signal Into Its Constituent Action Potentials - Part I: Technique, Theory, and Implementation," *IEEE Transactions on Biomedical Engineering,* vol. BME-29, pp. 149-157, 1982.

[31] D. Stashuk, "EMG signal decomposition: How can it be accomplished and used?," *Journal of Electromyography and Kinesiology,* vol. 11, pp. 151-173, 2001.

[32] H. B. Olsen, H. Christensen, and K. SÃ¸gaard, "An analysis of motor unit firing pattern during sustained low force contraction in fatigued muscle," *Acta Physiologica et Pharmacologica Bulgarica,* vol. 26, pp. 73-78, 2001.

[33] M. Kamo and S. Morimoto, "Discharge properties of human motor units during sustained contraction at low level force," *Journal of Electromyography and Kinesiology,* vol. 11, pp. 255-261, 2001.

[34] A. Kossev and P. Christova, "Discharge pattern of human motor units during dynamic concentric and eccentric contractions," *Electroencephalography and Clinical Neurophysiology - Electromyography and Motor Control,* vol. 109, pp. 245-255, 1998.

[35] P. A. McNulty and A. G. Cresswell, "Recruitment of single human low-threshold motor units with increasing loads at different muscle lengths," *Journal of Electromyography and Kinesiology,* vol. 14, pp. 369-377, 2004.

[36] S. Riek and P. Bawa, "Recruitment of motor units in human forearm extensors," *Journal of Neurophysiology,* vol. 68, pp. 100-108, 1992.

[37] A. Adam and C. J. De Luca, "Recruitment Order of Motor Units in Human Vastus Lateralis Muscle Is Maintained during Fatiguing Contractions," *Journal of Neurophysiology,* vol. 90, pp. 2919-2927, 2003.

[38] C. J. De Luca, R. S. LeFever, M. P. McCue, and A. P. Xenakis, "Behaviour of human motor units in different muscles during linearly varying contractions," *Journal of Physiology,* vol. Vol. 329, pp. 113-128, 1982.

[39] A. Fuglsang-Frederiksen and J. Ronager, "EMG power spectrum, turns-amplitude analysis and motor unit potential duration in neuromuscular disorders," *Journal of the Neurological Sciences,* vol. 97, pp. 81-91, 1990.

[40] P. R. W. Fawcett, F. L. Mastaglia, and F. Mechler, "Electrophysiological findings including single fibre EMG in a family with mitochondrial myopathy," *Journal of the Neurological Sciences,* vol. 53, pp. 397-410, 1982.

[41] E. N. Kamavuako, D. Farina, K. Yoshida, and W. Jensen, "Relationship between grasping force and features of single-channel intramuscular EMG signals," *Journal of Neuroscience Methods,* vol. 185, pp. 143-150, 2009.

[42] C. J. De Luca, A. Adam, R. Wotiz, L. D. Gilmore, and S. H. Nawab, "Decomposition of surface EMG signals," *Journal of Neurophysiology,* vol. 96, pp. 1646-1657, 2006.

[43] D. Stashuk, D. Farina, and K. SÃ¸gaard, "Decomposition of intramuscular EMG signals," in *Electromyography: Physiology, Engineering, and Non-Invasive Applications*, R. Merletti and P. Parker, Eds. New York, NY: Wiley-IEEE Pres, 2004, pp. 47-77.

[44] H. Nakamura, M. Yoshida, M. Kotani, K. Akazawa, and T. Moritani, "The application of independent component analysis to the multi-channel surface electromyographic signals for separation of motor unit action potential trains: Part I - Measuring techniques," *Journal of Electromyography and Kinesiology,* vol. 14, pp. 423-432, 2004.

[45] E. Chauvet, O. Fokapu, J. Y. Hogrel, D. Gamet, and J. DuchÃªne, "Automatic identification of motor unit action potential trains from electromyographic signals using fuzzy techniques," *Medical and Biological Engineering and Computing,* vol. 41, pp. 646-653, 2003.

[46] J. Lee, A. Adam, and C. J. De Luca, "A simulation study for a surface EMG sensor that detects distinguishable motor unit action potentials," *Journal of Neuroscience Methods,* vol. 168, pp. 54-63, 2008.

[47] D. Farina and C. Cescon, "Concentric-ring electrode systems for noninvasive detection of single motor unit activity," *IEEE Transactions on Biomedical Engineering,* vol. 48, pp. 1326-1334, 2001.

[48] D. Farina, W. Muhammad, E. Fortunato, O. Meste, R. Merletti, and H. Rix, "Estimation of single motor unit conduction velocity from surface electromyogram signals detected with linear electrode arrays," *Medical and Biological Engineering and Computing,* vol. 39, pp. 225-236, 2001.

[49] B. Bigland-Ritchie, E. F. Donovan, and C. S. Roussos, "Conduction velocity and EMG power spectrum changes in fatigue of sustained maximal efforts," *Journal of Applied Physiology Respiratory Environmental and Exercise Physiology,* vol. 51, pp. 1300-1305, 1981.

[50] R. Merletti, A. Holobar, and D. Farina, "Analysis of motor units with high-density surface electromyography," *Journal of Electromyography and Kinesiology,* vol. 18, pp. 879-890, 2008.

[51] A. Holobar, D. Farina, M. Gazzoni, R. Merletti, and D. Zazula, "Estimating motor unit discharge patterns from high-density surface electromyogram," *Clinical Neurophysiology,* vol. 120, pp. 551-562, 2009.

[52] D. Farina, A. Holobar, R. Merletti, and R. M. Enoka, "Decoding the neural drive to muscles from the surface electromyogram," *Clinical Neurophysiology,* In Press.

[53] D. Farina, R. Merletti, and R. M. Enoka, "The extraction of neural strategies from the surface EMG," *Journal of Applied Physiology,* vol. 96, pp. 1486-1495, 2004.

[54] M. J. Zwarts, G. Drost, and D. F. Stegeman, "Recent progress in the diagnostic use of surface EMG for neurological diseases," *Journal of Electromyography and Kinesiology,* vol. 10, pp. 287-291, 2000.

[55] N. K. Iwata and Y. Ugawa, "The effects of cerebellar stimulation on the motor cortical excitability in neurological disorders: A review," *Cerebellum,* vol. 4, pp. 218-223, 2005.

[56] J. P. Clarys, "Electromyography in sports and occupational settings: An update of its limits and possibilities," *Ergonomics,* vol. 43, pp. 1750-1762, 2000.

[57] F. Felici, "Neuromuscular responses to exercise investigated through surface EMG," *Journal of Electromyography and Kinesiology,* vol. 16, pp. 578-585, 2006.

[58] J. P. Clarys and J. Cabri, "Electromyography and the study of sports movements: A review," *Journal of Sports Sciences,* vol. 11, pp. 379-448, 1993.

[59] D. Staudenmann, K. Roeleveld, D. F. Stegeman, and J. H. van Dieen, "Methodological aspects of SEMG recordings for force estimation - A tutorial and review," *Journal of Electromyography and Kinesiology,* vol. 20, pp. 375-387, 2010.

[60] A. Rainoldi, R. Casale, P. Hodges, and G. Jull, "Applications in rehabilitation medicine and related fields," in *Electromyography Physiology, Engineering and Non Invasive Applications*, R. Merletti and P. Parker, Eds. New York, NY: Wiley-IEEE Press, 2004, pp. 403-433.

[61] P. Di Benedetto and T. Giorgini, "Chronic pelvic pain and role of the surface electromyographic (EMG) biofeedback in the diagnosis and treatment," *Europa Medicophysica,* vol. 36, pp. 91-101, 2000.

[62] C. Castellini and P. van der Smagt, "Surface EMG in advanced hand prosthetics," *Biological Cybernetics,* p. 1, 2008.

[63] M. Asghari Oskoei and H. Hu, "Myoelectric control systems-A survey," *Biomedical Signal Processing and Control,* vol. 2, p. 275, 2007.

[64] J. A. Doubler and D. S. Childress, "Design and evaluation of a prosthesis control system based on the concept of extended physiological proprioception," *Journal of Rehabilitation Research and Development,* vol. 21, pp. 19-31, 1984.

[65] A. H. Bottomley, "Myo-electric Control of Powered Prosthesis," *The Journal of bone and joint surgery. British volume,* vol. 47, pp. 411-415, 1965.

[66] C. K. Battye, A. Nightingale, and J. Whillis, "The Use of Myo-electric Currents in the Operation of Prosteses," *J Bone Joint Surg Br,* vol. 37-B, pp. 506-510, August 1, 1955 1955.

[67] J. E. Paciga, D. A. Gibson, and R. Gillespie, "Clinical evaluation of UNB 3-state myoelectric control for arm prostheses," *Bulletin of Prosthetics Research,* vol. 10, pp. 21-33, 1980.

[68] D. S. Dorcas and R. N. Scott, "A three-state myo-electric control," *Medical & Biological Engineering,* vol. 4, pp. 367-370, 1966.

[69] P. D. Richard, R. E. Gander, P. A. Parker, and R. N. Scott, "Multistate myoelectric control: The feasibility of 5-state control," *Journal of Rehabilitation Research and Development,* vol. 20, pp. 84-86, 1983.

[70] J. E. Paciga, P. D. Richard, and R. N. Scott, "Error rate in five-state myoelectric control systems," *Medical and Biological Engineering and Computing,* vol. 18, pp. 287-290, 1980.

[71] Liberating Technologies Inc, "Boston Arm Systems," Available: http://www.liberatingtech.com/products/LTI_Boston_Arm_Systems.asp, accessed on July 2010.

[72] Motion Control Inc, "The Utah Arm 3," Available: http://www.utaharm.com/, accessed on July 2010.

[73] S. C. Jacobsen, D. F. Knutti, R. T. Johnson, and H. H. Sears, "Development of the Utah artificial arm," *IEEE Transactions on Biomedical Engineering,* vol. 29, pp. 249-269, 1982.

[74] P. J. Kyberd and P. H. Chappell, "The Southampton hand: An intelligent myoelectric prosthesis," *Journal of Rehabilitation Research and Development,* vol. 31, pp. 326-334, 1994.

[75] D. Graupe and W. K. Cline, "Functional separation of EMG signals via ARMA identification methods for prosthesis control purposes," *IEEE Transactions on Systems, Man and Cybernetics,* vol. SMC-5, pp. 252-259, 1975.

[76] D. Graupe, J. Magnussen, and A. Beex, "A microprocessor system for multifunctional control of upper-limb prostheses via myoelectric signal identification," *IEEE Transactions on Automatic Control,* vol. 23, pp. 538-544, 1978.

[77] B. Hudgins, P. Parker, and R. N. Scott, "A new strategy for multifunction myoelectric control," *IEEE Transactions on Biomedical Engineering,* vol. 40, pp. 82-94, 1993.

[78] U. Kuruganti, B. Hudgins, and R. N. Scott, "Two-channel enhancement of a multifunction control system," *IEEE Transactions on Biomedical Engineering,* vol. 42, pp. 109-111, 1995.

[79] C. M. Light, P. H. Chappell, B. Hudgins, and K. Engelhart, "Intelligent multifunction myoelectric control of hand prostheses," *Journal of Medical Engineering and Technology,* vol. 26, pp. 139-146, 2002.

[80] Y. Al-Assaf and H. Al-Nashash, "Surface myoelectric signal classification for prostheses control," *Journal of Medical Engineering and Technology,* vol. 29, p. 203, 2005.

[81] P. C. Doerschuk, D. E. Gustafson, and A. S. Willsky, "Upper extremity limb function discrimination using EMG signal analysis," *IEEE Transactions on Biomedical Engineering,* vol. 30, pp. 18-29, 1983.

[82] K. Englehart, B. Hudgins, and P. A. Parker, "A wavelet-based continuous classification scheme for multifunction myoelectric control," *IEEE Transactions on Biomedical Engineering,* vol. 48, pp. 302-311, 2001.

[83] G. W. Choi, J. U. Chu, and G. H. Choe, "A study on the control system of myoelectric hand prosthesis," *Transactions of the Korean Institute of Electrical Engineers,* vol. 56, pp. 214-221, 2007.

[84] A. B. Ajiboye and R. F. F. Weir, "A heuristic fuzzy logic approach to EMG pattern recognition for multifunctional prosthesis control," *IEEE Transactions on Neural Systems and Rehabilitation Engineering,* vol. 13, pp. 280-291, 2005.

[85] A. Soares, A. Andrade, E. Lamounier, and R. Carrijo, "The development of a virtual myoelectric prosthesis controlled by an EMG pattern recognition system based on neural networks," *Journal of Intelligent Information Systems,* vol. 21, pp. 127-141, 2003.

[86] B. Karlik, M. O. Tokhi, and M. Alci, "A Fuzzy Clustering Neural Network Architecture for Multifunction Upper-Limb Prosthesis," *IEEE Transactions on Biomedical Engineering,* vol. 50, pp. 1255-1261, 2003.

[87] K. Englehart, B. Hudgins, and A. D. C. Chan, "Continuous multifunction myoelectric control using pattern recognition," *Technology and Disability,* vol. 15, pp. 95-103, 2003.

[88] P. Hortensius, A. Quanbury, and S. Onyshko, "A low-power multichannel electromyographic signal data acquisition system," *Journal of Medical Engineering and Technology,* vol. 11, pp. 11-16, 1987.

[89] T. A. Kuiken, G. Li, B. A. Lock, R. D. Lipschutz, L. A. Miller, K. A. Stubblefield, and K. B. Englehart, "Targeted muscle reinnervation for real-time myoelectric control of multifunction artificial arms," *JAMA - Journal of the American Medical Association,* vol. 301, pp. 619-628, 2009.

[90] J. W. Sensinger, B. A. Lock, and T. A. Kuiken, "Adaptive pattern recognition of myoelectric signals: Exploration of conceptual framework and practical algorithms," *IEEE Transactions on Neural Systems and Rehabilitation Engineering,* vol. 17, pp. 270-278, 2009.

[91] M. Zardoshti-Kermani, B. C. Wheeler, K. Badie, and R. M. Hashemi, "EMG feature selection for movement control of a cybernetic arm," *Cybernetics and Systems,* vol. 26, pp. 189-210, 1995.

[92] G. N. Saridis and T. P. Gootee, "EMG pattern analysis and classification for a prosthetic arm," *IEEE Transactions on Biomedical Engineering,* vol. 29, pp. 403-412, 1982.

[93] K. Momen, S. Krishnan, and T. Chau, "Real-time classification of forearm electromyographic signals corresponding to user-selected intentional movements for multifunction prosthesis control," *IEEE Transactions on Neural Systems and Rehabilitation Engineering,* vol. 15, pp. 535-542, 2007.

[94] C. Castellini, A. E. Fiorilla, and G. Sandini, "Multi-subject/daily-life activity EMG-based control of mechanical hands," *Journal of NeuroEngineering and Rehabilitation,* vol. 6, 2009.

[95] J. M. Fontana and A. W. L. Chiu, "Control of prosthetic device using Support Vector Machine signal classification technique," *American Journal of Biomedical Science,* vol. 1, pp. 336-343, 2009.

[96] M. F. Kelly, P. A. Parker, and R. N. Scott, "The application of neural networks to myoelectric signal analysis: A preliminary study," *IEEE Transactions on Biomedical Engineering,* vol. 37, pp. 221-230, 1990.

[97] A. Hiraiwa, K. Shimohara, and Y. Tokunaga, "EMG pattern analysis and classification by neural network," in *Proceedings of the IEEE International Conference on Systems, Man and Cybernetics*, 1989, pp. 1113-1115.

[98] P. A. Parker, J. A. Stuller, and R. N. Scott, "Signal processing for the multistate myoelectric channel," *Proceedings of the IEEE,* vol. 65, pp. 662-674, 1977.

[99] L. Zhizeng, W. Fei, and M. Wenjie, "Pattern classification of surface electromyography based on AR model and high-order neural network," in *Proceedings of the 2nd IEEE/ASME International Conference on Mechatronic and Embedded Systems and Applications, MESA 2006*, 2007.

[100] Y. Al-Assaf, "Surface myoelectric signal analysis: Dynamic approaches for change detection and classification," *IEEE Transactions on Biomedical Engineering,* vol. 53, p. 2248, 2006.

[101] A. Khadivi, K. Nazarpour, and H. S. Zadeh, "sEMG classification for upper-limb prosthesis control using higher order statistics," in *ICASSP, IEEE International Conference on Acoustics, Speech and Signal Processing - Proceedings*, 2005.

[102] L. J. Hargrove, G. Li, K. B. Englehart, and B. S. Hudgins, "Principal components analysis preprocessing for improved classification accuracies in pattern-recognition-based myoelectric control," *IEEE Transactions on Biomedical Engineering,* vol. 56, pp. 1407-1414, 2009.

[103] M. Zardoshti-Kermani, B. C. Wheeler, K. Badie, and R. M. Hashemi, "EMG feature evaluation for movement control of upper extremity prostheses," *IEEE Transactions on Rehabilitation Engineering,* vol. 3, pp. 324-333, 1995.

[104] M. Khezri and M. Jahed, "Real-time intelligent pattern recognition algorithm for surface EMG signals," *BioMedical Engineering Online,* vol. 6, 2007.

[105] D. Graupe, J. Salahi, and D. S. Zhang, "Stochastic analysis of myoelectric temporal signatures for multifunctional single-site activation of prostheses and orthoses," *Journal of Biomedical Engineering,* vol. 7, pp. 18-29, 1985.

[106] S. Karlsson, J. Yu, and M. Akay, "Enhancement of spectral analysis of myoelectric signals during static contractions using wavelet methods," *IEEE Transactions on Biomedical Engineering,* vol. 46, pp. 670-684, 1999.

[107] R. Merletti and L. R. Lo Conte, "Surface EMG signal processing during isometric contractions," *Journal of Electromyography and Kinesiology,* vol. 7, pp. 241-250, 1997.

[108] O. Paiss and G. F. Inbar, "Autoregressive modeling of surface EMG and its spectrum with application to fatigue," *IEEE Transactions on Biomedical Engineering,* vol. 34, pp. 761-770, 1987.

[109] K. A. Farry, I. D. Walker, and R. G. Baraniuk, "Myoelectric teleoperation of a complex robotic hand," *IEEE Transactions on Robotics and Automation,* vol. 12, pp. 775-788, 1996.

[110] S. Du and M. Vuskovic, "Temporal vs. spectral approach to feature extraction from prehensile EMG signals," in *Proceedings of the 2004 IEEE International Conference on Information Reuse and Integration, IRI-2004*, 2004, pp. 344-350.

[111] P. J. Gallant, E. L. Morin, and L. E. Peppard, "Feature-based classification of myoelectric signals using artificial neural networks," *Medical and Biological Engineering and Computing,* vol. 36, pp. 485-489, 1998.

[112] K. Englehart, B. Hudgins, P. Parker, and M. Stevenson, "Time-frequency representation for classification of the transient myoelectric signal," in *Annual International Conference of the IEEE Engineering in Medicine and Biology - Proceedings*, 1998, pp. 2627-2630.

[113] F. Hlawatsch and G. F. Boudreaux-Bartels, "Linear and quadratic time-frequency signal representations," *IEEE Signal Processing Magazine,* vol. 9, pp. 21-67, 1992.

[114] D. Zazula, S. Karlsson, and C. Doncarli, "Advanced signal processing techniques," in *Electromyography: Physiology, Engineering, and Non-Invasive Applications*, R. Merletti and P. Parker, Eds. New York, NY: Wiley-IEEE Pres, 2004, pp. 259-304.

[115] K. Englehart, B. Hudgins, P. A. Parker, and M. Stevenson, "Classification of the myoelectric signal using time-frequency based representations," *Medical Engineering and Physics,* vol. 21, pp. 431-438, 1999.

[116] R. R. Coifman and M. V. Wickerhauser, "Entropy-based algorithms for best basis selection," *IEEE Transactions on Information Theory,* vol. 38, pp. 713-718, 1992.

[117] S. Karlsson, J. Yu, and M. Akay, "Time-frequency analysis of myoelectric signals during dynamic contractions: A comparative study," *IEEE Transactions on Biomedical Engineering,* vol. 47, pp. 228-238, 2000.

[118] Y. Al-Assaf and H. Al-Nashash, "Myoelectric signal segmentation and classification using wavelets based neural networks," in *Proceedings of the 23rd Annual International Conference of the IEEE Engineering in Medicine and Biology Society*, 2001, pp. 1820-1823.

[119] M. F. Lucas, A. Gaufriau, S. Pascual, C. Doncarli, and D. Farina, "Multi-channel surface EMG classification using support vector machines and signal-based wavelet optimization," *Biomedical Signal Processing and Control,* vol. 3, pp. 169-174, 2008.

[120] H. Liu, X. Chen, and Y. Chen, "Wavelet transform and real-time learning method for myoelectric signal in motion discrimination," *Journal of Physics: Conference Series,* vol. 13, pp. 250-253, 2005.

[121] G. Wang, Z. Wang, W. Chen, and J. Zhuang, "Classification of surface EMG signals using optimal wavelet packet method based on Davies-Bouldin criterion," *Medical and Biological Engineering and Computing,* vol. 44, pp. 865-872, 2006.

[122] G. Wang, Z. Yan, X. Hu, H. Xie, and Z. Wang, "Classification of surface EMG signals using harmonic wavelet packet transform," *Physiological Measurement,* vol. 27, 2006.

[123] K. Englehart, B. Hudgins, P. A. Parker, and M. Stevenson, "Improving myoelectric signal classification using wavelet packets and principal components analysis," in *Proceedings Annual International Conference of the IEEE Engineering in Medicine and Biology*, 1999, p. 569.

[124] K. Englehart, B. Hudgins, and P. A. Parker, "Time-frequency based classification of the myoelectric signal: Static vs. dynamic contractions," in *Annual International Conference of the IEEE Engineering in Medicine and Biology - Proceedings*, 2000, pp. 317-320.

[125] S. Marsland, *Machine Learning: An Algorithmic Perspective*. Boca Raton, FL: CRC Press, 2009.

[126] R. Battiti, "Using mutual information for selecting features in supervised neural net learning," *IEEE Transactions on Neural Networks,* vol. 5, pp. 537-550, 1994.

[127] L. Cai, Z. Wang, and H. Zhang, "Surface EMG signal classification using wavelet transform," *Shengwu Yixue Gongchengxue Zazhi/Journal of Biomedical Engineering,* vol. 17, pp. 281-284, 2000.

[128] M. Dash and H. Liu, "Feature selection for classification," *Intelligent Data Analysis,* vol. 1, pp. 131-156, 1997.

[129] H. Liu and L. Yu, "Toward integrating feature selection algorithms for classification and clustering," *IEEE Transactions on Knowledge and Data Engineering,* vol. 17, pp. 491-502, 2005.

[130] R. N. Khushaba, A. Alsukker, A. Al-Ani, A. Al-Jumaily, and A. Y. Zomaya, "A novel swarm based feature selection algorithm in multifunction myoelectric control," *Journal of Intelligent and Fuzzy Systems,* vol. 20, pp. 175-185, 2009.

[131] C. M. Bishop, "Continuous latent variables," in *Pattern Recognition and Machine Learning* Secaucus, NJ: Springer-Verlag New York, Inc, 2006.

[132] N. F. Guler and S. Kocer, "Classification of EMG signals using PCA and FFT," *Journal of Medical Systems,* vol. 29, pp. 241-250, 2005.

[133] E. S. A. El-Dahshan, T. Hosny, and A. B. M. Salem, "Hybrid intelligent techniques for MRI brain images classification," *Digital Signal Processing: A Review Journal,* vol. 20, pp. 433-441, 2010.

[134] J. B. Tenenbaum, V. De Silva, and J. C. Langford, "A global geometric framework for nonlinear dimensionality reduction," *Science,* vol. 290, pp. 2319-2323, 2000.

[135] N. R. Pal and V. K. Eluri, "Two efficient connectionist schemes for structure preserving dimensionality reduction," *IEEE Transactions on Neural Networks,* vol. 9, pp. 1142-1154, 1998.

[136] J. Wu, J. Wang, and L. Liu, "Feature extraction via KPCA for classification of gait patterns," *Human Movement Science,* vol. 26, pp. 393-411, 2007.

[137] J. U. Chu, I. Moon, and M. S. Mun, "A real-time EMG pattern recognition system based on linear-nonlinear feature projection for a multifunction myoelectric hand," *IEEE Transactions on Biomedical Engineering,* vol. 53, pp. 2232-2239, 2006.

[138] J. Han and M. Kamber, *Data Mining: Concepts and Techniques*. San Francisco, CA: Morgan Kaufmann, 2006.

[139] X. Chen, X. Zhu, and D. Zhang, "Use of the discriminant Fourier-derived cepstrum with feature-level post-processing for surface electromyographic signal classification," *Physiological Measurement,* vol. 30, pp. 1399-1413, 2009.

[140] X. Chen, X. Zhu, and D. Zhang, "A discriminant bispectrum feature for surface electromyogram signal classification," *Medical Engineering and Physics,* vol. 32, pp. 126-135, 2010.

[141] Y. Huang, K. B. Englehart, B. Hudgins, and A. D. C. Chan, "A Gaussian mixture model based classification scheme for myoelectric control of powered upper limb prostheses," *IEEE Transactions on Biomedical Engineering,* vol. 52, pp. 1801-1811, 2005.

[142] A. D. C. Chan and K. B. Englehart, "Continuous myoelectric control for powered prostheses using hidden Markov models," *IEEE Transactions on Biomedical Engineering,* vol. 52, pp. 121-124, 2005.

[143] A. T. C. Au and R. F. Kirsch, "EMG-based prediction of shoulder and elbow kinematics in able-bodied and spinal cord injured individuals," *IEEE Transactions on Rehabilitation Engineering,* vol. 8, pp. 471-480, 2000.

[144] D. Graupe and H. Kordylewski, "Artificial neural network control of FES in paraplegics for patient responsive ambulation," *IEEE Transactions on Biomedical Engineering,* vol. 42, pp. 699-707, 1995.

[145] M. W. Jiang, R. C. Wang, J. Z. Wang, and D. W. Jin, "A method of recognizing finger motion using wavelet transform of surface EMG signal," in *Annual International Conference of the IEEE Engineering in Medicine and Biology - Proceedings*, 2005, p. 2672.

[146] F. H. Y. Chan, Y. S. Yang, F. K. Lam, Y. T. Zhang, and P. A. Parker, "Fuzzy EMG classification for prosthesis control," *IEEE Transactions on Rehabilitation Engineering,* vol. 8, p. 305, 2000.

[147] C. J. C. Burges, "A tutorial on support vector machines for pattern recognition," *Data Mining and Knowledge Discovery,* vol. 2, pp. 121-167, 1998.

[148] C. Cortes and V. Vapnik, "Support-vector networks," *Machine Learning,* vol. 20, pp. 273-297, 1995.

[149] P. Shenoy, K. J. Miller, B. Crawford, and R. P. N. Rao, "Online electromyographic control of a robotic prosthesis," *IEEE Transactions on Biomedical Engineering,* vol. 55, pp. 1128-1135, 2008.

[150] M. A. Oskoei and H. Hu, "Support vector machine-based classification scheme for myoelectric control applied to upper limb," *IEEE Transactions on Biomedical Engineering,* vol. 55, pp. 1956-1965, 2008.

[151] D. Gabor, "Theory of communication. Part 1: The analysis of information," *Journal of the Institution of Electrical Engineers - Part III: Radio and Communication Engineering,* vol. 93, pp. 429-441, 1946.

[152] P. Goupillaud, A. Grossmann, and J. Morlet, "Cycle-octave and related transforms in seismic signal analysis," *Geoexploration,* vol. 23, pp. 85-102, 1984.

[153] I. Daubechies, "Wavelet transform, time-frequency localization and signal analysis," *IEEE Transactions on Information Theory,* vol. 36, pp. 961-1005, 1990.

[154] S. G. Mallat, "Multiresolution Approximations and Wavelet Orthonormal Bases of L2(R)," *Transactions of the American Mathematical Society,* vol. 315, pp. 69-87, 1989.

[155] L. Brechet, M. F. Lucas, C. Doncarli, and D. Farina, "Compression of biomedical signals with mother wavelet optimization and best-basis wavelet packet selection," *IEEE Transactions on Biomedical Engineering,* vol. 54, pp. 2186-2192, 2007.

[156] Q. Zhang and Z. Luo, "Wavelet de-noising of electromyography," in *IEEE International Conference on Mechatronics and Automation, ICMA 2006*, 2006, pp. 1553-1558.

[157] C. C. Liu and D. Q. Dai, "Face recognition using dual-tree complex wavelet features," *IEEE Transactions on Image Processing,* vol. 18, pp. 2593-2599, 2009.

[158] Y. Liu, "Wavelet feature extraction for high-dimensional microarray data," *Neurocomputing,* vol. 72, pp. 985-990, 2009.

[159] K. Englehart, "Signal Representation for Classification of the Transient Myoelectric Signal," in *Dept. Electr. Comput. Eng.* New Brunswick, Canada: Univ. of New Brunswick, 1998.

[160] M. B. I. Reaz, M. S. Hussain, and F. Mohd-Yasin, "Techniques of EMG signal analysis: Detection, processing, classification and applications," *Biological Procedures Online,* vol. 8, p. 11, 2006.

[161] S. G. Mallat, "A theory for multiresolution signal decomposition: the wavelet representation," *IEEE Transactions on Pattern Analysis and Machine Intelligence,* vol. 11, pp. 674-693, 1989.

[162] I. Daubechies, *Ten lectures on wavelets* vol. 61. Philadelphia: SIAM, 1992.

[163] C. M. Bishop, "Sparse Kernel Machines," in *Pattern Recognition and Machine Learning* Secaucus, NJ: Springer-Verlag New York, Inc, 2006, pp. 325-358.

[164] J. Platt, "Fast training of support vector machines using sequential minimal optimization," in *Advances in Kernel Methods - Support Vector Learning*, B. Scholkopf, C. J. C. Burges, and A. J. Smola, Eds.: MIT Press, 1999, pp. 185-208.

[165] J. Platt, N. Cristianini, and J. Shawe-Taylor, "Large margin DAGs for multiclass classification," *Advances in Neural Information Processing Systems,* vol. 12, pp. 547-553, 2000.

[166] C. W. Hsu and C. J. Lin, "A comparison of methods for multiclass support vector machines," *IEEE Transactions on Neural Networks,* vol. 13, pp. 415-425, 2002.

[167] V. Franc, M. I. Schlesinger, and V. Hlavac, "Statistical Pattern Recognition Toolbox for Matlab," in *http://cmp.felk.cvut.cz/cmp/software/stprtool/index.html* Prague, Czech Republic, 1999.

[168] F. Melgani and Y. Bazi, "Classification of electrocardiogram signals with support vector machines and particle swarm optimization," *IEEE Transactions on Information Technology in Biomedicine,* vol. 12, pp. 667-677, 2008.

[169] F. Melgani and L. Bruzzone, "Classification of hyperspectral remote sensing images with support vector machines," *IEEE Transactions on Geoscience and Remote Sensing,* vol. 42, pp. 1778-1790, 2004.

[170] M. Yoshikawa, M. Mikawa, and K. Taiiaka, "A myoelectric interface for robotic hand control using support vector machine," in *IEEE International Conference on Intelligent Robots and Systems*, 2007, pp. 2723-2728.

[171] T. Fawcett, "An introduction to ROC analysis," *Pattern Recognition Letters,* vol. 27, pp. 861-874, 2006.

[172] L. Hargrove, K. Englehart, and B. Hudgins, "The effect of electrode displacements on pattern recognition based myoelectric control," in *28th Annual International Conference of the IEEE Engineering in Medicine and Biology Society. EMBS*, 2006, pp. 2203-2206.

[173] H. J. Hermens and B. Freriks, "The SENIAM project (Surface ElectroMyoGraphy for the Non-Invasive Assessment of Muscles)," 1996.

[174] M. Hall, E. Frank, G. Holmes, B. Pfahringer, P. Reutemann, and I. H. Witten, "The WEKA Data Mining Software: An Update," *SIGKDD Explorations,* vol. 11, pp. 10-18, 2009.